9-16-2014

Computational Techniques for Optimal Control of Quantum System

Gregory von Winckel

Gregory von Winckel

Candidate

Mathematics and Statistics

Department

This dissertation is approved, and it is acceptable in quality and form for publication:

Approved by the Dissertation Committee:

Evangelos A. Coutsias , Chairperson

Sanjay Krishna

Stephen Lau

Pavel Lushnikov

Louis A. Romero

Computational Techniques for Optimal Control of Quantum Systems

by

Gregory von Winckel

B.S.E., Electrical Engineering, University of Connecticut, 1998
M.S., Electrical Engineering, University of Connecticut, 2000
Ph.D., Electrical Engineering, University of New Mexico, 2006

DISSERTATION

Submitted in Partial Fulfillment of the
Requirements for the Degree of

Doctorate of Philosophy
Mathematics

The University of New Mexico

Albuquerque, New Mexico

December, 2011

Dedication

To Holly, who has had twice the patience.

Acknowledgments

I wish to express thanks to the advisory committee members Vageli Coutsias, Sanjay Krishna, Stephen Lau, Pavel Lushnikov, and Louis Romero. The University of New Mexico Office of Graduate Studies and Department of Mathematics and Statistics, both, in general, deserve my gratitude for not only the opportunity to pursue this work, but also the understanding of the unusual logistics of distance education taken to the extreme.

I owe many thanks to Alfio Borzì, Christian Clason, Julien Grond, Ulrich Höhenester, Karl Kunisch, and Stefan Volkwein for their fruitful collaboration, support, and many helpful discussions.

Computational Techniques for Optimal Control of Quantum Systems

by

Gregory von Winckel

B.S.E., Electrical Engineering, University of Connecticut, 1998

M.S., Electrical Engineering, University of Connecticut, 2000
Ph.D., Electrical Engineering, University of New Mexico, 2006

Ph.D., Mathematics, University of New Mexico, 2011

Abstract

The control of matter and energy at a fundamental level will be a cornerstone of new technologies for years to come. This idea is exemplified in a distilled form by controlling the dynamics of quantum mechanical systems via a time–dependent potential. The contributions detailed within this work focus on the computational aspects of formulating and solving quantum control problems efficiently.

The accurate numerical computation of optimal controls of infinite–dimensional quantum control problems is a very difficult task that requires to take into account the features of the original infinite–dimensional problem. An important issue is the choice of the functional space where the minimization process is defined. A systematic comparison of L^2– versus H^1–based minimization shows that the choice of the appropriate functional space matters and has many consequences in the implementation of some optimization techniques.

A matrix–free cascadic BFGS algorithm is introduced in the L^2 and H^1 settings and it is demonstrated that the choice of H^1 over L^2 results in a substantial performance and robustness increase. A comparison between optimal control resulting from function space minimization and the control obtained by minimization over Chebyshev and POD basis function coefficients is presented.

A theoretical and computational framework is presented to obtain accurate controls for fast quantum state transitions that are needed in a host of applications such as nano electronic devices and quantum computing. This method is based on a reduced Hessian Krylov–Newton scheme applied to a norm–preserving discrete model of a dipole quantum control problem. The use of second–order numerical methods for solving the control problem is justified proving existence of optimal solutions and analyzing first– and second–order optimality conditions. Criteria for the discretization of the non–convex optimization problem and for the formulation of the Hessian are given to ensure accurate gradients and a symmetric Hessian. Robustness of the Newton approach is obtained using a globalization strategy with a robust line-search procedure. Results of numerical experiments demonstrate that the Newton approach presented in this dissertation is able to provide fast and accurate controls for high–energy state transitions.

Control of bound–to–bound and bound–to–continuum transitions in open quantum systems and vector field control of two–dimensional systems is presented. An efficient space–time spectral discretization of the time–dependent Schrödinger equation and preconditioning strategy for a fast approximate solution with Krylov methods is outlined.

Contents

List of Figures

List of Tables

Glossary

BFGS	Broyden–Fletcher–Goldfarb–Shanno method
CGL	Chebyshev–Gauss–Lobatto quadrature
DG	Discontinuous Galerkin method
FCT	Fast Cosine Transform
FFT	Fast Fourier Transform
HZ–NCG	Hagar and Zhang's implementation of the nonlinear conjugate gradient method
KKT	Karush–Kuhn–Tucker conditions
KN	Krylov–Newton method
MCN	Modified Crank–Nicolson method
NCG	Nonlinear conjugate gradient method
PDE	Partial differential equation
PML	Perfectly matched layer
POD	Proper orthogonal decomposition

SD	Steepest descent method
SMW	Sherman–Morrison–Woodbury formula
TDSE	Time–dependent Schrödinger equation
TSSP	Time–splitting spectral scheme

Chapter 1

Introduction

Optimal control of quantum systems can be viewed as a specific instance of PDE–constrained optimization. The optimization problem arises by formulating a cost functional based on a quantum mechanical observable, such as the probability of finding a particle in a particular state, which is to be minimized or maximized. An equality constraint is added which requires the dynamics of the particle to satisfy the appropriate evolution equation, such as the time–dependent Schrödinger equation or the Gross–Pitaevskii equation. The equality constraint is enforced by Lagrange multiplier methods. The optimal control method is, of course, not the only approach for controlling quantum mechanical systems. Quantum feedback control based on classical control theory[91] has many interesting applications and has been the subject of much attention as well.

Quantum control is a challenging problem both theoretically and numerically as the control problem is inherently nonlinear in nature. Even though the TDSE is a linear equation, the control term appears in the Hamiltonian operator, usually in the potential part, where it multiplies with the dependent variable, the quantum mechanical wavefunction. Consequently, cost functionals which depend on the wavefunction

are non-convex and globalization methods are needed to compute minima.

The current work is concerned specifically with the Lagrangian approach that was first applied to the control of quantum systems in 1988 by Peirce, Dahleh, and Rabitz [32] and moreover with the computational aspects of solving the first– and second–order optimality conditions efficiently and accurately. The computational cost of PDE–constrained optimization problems is that typically the PDE itself must be solved a very large number of times. There are, therefore, two ways in which the process can be expedited: one can try to make better use of the information obtained from each PDE solve so that the total number of solves can be reduced and one can choose a discretization which reduces the time of each PDE solve.

Chapter 2 is concerned with the choice of space of the control function with an application to optimal splitting of a Bose–Einstein condensate. It is shown that the standard L^2 leads to discontinuities in the control at the final time which back–propagate leading to a significant deterioration in convergence. An H^1 space formulation is introduced and a limited memory BFGS method is developed to use H^1 inner–product, giving globally time–continuous optimal controls and greatly improved convergence behavior. Additionally a reduced space method is introduced based on orthogonal polynomial expansion. This chapter is self–contained and was originally published in Inverse Problems in 2008 [40].

Chapter 3 contains the first application of a Newton method for the solution of an optimal quantum control problem. The implications of solving the discretized optimality system versus solving the equations which arise by discretizing the cost functional first and then taking variations afterward are considered as well. A novel robust linesearch method, based on the underlying physics, and new theoretical analysis of the first– and second–order optimality conditions are presented. Chapter 3 is also self–contained and was published in SIAM Journal of Scientific Computing

in 2009 [84]. An additional article detailing the algorithm with accompanying codes will be was appeared in Computer Physics Communications in 2010 [87].

Extension of the optimal control approach to open quantum systems is treated in chapter 4. By adding a perfectly matched layer to the computational domain, it becomes possible to accurately simulate loss of probability to the environment. This makes the control problem more challenging still, particularly when a short time horizon is desired. The results of chapters 2 and 3 demonstrate that to elicit a change of state in a short interval, the norm of the control must be large, however, when the system is open, an intense control field will cause the particle to delocalize and leave the confining potential. To prevent this, inequality state constraints are introduced which require the projection of the state onto the eigenspace of bound states to satisfy a certain threshold. The inequality constraint introduces terms of lower regularity and a semi–smooth Newton method is presented to solve the second–order optimality conditions. It is also shown in chapter 4 that the standard final–time cost of quantum control can be transformed into a family of equivalent time–distributed costs by invoking the Ehrenfest Theorem. For the first time, the Wirtinger calculus is applied to quantum control problems to demonstrate a simpler way of deriving optimality conditions.

As a further application of the optimal control framework, control of particles confined in multiple dimensions is considered in chapter 5. A lens-shaped quantum dot is modeled in two dimensions using a conforming simplex mesh and spectral element discretization. In the two–dimensional case, the control function is no longer a scalar function of time, but rather vector–valued. It is observed that a control field corresponding to a lateral electric field can induce transitions between bound states. This is significant as this is the situation of quantum dot photodetectors subjected to normally–incident light.

Chapter 6 develops an efficient space–time spectral discretization of the state

equation. The spectral discretization in time is motivated by two factors: the control which satisfies the first–order optimality system is a C^∞ function on the open time interval and the quantum dispersion relation indicates that the frequency of oscillations in time are much higher than those in space. Therefore a spectral discretization is the ideal for approximating highly oscillatory smooth functions. A space–time preconditioning strategy is detailed for rapidly solving the state equation with an iterative Krylov solver. This preconditioner is shown to reduce the condition number of the matrix to be inverted by as many as four orders of magnitude in the test cases and reduces the number of Krylov solver iterations from over a thousand to under ten.

The final chapter covers the directions of future work and extending the contributions of chapters 2 through 6 to more efficient and faster algorithms for solving quantum optimality systems.

Chapter 2

Choice of control space

2.1 Introduction

Recent years have witnessed large interest in controlling quantum phenomena in a variety of quantum systems through appropriate tailoring of external control fields. For this purpose, each field of research has come up with its own strategies. For instance, quantum-optical implementations in atoms benefit from the long atomic coherence and adiabatic population transfer. In contrast, in quantum chemistry direct feedback from experiments is the method of choice. Therefore, there exists no clear consensus of how to optimally tailor the system's control, and it is only recently that optimal control theory has been recognized as a powerful framework for investigating quantum control problems of various complexity [42, 11, 13, 34]. Along with this development, it has become clear that the numerical solution of optimal control problems requires additional insight and care in the development of solution strategies. It is the purpose of this paper to explore and remark upon some important aspects and details in the development of computational techniques for quantum control problems that are less known in the quantum control community.

For a general discussion on computational techniques for control problems see [56].

To illustrate the challenge given by quantum control problems, we need to discuss their formulation in detail. These problems consist of an evolutionary quantum system, described by Schrödinger-type equations, including a bilinear control mechanism and a functional modeling the purpose of the control and the cost of its action. Therefore the objective functional depends on the state configuration and features describing the desired target as well as the control fields. The resulting task is to minimize the objective subject to the constraint given by the dynamics equations. Therefore, we have an infinite dimensional optimization problem where the constraint is represented by a time-dependent Schrödinger equation and a bilinear control structure.

It turns out that quantum control problems possess very flat minima that are sensitive to problems' discretization parameters. Moreover, some of these local minima appear to be a consequence of discretization and eventually disappear when sufficiently fine mesh is used. This fact renders the accurate computation of optimal controls very difficult and requires to take into account the features of the original infinite dimensional problem. As a benchmark for our discussion we consider the Bose–Einstein condensates control problem [58] governed by the nonlinear time-dependent Gross–Pitaevskii equation [48] with the objective to approach a final target state by means of a smooth varying magnetic control field.

The bilinear control structure typical of quantum mechanical problems, the presence of nonlinear wavefunction evolution equations in complex Hilbert spaces, the possibility of final observations only, make quantum control problems very difficult to solve. This means that known optimal strategies may fail or not be able to provide the expected performance. For this reason, we present a systematic investigation of computational techniques with a focus on the choice of the functional space where the minimization process is defined. Our interest is motivated by the fact that usually

quantum control problems (and corresponding gradients) are formulated and solved on L^2 spaces while the cost of the controls in the objective may be of H^1 type, a natural choice related to the regularity properties typical of quantum models.

Our present contribution to the field of computational techniques for quantum control problems is to show that the choice of the appropriate minimization space matters and has many consequences for the implementation and performance of the optimization techniques considered in this paper.

In particular, we contribute on the following issues: 1) Discussion on the formulation of the gradient in the L^2 and H^1 spaces. 2) Construction of a nonlinear conjugate gradient (NCG) and of the standard and cascadic Broyden-Fletcher-Goldfarb-Shanno (BFGS) schemes in the L^2 and H^1 spaces. 3) Discussion of the globalization step depending on the accuracy of discretization. 4) Numerical performance of the L^2- and H^1-based optimization with NCG and BFGS schemes and with the Newton method resulting from an Hessian including only the regularization term. 5) Discussion on reduced space minimization procedures (a natural choice in the physics community) considered as alternative or complementary to the adjoint approach.

In the next section, we discuss the formulation of the optimal control of the transport of Bose–Einstein condensates and consider two possible choices of the functional space where necessary first-order optimality conditions are formulated, the L^2 and H^1 spaces. For each of these two choices there results a coupled system of two nonlinear Schrödinger equations, with opposite time orientation, and an equation for the control. These are the so-called state and adjoint equations and the optimality condition. Sequential solution of these equations provides the gradient in the appropriate space. The notion of the gradient is used in Section 2.3 where we define the Hager–Zhang NCG scheme and the BFGS scheme in a general functional space. The choice of line-search method is discussed and we investigate the influence of discretization errors on the globalization step. To formulate a cascadic BFGS scheme

we consider interpolating the BFGS state history along iterations thus obtaining an improvement in efficiency with respect to the one-grid approach. This is the first step towards the formulation of a multilevel BFGS scheme.

To solve the nonlinear optimality system, we proceed in Section 2.4 by introducing a time-splitting spectral discretization [44, 45] adapted to the resulting state and adjoint equations and use finite differences to discretize the optimality condition. Thus we obtain second-order accuracy in time-discretization and spectral accuracy in space.

In Section 2.5 results of numerical experiments are reported to compare the computational performance of the solution strategies resulting from two distinct functional analytical settings. The BFGS scheme can require twice as much CPU time to reduce the cost functional to a specified value as the NCG scheme, however, with similar computational effort the BFGS scheme may solve the control problem to a degree of accuracy of at least one order of magnitude better than the NCG scheme can do. Furthermore within each computational scheme, minimization in the H^1-based formulation allows to attain the same tolerance for the norm of the gradient in one order of magnitude less of CPU time. In addition, we obtain that the H^1-based minimization is more robust with respect to changes of value of the weight of the cost of the control. That is, we obtain a dramatic increase in performance and robustness when we move from L^2- to H^1-based optimization. We also compare the H^1- based BFGS scheme with the Newton method resulting from an Hessian including only the regularization term. We show that the former outperforms the latter and this fact becomes even more evident as the discretization is refined and the nonlinearity of the Gross–Pitaevskii equation increased.

An important aspect of quantum control problems is that they may possess many local minima. This fact becomes evident comparing solutions obtained with the L^2- and the H^1-based optimization. Now, a possible way to (statistically) explore the

space of solutions is to construct reduced control spaces and for this purpose one needs a robust and efficient optimization scheme like the cascadic H^1-based BFGS method that allows to consider a large range of problems and optimization parameters. The discussion on the construction of reduced control spaces is presented in Section 2.6 where we consider direct minimization with polynomial basis functions without the need of introducing the adjoint equation and optimization with an explicit construction of the gradient. A link between adjoint formulation and direct minimization is given by discussing direct minimization on a POD basis determined through the adjoint formulation. We obtain that the adjoint formulation is more robust and accurate and point out the limitation of the reduced control space approach depending on the choice of parameters.

A section of conclusion completes the exposition of our work.

2.2 Quantum optimal control problems

Recently, quantum optimal control of transport of Bose–Einstein condensates in magnetic microtraps was proposed [58] to solve the problem first considered in [54] for a trapped-atom interferometer setup where a dilute Bose–Einstein condensate should be split from a single to a double well ground state. A Bose–Einstein condensate is a state of matter formed by bosons (e.g., helium-4, rubidium) cooled to temperatures very near to absolute zero. Under such conditions, the atoms with magnetic spin collapse into the lowest quantum state sharing the same wavefunction, and quantum effects become apparent on a macroscopic scale. Coherent manipulation of this wavefunction, as the splitting mentioned above, is one of the ultimate goals of modern atom optics, and it is a promising approach towards full control of matter waves on small scales; see [49, 50, 54, 55, 51], and references therein.

The mean-field dynamics of a coherent Bose–Einstein condensate is described by

the Gross–Pitaevskii equation [48]

$$i\frac{\partial}{\partial t}\,\psi(x,t) = \left(-\frac{1}{2}\nabla^2 + V_\lambda(x,t) + g\,|\psi(x,t)|^2\right)\psi(x,t), \tag{2.1}$$

where $x \in \Omega$ and $t \in [0,T]$, with g a coupling constant related to the scattering length of the atoms, density, and transversal confinement. We set $\hbar = 1$, and measure mass in units of the atom mass and length in units of micrometers. We assume that the quantum state wavefunction $\psi(x,t)$ is normalized to one $\int_\Omega |\psi(x,t)|^2 dx = 1$, $t \geq 0$, and therefore g in (2.1) incorporates the number of atoms N_A. Alternatively as in, e.g., [48], we could choose to normalize the wavefunction to N_A in the condensates, then g represents only the strength of interatomic interaction.

Notice that, in principle, the evolution of the Bose–Einstein condensate is defined in unbounded spaces while the fact that V is a confinement potential results in a wavefunction ψ whose support is localized in a bounded region. Therefore, with Ω we represent a spatial domain that is large enough to represent the support of ψ during evolution and we use periodic boundary conditions.

We consider confining potentials $V_\lambda(x,t) = V(x,\lambda(t))$ that are produced by magnetic microtraps whose variation is described by a control function $\lambda(t)$. We assume that $\lambda(t)$ is real and single-valued. We treat the case typical in experimental settings where the initial and final potential configuration are given, therefore we require that $\lambda(t)$ takes initial and final values of zero and one, respectively. These two extremal values correspond to the case where the potential $V_\lambda(x,t)$ is convex and to the case where it has a double well structure. Furthermore we require that V_λ is spatially symmetric with respect to the origin of coordinates $V_\lambda(x,t) = V_\lambda(-x,t)$ and $V_\lambda(x,\cdot) \in C^2(\Omega)$, and assume that V_λ is twice continuously differentiable in λ.

Suppose that initially the system is in the ground state ψ_0 for the potential $V(x,\lambda)|_{\lambda=0}$. Upon varying $\lambda(t)$ in the time interval $t \in [0,T]$ from zero to one, the system will pass through a sequence of states and will end up in the final state $\psi(T)$.

Our purpose is to determine an optimal time evolution of $\lambda(t)$ that allows to channel the system from the initial state ψ_0 at time zero to a desired state ψ_d at final time T. In accordance to [54], we assume ψ_d to be the ground state for the potential $V(x,\lambda)|_{\lambda=1}$ at time T. The ground state for a given potential $V(x,\lambda)$ is defined as the stationary state $\phi(x)$ with $\int_\Omega |\phi(x)|^2 dx = 1$ that minimizes the energy [43]

$$E_\lambda(\phi) = \int_\Omega \left(\frac{1}{2} |\nabla \phi(x)|^2 + V_\lambda(x) \, |\phi(x)|^2 + \frac{g}{2} \, |\phi(x)|^4 \right) dx. \tag{2.2}$$

We choose the control potential proposed in [60] to create condensates of trapped atoms coupled with a radio-frequency fields. We have that

$$V(x,\lambda) = -\frac{\lambda^2 \, d^2}{8c} \, x^2 + \frac{1}{c} \, x^4, \tag{2.3}$$

where $c = 40$ and d is a parameter corresponding to twice the distance of the two minima in the double well potential. The stationary state wavefunctions for the initial and final potentials are depicted for weak and strong nonlinearity in figure 2.1.

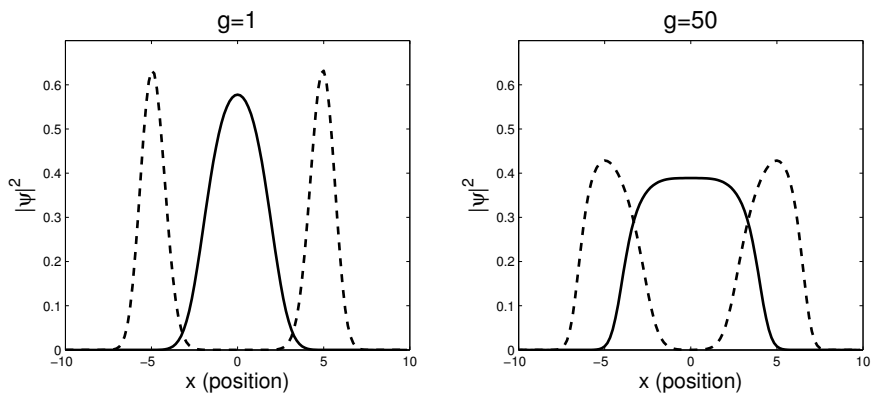

Figure 2.1: Stationary solutions of the Gross-Pitaevskii equation for nonlinearity strength $g = 1$ and $g = 50$ The initial state ψ_0 is shown in solid line and the target state ψ_d is represented by the dashed line.

For our purpose, in order to define a well-defined control problem, we consider the following cost functional [58]

$$J(\psi,\lambda) = \frac{1}{2}\big(1 - \big|\langle\psi_d, \psi(T)\rangle\big|^2\big) + \frac{\gamma}{2}\int_0^T \left(\dot{\lambda}(t)\right)^2 dt \tag{2.4}$$

with $\langle u, v\rangle = \int_\Omega u(x)^* v(x)\, dx$ the usual inner product in complex spaces, where the $*$ denotes complex conjugate, and $\|u\| = \langle u, u\rangle^{1/2}$.

The goal of the first term of the cost functional is to track the state ψ to a given terminal state ψ_d at $t = T$. Exact tracking would result in $\big|\langle\psi_d, \psi(T)\rangle\big|^2 = 1$. This choice of the form of the functional is different than the one given by $\frac{1}{2}\|\psi(T) - \psi_d\|^2$ as used in, e.g., [8]. In fact, in (2.4), the final wavefunction is required to match the desired target function only up to a global phase $e^{i\varphi T}$ which cannot be specified. That is, we are free to specify the target function up to a phase shift.

The second term in the cost functional represents H^1 costs and aims at penalizing fast varying confinement potentials that are more difficult to realize in real experiments. This regularization term ensures existence of at least one optimal control. The regularization parameter $\gamma > 0$ allows to vary the relative importance of the objectives represented by the tracking and the cost of control.

The control problem under consideration is therefore to minimize $J(\psi, \lambda)$ subject to the condition that $\psi(x, t)$ fulfills the Gross–Pitaevskii equation (2.1) with given initial conditions.

To solve this problem we introduce the Lagrange function

$$L(\psi, p, \lambda) = J(\psi, \lambda) + \Re e\left(p\,\Big|\, i\dot{\psi} - \left(-\frac{1}{2}\nabla^2 + V_\lambda + g|\psi|^2\right)\psi\right), \tag{2.5}$$

with $(u|v) = \int_0^T \int_\Omega u(x,t)^*\, v(x,t) dx\, dt$, and $p(x, t)$ is the Lagrange multiplier.

By formally equating to zero the Frechét derivatives of L with respect to the triple (ψ, p, λ), we obtain the following optimality system characterizing the solution

to our optimal control problem. We have

$$i\frac{\partial \psi}{\partial t} = \left(-\frac{1}{2}\nabla^2 + V_\lambda + g|\psi|^2\right)\psi \tag{2.6}$$

$$i\frac{\partial p}{\partial t} = \left(-\frac{1}{2}\nabla^2 + V_\lambda + 2g|\psi|^2\right)p + g\,\psi^2\,p^* \tag{2.7}$$

$$\gamma\,\frac{d^2\lambda}{dt^2} = -\Re e\langle\psi,\,\frac{\partial V_\lambda}{\partial \lambda}\,p\rangle\,, \tag{2.8}$$

which has to be solved together with the initial and terminal conditions

$$\psi(0) = \psi_0 \tag{2.9}$$

$$ip(T) = -\langle\psi_d, \psi(T)\rangle\,\psi_d \tag{2.10}$$

$$\lambda(0) = 0\,, \quad \lambda(T) = 1. \tag{2.11}$$

Equation (2.10) follows from computing time integration by parts to determine the Frechét derivative with respect to the variable ψ. Notice that while the state equation (2.6) with initial condition $\psi(0) = \psi_0$ evolves forward in time, the adjoint equation (2.7) with terminal condition (2.10) is marching backwards. The control equation (2.8) provides the optimality condition that determines the optimal control. Because of H^1 regularization we have a natural setting to impose the required Dirichlet boundary conditions on the control function, $\lambda(0) = 0$ and $\lambda(T) = 1$.

We have that (2.6) is uniquely solvable for every $\lambda \in H^1(0,T;\mathbb{R})$ such that V_λ is a symmetric double well potential; see [61]. Thus, it is meaningful to introduce the so-called reduced cost functional $\hat{J} : H^1(0,T;\mathbb{R}) \to \mathbb{R}$ given by

$$\hat{J}(\lambda) = J(\psi(\lambda), \lambda), \tag{2.12}$$

where $\psi(\lambda)$ denotes the unique solution to (2.6) for given λ. One can show that the gradient of $\hat{J}$ with respect to λ is given by

$$\nabla\hat{J}(\lambda) = -\gamma\,\frac{d^2\lambda}{dt^2} - \Re e\langle\psi,\,\frac{\partial V_\lambda}{\partial \lambda}\,p\rangle, \tag{2.13}$$

where ψ and p solve the state and the adjoint equations with given λ.

Now, the Taylor series of the reduced cost functional $\hat{J}(\lambda)$ in a Hilbert space is

$$\hat{J}(\lambda + \epsilon\varphi) = \hat{J}(\lambda) + \epsilon \left(\nabla \hat{J}(\lambda), \varphi\right)_X + \frac{\epsilon^2}{2} \left([\nabla^2 \hat{J}(\lambda)]\varphi, \varphi\right)_X + O(\epsilon^3)$$

The actual gradient will depend on the choice of which inner product space we use. If we choose the space $X = L^2(0, T; \mathbb{R})$, we have the inner product $(u, v) = \int_0^T u(t)v(t)dt$ and the gradient is

$$\nabla \hat{J}(\lambda) = -\gamma \frac{d^2\lambda}{dt^2} - \Re e\langle \psi, \frac{\partial V_\lambda}{\partial \lambda} p\rangle \tag{2.14}$$

In the case of the $X = H^1(0, T; \mathbb{R})$ formulation, we can determine the formula for the gradient because the Taylor series must be identical term-by-term regardless of the choice of X. Since we know the gradient in L^2 given by (2.14), we can determine the gradient in H^1 by requiring

$$\left(\nabla \hat{J}_{H^1}(\lambda), \varphi\right)_{H^1} = \left(\nabla \hat{J}_{L^2}(\lambda), \varphi\right)_{L^2}$$

Using the definition of the H^1 inner product $(u, v)_{H^1} = (u', v')_{L^2}$, we have the relation

$$\left(\nabla \hat{J}'_{H^1}(\lambda), \varphi'\right)_{L^2} = \left(\nabla \hat{J}_{L^2}(\lambda), \varphi\right)_{L^2}$$

which must hold for all test functions φ. Integrating by parts shows that the H^1 gradient must satisfy the one-dimensional Poisson equation with homogeneous Dirichlet conditions. That is,

$$\frac{d^2}{dt^2}[\nabla \hat{J}(\lambda)] = \gamma \frac{d^2\lambda}{dt^2} + \Re e\langle \psi, \frac{\partial V_\lambda}{\partial \lambda} p\rangle, \tag{2.15}$$

with $[\nabla \hat{J}(\lambda)](0) = 0$ and $[\nabla \hat{J}(\lambda)](T) = 0$. Two important differences between the L^2 and H^1 formulations are immediately apparent. First, the L^2 gradient does not vanish at $t = T$ and second, the H^1 gradient possesses the same degree of smoothness as λ, while the L^2 gradient does not.

2.3 Optimization methods in L^2 and H^1 spaces

We discuss the minimization of $\hat{J}(\lambda)$, representing the reduced cost functional $J(\psi(\lambda), \lambda)$, where $\psi(\lambda)$ denotes the solution to the state equation (2.6). Denote with $g(\lambda) = \nabla \hat{J}(\lambda)$. In the following, we denote with X both the $L^2(0, T; \mathbb{R})$ and the $H^1(0, T; \mathbb{R})$ spaces with corresponding inner product $(\cdot, \cdot)_X$ and norm $\| \cdot \|_X$. The discussion below focuses on NCG and BFGS schemes in L^2 and H^1 spaces with application to quantum control problems. In the numerical experiments section we compare these schemes with the method of steepest descent with the H^1 form of the gradient. This scheme can be viewed as a Newton method where one only uses the Hessian arising from the regularization term. For a discussion on these techniques with an emphasis on implementation issues see [56].

We formulate the NCG scheme in a continuous setting. In the common NCG variants, the basic idea is to avoid matrix operations and express the search directions recursively as

$$d_{k+1} = -g_{k+1} + \beta_k \, d_k, \tag{2.16}$$

for $k = 1, 2, \ldots$, where k is the iteration index. We take $d_1 = -g_1$. In general, for convergence it is required that d_k is a descent direction for any k, i.e. $(g_k, d_k)_X < 0$ holds.

The iterates for a minimum point are given by

$$\lambda_{k+1} = \lambda_k + \tau_k \, d_k, \tag{2.17}$$

where $\tau_k > 0$ is a step length. The parameter β_k is chosen so that (2.16)–(2.17) reduces to the linear CG scheme if $\hat{J}$ is a strictly convex quadratic function and τ_k is the exact one-dimensional minimizer of $\hat{J}$ along d_k. Notice that linesearch is important: In the first application of the NCG scheme on quantum control problems

[66], a NCG method with a special rule concerning the value of step length results in an algorithm that is not always robust and convergence slow-down can be observed.

We use the NCG scheme of Hager and Zhang [53] based on the formula

$$\beta_k = \beta_k^{HZ} := \frac{(\sigma_k, g_{k+1})_X}{(d_k, y_k)_X}, \qquad \sigma_k = y_k - 2d_k \frac{(y_k, y_k)_X}{(y_k, d_k)_X}, \tag{2.18}$$

where $y_k = g_{k+1} - g_k$. Our choice is motivated by results of numerical experiments. In fact, the Hager-Zhang NCG formula results to be the most efficient among the known [29] formulas.

Convergence of the proposed NCG scheme is established requiring that the step length τ_k, satisfies the Armijo condition of sufficient decrease of $\hat{J}$'s value given by

$$\hat{J}(\lambda_k + \tau_k d_k) \leq \hat{J}(\lambda_k) + \delta\, \tau_k\, (g_k, d_k)_X \tag{2.19}$$

together with the Wolfe condition

$$(g(\lambda_k + \tau_k d_k), d_k)_X > \sigma\, (g_k, d_k)_X, \tag{2.20}$$

where $0 < \delta < \sigma < 1/2$; see [29]. The last condition means that the graph of $\hat{J}$ should not increase too fast beyond the minimum.

We implement the following NCG scheme

NCG Scheme *Step 1.* Given $k = 1$, λ_1, $d_1 = -g_1$, if $\|g_1\|_X < tol$ then stop. *Step 2.* Compute $\tau_k > 0$ satisfying (2.19)–(2.20). *Step 3.* Let $\lambda_{k+1} = \lambda_k + \tau_k\, d_k$. *Step 4.* Compute $g_{k+1} = \nabla \hat{J}(\lambda_{k+1})$. If $\|g_{k+1}\|_X < tol_{abs}$ or $\|g_{k+1}\|_X < tol_{rel}\, \|g_1\|_X$ or $k = k_{\max}$ then stop. *Step 5.* Compute β_k by (2.18). *Step 6.* Let $d_{k+1} = -g_{k+1} + \beta_k\, d_k$. *Step 7.* Set $k = k + 1$, goto Step 2.

Time dependent quantum control problems represent a class of PDE-constrained minimization problems where much less experience of computational optimization is available. In the following, we discuss function space BFGS optimization that uses only gradient information and whose performance is strictly depending on the choice of the space where the optimization procedure is defined.

The BFGS algorithm is a quasi-Newton method which makes successive rank-two updates to a matrix B such that it serves as an approximation to the true Hessian. Typically, the BFGS scheme exhibits convergence rates superior to those of NCG schemes at the expense of additional computational effort. The search direction at the kth step is given by $p_k = -B_k^{-1} g_k$. Just as with the HZ-NCG scheme, the gradient is denoted $g_k = \nabla \hat{J}(\lambda_k)$ and the difference between two successive updates of λ is $s_k = \alpha_k p_k$ where α_k is the step length. The difference between two successive gradients is dented by $y_k = g_{k+1} - g_k$. The matrix B can be formed explicitly via the well-known recurrence formula.

$$B_{k+1} = B_k - \frac{(B_k s_k)(B_k s_k)^\top}{s_k^\top B_k s_k} + \frac{y_k y_k^\top}{y_k^\top s_k}, \tag{2.21}$$

To compute the search direction, it is necessary to invert the matrix B. We denote its inverse as $H = B^{-1}$. Using the Sherman-Morrison-Woodbury formula, we can also establish a recurrence for H.

$$H_{k+1} = H_k + \frac{s_k^\top y_k + y_k^\top H_k y_k}{(s_k^\top y_k)^2}(s_k s_k^\top) - \frac{H_k y_k s_k^\top + s_k y_k^\top H_k}{s_k^\top y_k} \tag{2.22}$$

In the case where the control λ and the gradient of the objective function $\nabla \hat{J}$ are elements in a function space, it is not immediately obvious how to directly use this formula since it requires forming outer products. To compute the search direction, however, we only need the action of H on a vector g and it is not necessary to construct the matrix. Supposing X is either $L^2(0, T; \mathbb{R})$ or $H^1(0, T; \mathbb{R})$ and that x, $y \in X$, then we can denote the function space analog of the outer product as a

dyadic operator $x \otimes y : X \to X$. The action of this operator on a third element $z \in X$ can be expressed in terms of the inner product $(x \otimes y)z = (y, z)_X x$. From the recursion relation for H, we obtain the following sum formula for the search direction

$$p_k = -H_0 g_k - \sum_{j=0}^{k-1} c_j [d_j (s_j, g_k)_X s_j - (z_j, g_k)_X s_j - (s_j, g_k)_X z_j] \tag{2.23}$$

where $c_j = (s_j, y_j)_X^{-1}$, $d_j = 1 + c_j (y_j, z_j)$ and we also have a similar sum formula for the term $z_k = H_k y_k$.

$$z_k = H_0 y_k + \sum_{j=0}^{k-1} c_j \left\{ [d_j (s_j, y_k)_X - (z_j, y_k)_X] s_j - (s_j, y_k)_X z_j \right\}. \tag{2.24}$$

In the numerical implementation, these functions are approximated on a uniform grid. The function space L^2 or H^1 inner product is in either case approximated by a vector inner product with a weighting matrix. This can be written as $(u, v)_{L^2} \approx u^\top M v$ and $(u, v)_{H^1} \approx u^\top K v$ where the stiffness matrix $K = D^\top M D$. The finite difference matrix D is Toeplitz tridiagonal for taking centered differences except for the first and the last rows which use non-centered differences to account for the boundary. The mass matrix M is diagonal and contains the quadrature weights for the composite Simpson's rule. If the PDE itself were to be discretized with a higher order scheme, then it would be desirable to use correspondingly higher order quadrature and differentiation rules for the inner products. In all numerical tests, M was taken to be the identity matrix.

With both the NCG and BFGS schemes, the new control λ_{k+1} is composed of a linear combination of the original control and the gradients at every step. Unlike the NCG formulas, the matrix-free BFGS formula requires progressively more computation for each optimization step, so it is important that the improved convergence properties at least compensate for the increased computational effort. The BFGS algorithm is given below.

BFGS Scheme *Step 1.* Take a steepest descent step. *Step 2.* Let $y_k = g_k - g_{k-1}$ and $s_k = \alpha_k p_k$ *Step 3.* if $|(s_k, y_k)_X| < \epsilon$ or $||g_k||_X < tol$ stop. *Step 4.* Compute new search direction $p_k = -H_k g_k$ using (2.23). *Step 5.* Perform linesearch to get new α_k. If no descent step is found, stop. *Step 6.* Increment k and go to Step 2.

Previous experience in quantum control computation [7] has demonstrated that cascadic acceleration is an efficient method to accelerate convergence of NCG iteration. In this paper, we show that this is also true in combination with a BFGS algorithm.

The basic approach of the cascadic method is to begin with a coarse grid approximation to the optimal control problem, take a suitable number of optimization steps and then interpolate on to a finer grid before proceeding.

In the case of NCG, the computation of the next state depends only on the previous state and as such, one need only interpolate the current state and search direction to proceed to the next level of refinement. In the matrix-free BFGS algorithm, a history of vectors must be maintained. These are the s_j vectors which are the search steps themselves, the y_j which are the differences between successive gradients, and also the z_j vectors which are elements in the space spanned by $s_0, ..., s_{j-1}$. The set of these vectors, which increases with successive BFGS steps, must each be interpolated on to the next finest grid in the cascadic scheme. In all of the numerical experiments, cubic splines are used rather than linear interpolation because the latter is not suitable for use with the H^1 norm.

We now discuss the linesearch algorithm. We are faced with the following difficulty. First, using a large step length α at the beginning of a backtracking sweep is dangerous. In fact, large control potentials may result that lead to highly oscillatory wave functions such that the cost functional and its gradient can cease to be

Cascadic BFGS Scheme *Step 1.* If on the finest grid, proceed with BFGS minimization until unable
to take another descent step otherwise go to Step 2.
Step 2. Letting the current state be λ_k, back up one iteration to the last state from which a suitable search length was found.
Step 3. Interpolate the λ_{k-1} and all of the history vectors s_j, y_j, and z_j for $j = 0...k-1$.on to the next finer grid.
Step 4. Go to step 2, using the most recent s vector as a search direction.

physically meaningful or the discretization fineness is not accurate enough to resolve all scales of the problem. As shown in Figure 2.2, spurious local minima may appear along the search direction. However, as minimization proceeds, the objective becomes more flat and local minima are no longer present. Moreover, in our experiments the global minimum along the search path always appears at a small step length, as can be seen in Figure 2.2. Therefore starting with a large α requires many backtrack evaluations and a backtrack algorithm may be trapped in some local minimum away from the global one. On the other hand, starting a backtracking sweep with small α will be at the cost of an efficient linesearch process.

To overcome these difficulties we implement a robust bisection approach, that uses approximate finite-differences derivatives of the objective function with respect to the step length.

Although there were almost always multiple local minima along the search direction, it appeared that the global minimum was always the nearest critical point to the origin in every numerical experiment. We do not know of any explanation to this phenomena at this time. As such, the bisection algorithm always attains the global minimum along the search direction. The parameters m, δ used were chosen based on empirical studies. One suitable pair of values was found to be $\delta = 0.01$ and

$m = 1.1$. We choose $tol_{BLS} = 10^{-6}$.

In the bisection scheme, the use of the numerical derivative of the linesearch function $\phi(\alpha) = \hat{J}(\lambda + \alpha p)$ instead of the functional derivative is motivated by results given in [47] and the fact that, along a given search direction, it requires fewer functional evaluations. In [47], it is shown that away from the global minimum the numerical derivative remains consistent with the behavior of the functional along the search direction while the functional derivative may be inconsistent, e.g., negative for an increasing functional value. The difference between the two derivatives reflects the difference between the discretize-then-optimize approach and the optimize-then-discretize approach. This difference results in an error denoted by $E(\epsilon, \varphi)$ and defined as follows

$$E(\epsilon, \varphi) = \left| \frac{\hat{J}(\lambda + \epsilon\varphi) - \hat{J}(\lambda - \epsilon\varphi)}{2\epsilon} - \left(\varphi, \nabla \hat{J}(\lambda)\right)_X \right| \tag{2.25}$$

where φ represents the search direction. The behavior of this error with respect to α and the mesh fineness is seen in the right panel of Figure 2.2. Notice that the search direction in the bisection scheme is always provided by the functional gradient since the quantum optimal control problem is well resolved in the vicinity of the minimizer (see also [47]).

We remark that choosing ϵ sufficiently small, $E(\epsilon, \varphi)$ becomes independent on ϵ and this error scales quadratically with the time-step size, δt. This is consistent with the order of the split operator of the time-stepping scheme.

No restarting was used in either of the BFGS schemes, however, the HZ-NCG scheme was restarted whenever $(g_k, g_{k-1}) \geq 0.1||g_k||^2$. The stopping condition was taken to be the first iteration in which the linesearch was unable to find a step length which reduces the objective function.

Bisection linesearch (BLS) algorithm

Step 1. Set $\alpha_L = 0,\ \alpha_R = 0$.

Step 2. If $\phi(\alpha_R) > \phi(0)$ go to Step 4

Step 3. If $\phi(\alpha_R) < \phi(0)$ set $\alpha_R \leftarrow m\,(\alpha_R + \delta)$ and go to Step 2.

Step 4. Set α_M as the midpoint between α_L and α_R.

Step 5. If the distance between α_L and α_R is less than tol_{BLS} quit.

Step 6. If $\phi'(\alpha_M)$ has the same sign as $\phi'(\alpha_L)$ set $\alpha_L = \alpha_M$ otherwise set $\alpha_R = \alpha_M$.

Step 7. Go to Step 4.

2.4 Discretization method

In this section, we discuss the discretization of (2.6) and (2.7) using a unconditionally stable explicit second-order norm-preserving time-splitting spectral scheme (TSSP) [45, 44]. These properties make the TSSP scheme particularly suitable for computation on a hierarchy of grids. To introduce the time-splitting technique and the corresponding notation we discuss the discretization of the forward equation. For the backward adjoint equation additional work is required to implement the time-splitting method appropriately. This is due to the presence of the term $g\,\psi^2\,p^*$ in the adjoint equation. This problem is discussed in detail below.

For ease of notation we take $\Omega = (-L/2, L/2) \subset \mathbb{R}$ where L is large enough so that the support of the state and adjoint variables are well within the domain. Assume the interval $(-L/2, L/2)$ is divided in N subintervals of size $h = L/N$. In all of the numerical experiments, $N = 128$ was used and it was found that increased spatial resolution did not contribute to increased performance as the time discretization was always the limiting factor. Subinterval end-points are denoted by $x_j = (j - 1)\,h - L/2$, $j = 1, \ldots, N$, where we take N to be an integer power of 2. The point x_{N+1} corresponds to $x = L/2$. Further we assume that the time interval $(0, T)$

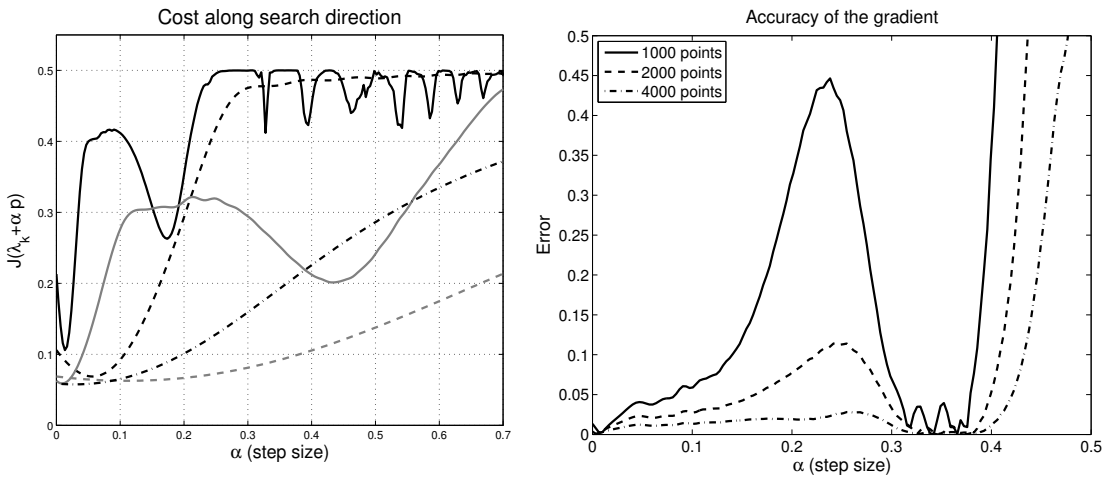

Figure 2.2: The cost functional along the search direction for successive descent steps (left). Error $E(\epsilon, h)$ for different mesh fineness and different step length (right). We use a 5-point centered difference of $\hat{J}$ with $\epsilon = 10^{-4}$ and a test function. We have $T = 7.5$, $g = 10$, and $\gamma = 10^{-7}$.

is divided in M subintervals thus the time step-size is given by $\delta t = T/M$. The approximation to $\psi(x,t)$ at x_j for the time $t_m = m\,\delta t$ is denoted with ψ_j^m. We set $\mu_k = \frac{2\pi}{L}k$. We assume that the function ψ is periodic in $(-L/2, L/2)$ in the sense that $\psi(-L/2^+) = \psi(L/2^-)$.

For a given continuous periodic function ψ, consider the polynomial

$$I_N\psi(x) = \sum_{k=-\lfloor \frac{N}{2}-1 \rfloor}^{\frac{N}{2}} \tilde{\psi}_k\, e^{i\mu_k x}, \tag{2.26}$$

where

$$\tilde{\psi}_k = \frac{1}{N}\sum_{j=1}^{N} \psi(x_j)\, e^{-i\,\mu_k x_j} \qquad \text{with} \quad x_j = (j-1)\,h - L/2. \tag{2.27}$$

The function $I_N\psi(x)$ is the $\frac{N}{2}$-degree trigonometric interpolant of ψ at the nodes x_j, i.e.

$$I_N\psi(x_j) = \psi(x_j) \qquad j = 1, \ldots, N. \tag{2.28}$$

This polynomial is the discrete Fourier series of ψ.

The Fourier pseudospectral derivative of ψ is defined by $D_N\psi = (I_N\psi)'$. That is,

$$D_N\psi(x) = \sum_{k=-\left(\frac{N}{2}-1\right)}^{\frac{N}{2}} \tilde{\psi}'_k\, e^{i\,\mu_k x} \qquad \text{where} \qquad \tilde{\psi}'_k = i\mu_k\tilde{\psi}_k.$$

Further, the Laplacian is given by

$$D_N^2\psi(x) = \sum_{k=-\left(\frac{N}{2}-1\right)}^{\frac{N}{2}} \tilde{\psi}''_k\, e^{i\mu_k x} \qquad \text{where} \qquad \tilde{\psi}''_k = -\mu_k^2\tilde{\psi}_k.$$

Now let $H = H_0 + V$, where $H_0 = -\frac{1}{2}\nabla^2$ is the free Hamiltonian and $V = V_\lambda + g|\psi|^2$ represents the effective potential including the magnetic confinement potential. Next we illustrate the time-splitting spectral scheme for the Gross–Pitaevskii equation written as follows; see [44] for more details.

$$i\frac{\partial\psi}{\partial t} = (H_0 + V)\,\psi.$$

The time-splitting scheme for this equation can formally be written in the following form

$$\psi^{m+1} = e^{-i\frac{\delta t}{2}V^{m+1}} e^{-i\delta t\,H_0} e^{-i\frac{\delta t}{2}V^m}\,\psi^m. \tag{2.29}$$

From time t_m to time t_{m+1} we have three steps. For a $\delta t/2$ time step we first solve

$$i\frac{\partial\psi}{\partial t} = V\,\psi.$$

For $j = 1, \ldots, N$, we obtain

$$\psi_j^+ = \exp\left(-i(V_\lambda(x_j, t_m) + g|\psi_j^m|^2)\,\delta t/2\right)\,\psi_j^m. \tag{2.30}$$

With this value, we compute a full time step for the equation $i\frac{\partial\psi}{\partial t} = H_0\,\psi$ obtaining

$$\psi_j^{++} = \sum_{k=-\left(\frac{N}{2}-1\right)}^{\frac{N}{2}} \tilde{\psi}_k^+\, e^{\left(-i\mu_k^2\,\delta t/2\right)}\, e^{i\mu_k x_j}, \qquad j = 1, \ldots, N, \tag{2.31}$$

where

$$\tilde{\psi}_k^+ = \frac{1}{N}\sum_{j=1}^{N} \psi_j^+ \, e^{-i\,\mu_k x_j}.$$

The final step consists in another $\delta t/2$ time step of the evolution governed by V with ψ^{++} as initial condition. Hence we have

$$\psi_j^{m+1} = \exp\left(-i(V_\lambda(x_j, t_{m+1}) + g|\psi_j^{++}|^2)\,\delta t/2\right)\psi_j^{++}, \qquad j = 1, \ldots, N. \tag{2.32}$$

Additional work is required to implement the time-splitting scheme for the adjoint equation (2.7) because of the presence of the term $g\,\psi^2\,p^*$ that prevents a straightforward application of an exponential solution formula. We proceed as follows. The adjoint equation can be written in the following form

$$i\frac{\partial}{\partial t}(p_r + i\,p_i) = \left(-\frac{1}{2}\nabla^2 + A\right)\,(p_r + i\,p_i) + (a_r + i\,a_i)\,(p_r - i\,p_i),$$

where $p = p_r + i\,p_i$, $A = V_\lambda + 2g|\psi|^2$, and $g\,\psi^2 = a_r + i\,a_i$. We focus on the first and third step of the time-splitting formula and therefore we consider

$$\frac{d}{dt}(p_r + i\,p_i) = -iA\,(p_r + i\,p_i) - i(a_r + i\,a_i)\,(p_r - i\,p_i).$$

This equation is equivalent to the following system of differential equations

$$\dot{p}_r = Ap_i + (a_i p_r - a_r p_i) \tag{2.33}$$

$$\dot{p}_i = -Ap_r - (a_r p_r + a_i p_i). \tag{2.34}$$

We now introduce the Pauli matrices to write this system in a form suitable for exponential representation. The Pauli matrices are

$$\sigma_1 = \begin{pmatrix} 0 & 1 \\ 1 & 0 \end{pmatrix}, \qquad \sigma_2 = \begin{pmatrix} 0 & -i \\ i & 0 \end{pmatrix}, \quad \text{and} \quad \sigma_3 = \begin{pmatrix} 1 & 0 \\ 0 & -1 \end{pmatrix},$$

and we write $\bar{\sigma} = (\sigma_1, \sigma_2, \sigma_3)$.

Therefore the system (2.33)–(2.34) can be written as follows

$$\frac{d}{dt}\begin{pmatrix} p_r \\ p_i \end{pmatrix} = i(\bar{u}\cdot\bar{\sigma})\begin{pmatrix} p_r \\ p_i \end{pmatrix},$$

where $\bar{u} = (ia_r, A, -ia_i)$. We can now use the exponential representation to obtain

$$\begin{pmatrix} p_r \\ p_i \end{pmatrix}(t+\delta t) = \exp\left(i\,\bar{u}\cdot\bar{\sigma}\,\delta t\right)\begin{pmatrix} p_r \\ p_i \end{pmatrix}(t). \tag{2.35}$$

Further, we use the fact that

$$\begin{aligned}\exp\left(i\,\bar{u}\cdot\bar{\sigma}\,\delta t\right) &= \cos\left(|\bar{u}|\,\delta t\right)\,I + i\,\sin\left(|\bar{u}|\,\delta t\right)\,\frac{\bar{u}}{|\bar{u}|}\cdot\bar{\sigma} \\ &= \cos\left(|\bar{u}|\,\delta t\right)\begin{pmatrix} 1 & 0 \\ 0 & 1 \end{pmatrix} + \sin\left(|\bar{u}|\,\delta t\right)\,\frac{1}{|\bar{u}|}\begin{pmatrix} a_i & A-a_r \\ -A-a_r & -a_i \end{pmatrix},\end{aligned}$$

where $|\bar{u}| = \sqrt{a_r^2 + a_i^2 + A^2}$. We can therefore use this formula in (2.35) and replace δt with $-\delta t/2$ to obtain the (backward) time evolution of the adjoint variable for the first and third step of the time-splitting procedure. Notice that in this case because of the terms A and a_r, a_i, also the values of the wavefunction ψ at intermediate half time-steps are required. For this purpose, the ψ function is also computed in the backward evolution using (2.30)–(2.32) with δt replaced by $-\delta t$. This is possible since the time-splitting scheme is time-reversible.

Evaluation of the gradient of the reduced cost functional is given by the following

$$\nabla\hat{J}(\lambda)^m = -\gamma\,\frac{\lambda^{m+1} - 2\lambda^m + \lambda^{m-1}}{\delta t^2} - \Re e\sum_{j=1}^{N} h\,(p_j^m)^*\,\frac{\partial V_\lambda}{\partial\lambda}|_{\lambda=\lambda^m}\,\psi_j^m.$$

The initial state $\psi(x,0)$ and the target state $\psi_d(x)$ are obtained by solving the stationary Gross-Pitaevksii equation $-\frac{1}{2}\nabla^2\psi + V\psi + g|\psi|^2\psi = 0$ with λ equal to zero or one respectively. The nonlinear problem is solved using Newton's method.

2.5 Numerical investigation

In this section we discuss the computational performance of the NCG scheme and of the BFGS scheme corresponding to the L^2 and H^1 functional space formulation. Results of numerical experiments show dramatic quantitative and qualitative differences concerning efficiency and robustness of the schemes discussed in this paper. Efficiency is measured in terms of CPU time taking into account that the optimization process may be stopped earlier because the scheme is not able to find an appropriate minimizing direction. Robustness concerns the ability of the scheme to provide a minimizing sequence also in the case of fast control, that is, short time horizon T, large nonlinearity, i.e. large g, and less penalization, that is, small γ.

Some of the results that are discussed in this section are summarized in Figure 2.3 that shows a series of optimal control curves corresponding to different time horizons, obtained by minimizing in the L^2 and H^1 spaces. We see that, as T becomes shorter, a more oscillatory optimal control results. Much less oscillating solutions are obtained with H^1 space minimization. Indeed we see that with the same setting, the controls obtained in the two functional space settings are different. These curves are obtained with a regularization parameter $\gamma = 10^{-4}$. More computational effort is required for short time horizons. In all experiments we use $N = 128$.

The influence of the regularization parameter γ on the solution of the optimization is shown in Figure 2.4 corresponding to L^2 and H^1 spaces. We see that γ plays an important role in the L^2-based optimization as it forces the solution to have a finite H^1 norm, while this will always be the case by construction with the H^1-based formulation. For either space, the optimal solution should approach the straight line as $\gamma \to \infty$ so it is reasonable that the optimal control curve for $\gamma = 1$ is very similar in both spaces. As γ is reduced however, the L^2 and H^1 solutions become quite different. In the L^2 space, the limit as $\gamma \to 0$ small gives a control function $\lambda(t)$

which has a steep gradient at $t = T$. On the other hand, since the H^1-based scheme produces $\lambda \in H^1$ at every optimization step, the precise value of regularization term is not essential to obtain a smooth control. Rather in this case the γ term only serves to penalize highly oscillatory solutions. In the limit as $\gamma \to 0$, the H^1-based solution approaches a smooth curve which gives a small cost functional. Since the theoretical lower bound on J is $\frac{\gamma}{2T}$ (assume $\psi(T) = \psi_d$ and $\lambda(t) = t/T$ which minimizes the H^1 norm), the smallest value of the cost functional occurs when $\gamma \approx 0$.

Figure 2.5 depicts how fast in terms of CPU time, the optimal control is attained for various values of γ. Since the γ penalty term sets a lower bound on the objective function, each curve will approach a different minimum value. For the H^1-based minimization, the performance curves rapidly converge to the $\gamma = 0$ limit for decreasing γ. Ultimately Figures 2.4 and 2.5 demonstrate that the H^1-based minimization is robust with respect to γ as the optimal control is always an H^1 function even when $\gamma = 0$.

The relative performance of the HZ-NCG, BFGS, and cascadic BFGS methods for the H^1-based minimization is depicted for long and short control times T in Figure 2.3 and for small and large nonlinearities in Figure 2.6. In each case, $M = 3200$ grid points were used and $\gamma = 10^{-4}$. Although the HZ-NCG method exhibits superior convergence properties for an NCG scheme, it does not minimize the cost functional as quickly as the BFGS methods do. When the nonlinearity becomes large or T becomes shorter, the optimal control function becomes more highly oscillatory and further away from the initial linear control function. Furthermore, the BFGS algorithm reaches the minimum in less computational time than the HZ-NCG method, and what is significant is that its advantage is greatest in the cases where the optimization problem is more difficult due to large nonlinearity or control time. The cascadic BFGS approach does not attain a minimum as small as the regular BFGS when the problem is easier. This is assumed to be due to the fact that interpolating

the state vectors which form the action of the H matrix leads to a worse approximation of H. However, in the difficult settings the cascadic BFGS method has a significant performance increase.

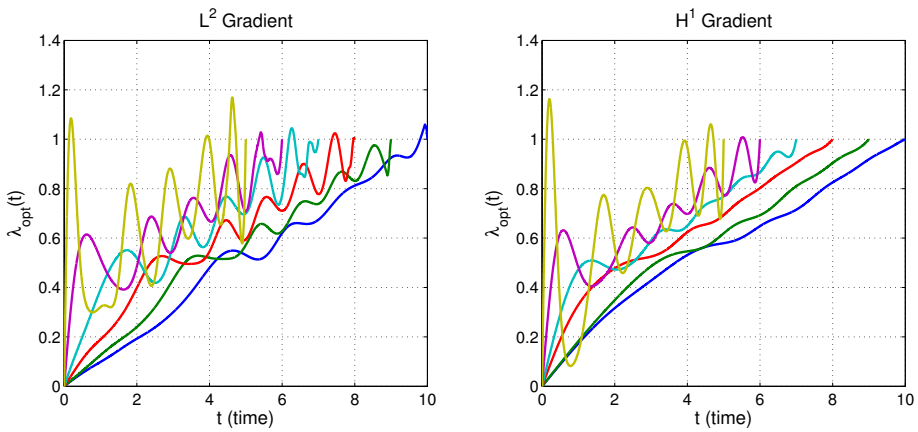

Figure 2.3: The optimal control function in the L^2 and H^1 settings for decreasing time horizons. As T becomes smaller, λ becomes a more oscillating function.

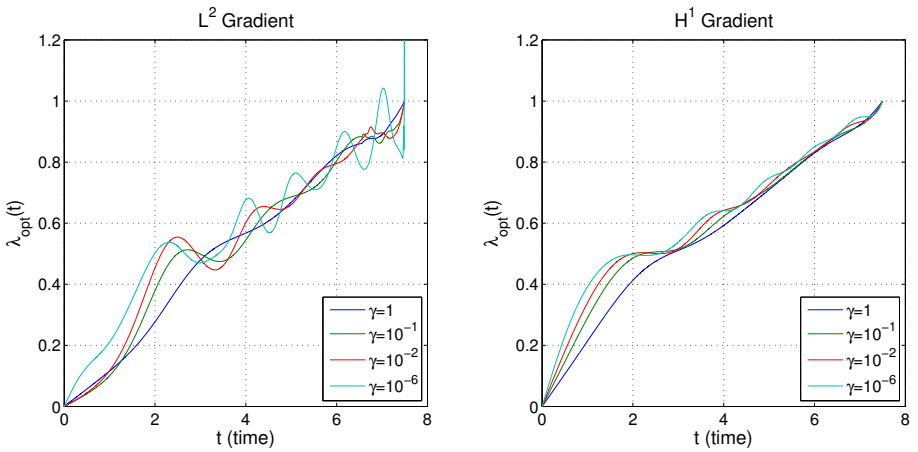

Figure 2.4: Dependence of the optimal control function on the regularization parameter γ for the L^2 and H^1 spaces. More oscillating controls are obtained with smaller γ. $M = 3200$ time steps with $g = 10$ and $T = 7.5$.

Additional results are reported in the Tables 2.1 – 2.5 that allow a more detailed discussion. Table 2.1 shows that, in the limiting case where the strength of the

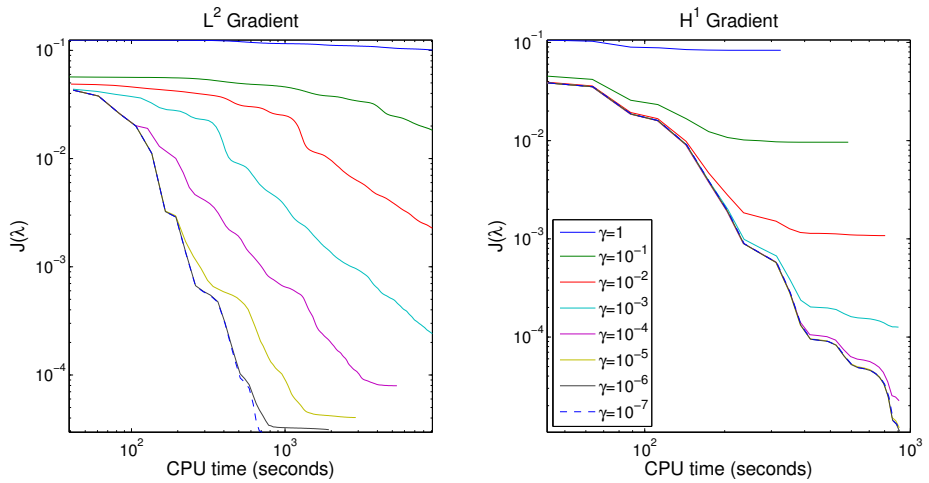

Figure 2.5: Effect of the regularization parameter, γ on the convergence in the L^2 and H^1 settings. Faster convergence is obtained with smaller γ.

nonlinearity is small, the accuracy of the gradient does indeed scale quadratically with respect to the time step size. The numerical error of the H^1 gradient is computed using the same test function $\varphi(t) = \sin(4\pi t/T)e^{-t/T}$ as before. The numerical error of the H^1 and L^2 gradients was observed to be similar. This is reasonable as the time discretization scheme has a quadratic error term, as do the numerical differentiation and integration formulas used to compute the inner products. As the nonlinearity becomes large, the quality of the gradient approximation deteriorates.

mesh	$g = 0.01$	$g = 1$	$g = 10$	$g = 100$
400	1.9836×10^{-4}	5.7461×10^{-3}	3.7687×10^{-2}	5.7021×10^{0}
800	5.1216×10^{-5}	1.4370×10^{-3}	1.2923×10^{-2}	5.5529×10^{-2}
1600	1.3005×10^{-5}	3.5915×10^{-4}	4.9711×10^{-3}	3.0740×10^{-2}
3200	3.2762×10^{-6}	8.9755×10^{-5}	2.1118×10^{-3}	1.7823×10^{-2}
6400	8.2191×10^{-7}	2.2427×10^{-5}	9.6235×10^{-4}	9.8638×10^{-3}

Table 2.1: Estimated numerical error of the gradient formula with $X = H^1$ for $T = 6$ and $\gamma = 10^{-4}$, for increasing mesh refinement and strength of the nonlinear term.

Tables 2.2 and 2.3 show the computational performance of the the HZ-NCG

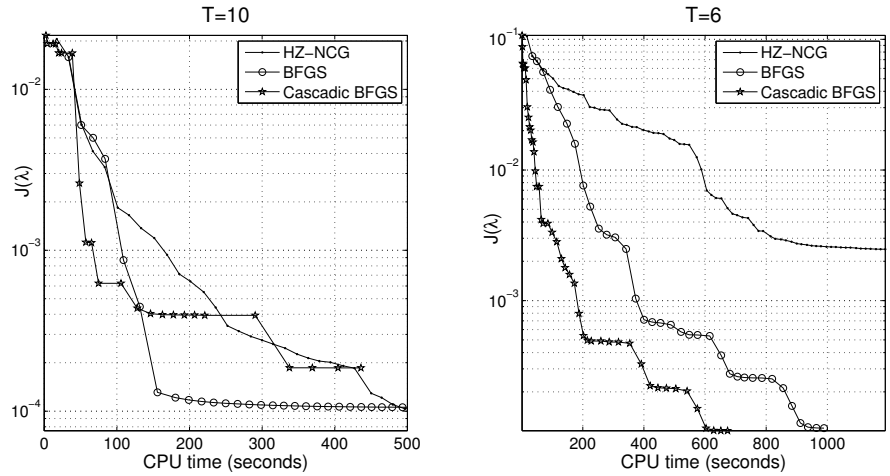

Figure 2.6: Reduction of cost function over CPU time using HZ-NCG, BFGS, and cascadic BFGS. The cascadic scheme gives superior performance for shorter time horizons.

mesh	$\hat{J}$	$\|\|\nabla\hat{J}\|\|_{L^2}$	iterations	CPU time (sec)
400	2.9676×10^{-3}	4.4182×10^{-2}	81	1.6271×10^{2}
800	1.6492×10^{-3}	2.113×10^{-2}	110	4.1789×10^{2}
1600	1.8103×10^{-3}	1.1400×10^{-2}	155	1.1932×10^{3}
3200	3.4755×10^{-3}	1.13815×10^{-1}	76	1.1985×10^{3}

Table 2.2: Results with L^2-based HZ-NCG minimization with g=10 and T=6.

scheme using the L^2 and H^1 space minimization, respectively. With the nonlinearity strength $g = 10$ and final time $T = 6$, this is a difficult optimization problem, the optimal control being far away from the original linear function. The CPU usage in

mesh	$\hat{J}$	$\|\|\nabla\hat{J}\|\|_{L^2}$	iterations	CPU time (sec)
400	3.0295×10^{-2}	2.7397×10^{-1}	24	3.3911×10^{1}
800	2.2888×10^{-3}	2.9977×10^{-2}	217	7.9421×10^{2}
1600	1.1995×10^{-3}	1.8310×10^{-2}	153	1.1986×10^{3}
3200	2.4388×10^{-3}	4.5315×10^{-3}	74	1.1883×10^{3}

Table 2.3: Results with H^1-based HZ-NCG minimization with g=10 and T=6.

mesh	$\hat{J}$	$\|\|\nabla\hat{J}\|\|_{L^2}$	iterations	CPU time (sec)
400	1.8922×10^{-3}	5.8348×10^{-2}	25	6.1990×10^{1}
800	1.2472×10^{-3}	9.7978×10^{-2}	34	1.7211×10^{2}
1600	3.5128×10^{-4}	1.3702×10^{-2}	105	9.6031×10^{2}
3200	1.1394×10^{-4}	5.8215×10^{-3}	500	8.1292×10^{3}

Table 2.4: Results with L^2-based BFGS minimization with g=10 and T=6.

mesh	$\hat{J}_{min}$	$\|\|\nabla\hat{J}_{min}\|\|_{L^2}$	iterations	CPU time (sec)
400	1.6605×10^{-2}	1.4288×10^{-1}	15	3.8407×10^{1}
800	5.5963×10^{-4}	4.5284×10^{-2}	62	2.8107×10^{2}
1600	2.9634×10^{-4}	1.0733×10^{-2}	30	3.6334×10^{2}
3200	1.0562×10^{-4}	3.6378×10^{-3}	37	9.6153×10^{2}

Table 2.5: Results with H^1-based BFGS minimization with g=10 and T=6.

both spaces is comparable. We see that, at convergence and similar computational effort, the H^1-based approach produces a smaller objective and substantially smaller norm of the gradient on the finest mesh than the L^2-based approach.

The advantage of the H^1-based minimization on the L^2-based scheme is more evident in Tables 2.4 and 2.5 which show the performance of the BFGS scheme in the L^2 and H^1 spaces, respectively. The L^2-based BFGS method requires progressively more iterations to reach the minimum, whereas the H^1 approach requires fewer iterations on the finest mesh, similar to NCG. Compared to the previous two tables, the BFGS scheme provides at least one order of magnitude better results in terms of the value of the objective and concerning CPU times.

The method of steepest descent with the H^1 form of the gradient can alternately be viewed as a Newton method where one only uses the Hessian arising from the regularization term. Recall the original L^2 formulation of the gradient in equation (2.14). The exact Hessian of the regularization term is the operator $\gamma\partial_t^2$ with the appropriate boundary conditions. Applying the inverse of this Hessian would map

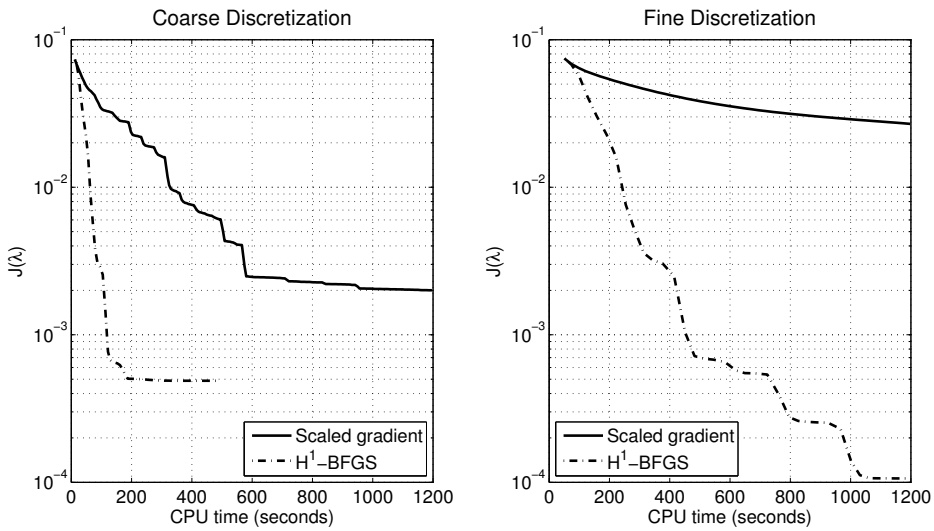

Figure 2.7: Comparison of H^1-BFGS with a scaled gradient method. Left plot is for a coarsely discretized governing equation with 1000 time steps and the right plot is for 4000 time steps. We have $\gamma = 10^{-4}$, $g = 10$, and $T = 6$.

functions in the space H^{-1} into H^1 as well. We see in figures 2.7 and 2.8, however, that this does not compare favorably to the H^1-BFGS method where we are approximating a Hessian-like operator for the full problem and not just the regularization term. In the BFGS method described above, the gradient is already in H^1 so the action of the BFGS operator B and its inverse H will map H^1 back into itself.

2.6 A basis function approach

We have considered only minimization schemes which use the optimality conditions. One might observe that the optimal control functions λ frequently resemble low-order polynomials. Therefore, one could use the adjoint framework of this paper to explore the space of control functions to determine their features and then start a procedure to define a reduced space of the controls. In fact, a statistical approach [65] to

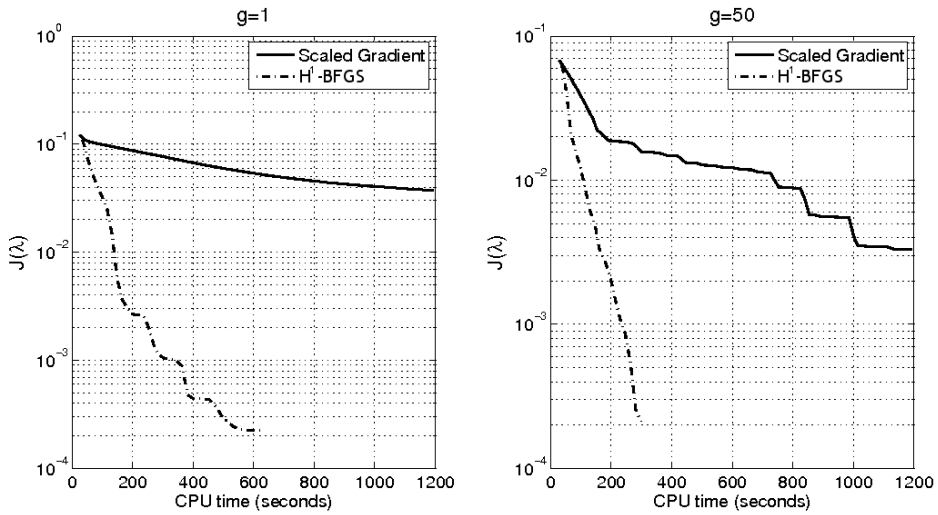

Figure 2.8: Comparison of H^1-BFGS with a scaled gradient method for weak and strong nonlinearity. We have $\gamma = 10^{-4}$, $T = 6$, and 2500 time steps.

quantum control problems interpreted as inverse problems would require to reduce the dimensionality of the problem by writing the control function λ in terms of a suitable series of basis functions. The problem is to determine what is a suitable basis for this approach. Two possibilities are considered. On the one hand, based on the regularity of the solution of the adjoint problem and on approximation properties of known interpolation polynomials, we choose a polynomial basis function and perform direct minimization on the coefficients of the polynomial expansion of the control function. On the other hand, with the adjoint method we can compute a set of optimal controls corresponding to different problem parameters and using the POD [59] a reduced model in using POD expansion coefficients. Clearly, in both cases the solution of the optimality system as described in the previous sections is an essential step. We show that the range of validity of the reduced space approach remains limited by the set of parameters used in the adjoint formulation in order to construct the reduced POD basis.

Next, we discuss a polynomial basis functions approach. Let us assume that λ

can be accurately represented in terms of Chebyshev polynomials. That is,

$$\lambda(t) = \frac{t}{T} + \sum_{k=1}^{N_k} a_k \phi_k \left(1 - \frac{2t}{T}\right), \qquad \phi_k(\cdot) = T_{k-1}(\cdot) - T_{k+1}(\cdot) \tag{2.36}$$

where $T_k(\cdot)$ is the kth Chebyshev polynomial of the first kind. We can then attempt to minimize the functional $\hat{J}(\mathbf{a})$ with respect to the coefficients $\mathbf{a} = (a_1, \ldots, a_{N_k})$, using any optimization toolbox. Much as choosing to minimize in the H^1 space before immediately give an update in the correct space, these basis functions are inherently in H^1 and vanish at the boundaries. It is also possible to define a gradient of the objective function with respect to the expansion coefficients. The kth element of the gradient is

$$[\nabla_a \hat{J}(\mathbf{a})]_k = \int_0^T \gamma \frac{d\lambda}{dt}\frac{d\phi_k}{dt} + \Re e\langle \psi, \frac{\partial V_\lambda}{\partial \lambda}\, p\rangle \phi_k dt$$

In contrast to the previous sections, this gradient is defined on the space ℓ^2. Interestingly, although the optimal control obtained using the BFGS method above may be well approximated by polynomials of order 20 or less in most situations, the minimum obtained via basis search in the equivalent number of degrees of freedom invariably produces a significantly different control. The basis minimization typically does not produce quite as optimal a solution as the H^1-based minimization and gives a cost functional value typically 5 to 10 times larger. Figure 2.9 shows the model problem where $g = 50$, $T = 5$, $\gamma = 10^{-7}$ and the nonlinear Schrödinger equation is solved over 4000 time steps.

As discussed at the beginning of this section, instead of assuming the optimal control to be close to a low order polynomial that can be well approximated in a polynomial basis, one can define a proper orthogonal decomposition (POD) of solutions to determine a natural set of basis functions for the problem. In the case of our model problem, it has been shown in Figure 2.3, that the control function depends strongly on the time horizon and much less on, e.g., the optimization parameter. Therefore it is reasonable to construct a POD basis using the optimal

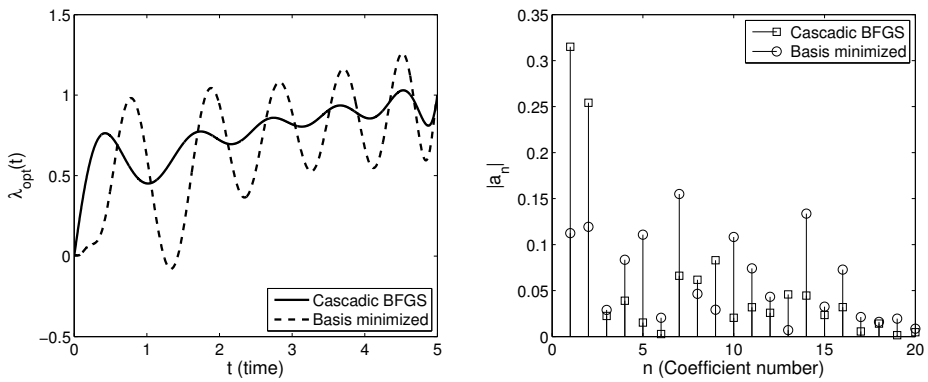

Figure 2.9: Optimal control from basis minimization versus solution of the optimality system. The right plot shows the amplitudes of the expansion coefficients of the control obtained with the two methods.

controls obtained from different time horizons and scaling them to the time interval corresponding to a desired T where further calculations are required. To describe this procedure, let $\sigma_j(t) = \lambda_j(t) - t/T$. Given various control time horizons $T_1, ..., T_m$, with corresponding optimal controls $\sigma_1, ..., \sigma_m$, the POD basis functions are obtained from the eigenvalue decomposition of the correlation matrix A where

$$A_{jk} = \int_0^T \sigma_j(t)\sigma_k(t)dt, \qquad A = V^\top SV. \tag{2.37}$$

The kth POD basis function is

$$\phi_k(t) = \frac{1}{\sqrt{s_k}} \sum_{j=1}^{m} V_{jk}\sigma_j(t), \qquad s_k = S_{kk} \tag{2.38}$$

To construct a POD basis, we compute the optimal control functions for $T = 5$ through $T = 10$ at 0.5 intervals, obtaining eleven different optimal control functions using H^1-based BFGS on a 4000 point grid with $\gamma = 10^{-7}$ and $g = 10$. It results that, the POD eigenvalues decay exponentially as depicted in Figure 2.9. Now, we can choose the first four POD functions to form a reduced-order model. We find that the POD-based control solution for the problem with $T = 6.75$ and $g = 10$ and $\gamma = 10^{-7}$ requires 53.7 seconds and gives a cost functional of $J = 2.2785 \times 10^{-5}$. In

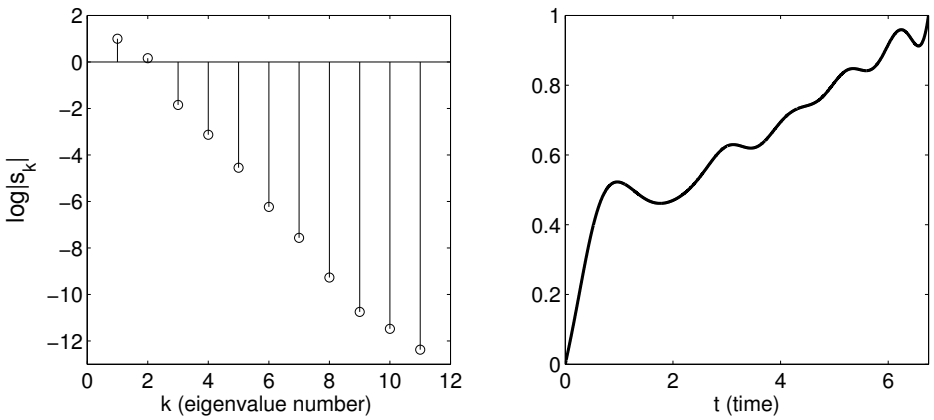

Figure 2.10: Natural logarithm of the eigenvalues of the POD correlation matrix (left). The optimal control obtained using the first four POD functions.

contrast, the polynomial minimization with four basis functions reaches the minimum $J = 4.1595 \times 10^{-3}$ in 78.1 seconds. Using eight polynomials gave a slightly better minimum than the POD test with $J = 7.4717 \times 10^{-6}$ at the added expense 330.5 seconds of CPU time. Solving the optimality system with the same parameters we obtain a minimum of $J = 1.9456 \times 10^{-6}$ and requires 894.1 seconds of CPU time.

It appears that the ability of the POD basis to capture the critical behavior in fewer terms is specific to the problem parameter set. For example, if we compute the POD basis for a problem with nonlinearity $g = 10$ and then attempt with this basis to find the optimal control when $T = 6$ and $g = 50$, the performance is significantly worse. Although the CPU time is comparable, 64.5 seconds, the minimum is $J = 6.0742 \times 10^2$. The polynomial bases, which have no problem-specific structure, yields a minimum of $J = 1.0245 \times 10^{-2}$ in 79.9 seconds using four basis functions and $J = 1.4632 \times 10^{-5}$ in 317.2 seconds using eight basis functions. The cascadic H^1-based BFGS scheme obtained a minimum of $J = 4.2709 \times 10^{-5}$ in 844.7 seconds of CPU time. The magnitude of the POD coefficients and an optimal control obtained though POD basis minimization appear in figure 2.10.

Chapter 3

The Krylov-Newton method

3.1 Introduction

The control of quantum electronic states in physical systems has a host of applications such as quantum computers [5], control of photochemical processes [36], and semiconductor lasers [18, 30]. Quantum computers, in particular, have been the subject of much research interest since they hold the promise of performing complex calculations in polynomial time. In a quantum computer the classical logic states 0 and 1 are replaced by states of a quantum system. One such possibility is a two-level system where the occupancy of the ground state could be analogous to the logical 0 and the first excited state represents logic state 1.

In most of the envisioned applications, it is important to define fast control mechanisms that cannot be constructed based on perturbation theory strategies or on a-priori parameterized control fields. This fact motivates the increasing interest in the optimal control theory framework [23] within which many recent successful results for quantum control problems [7, 46, 9, 22, 25, 26, 27, 33, 34] have been obtained. A pioneering work in this field was done by Peirce, Dahleh, and Rabitz [32] who in-

vestigated the optimal dipole control of a diatomic molecule represented by a Morse potential. The focus in this and in other early papers (see [11, 13]) was to validate the ability of the optimal control framework to provide suitable quantum control mechanisms. However, computational difficulties due to the structure of the optimality system with bilinear control and the non-convexity of the optimization problem led to research focused more on finite-dimensional Schrödinger equations; see, e.g., [7, 9, 27, 34]. In this case, the computational schemes of choice have been the monotonic iterative scheme [27, 34] and accelerated versions of the gradient scheme [7, 8]. These first-order schemes perform well for finite-level quantum systems and provide acceptable results [26, 40] when applied to infinite-dimensional systems. However, they cannot provide second-order convergence typical of the Newton method and their convergence behavior may not be robust with respect to changes of values of discretization and optimization parameters.

It is the purpose of this work to develop an accurate, efficient, and robust Newton scheme for infinite-dimensional quantum systems in the most representative case of a dipole control structure. We remark that, although the application of the Newton scheme to solve constrained optimization problems is well known, its use for solving quantum control problems has been less successful. The reason for this fact is manifold and will be illustrated in this paper. In particular, we discuss the accurate construction of the gradient and the setting of the Hessian of the reduced optimization problem. The former requires: 1) an appropriate discretization scheme that is norm-preserving and second-order accurate also in the case of time-varying potential; 2) a discretize-before-optimize approach to avoid any inconsistency between the optimality condition and its discrete approximation; 3) a gradient which is defined in the same functional space where the control function is sought. This last point is automatically fulfilled in a full Newton scheme. Point 2) results are necessary as in our experience bilinear control problems have very flat minima and therefore are prone to gradient inconsistency when using a optimize-before-discretize approach.

The other important aspect for a successful development of the Newton scheme for solving our problem is the construction (in the sense of application) of the Hessian. For this purpose, we notice that a formal derivation of this operator, which does not take into consideration the fact that quantum control problems are defined in complex Hilbert spaces, results in non-symmetric Hessians and thus in non-converging schemes; see a related discussion in [4]. For this purpose, we introduce a real-valued matrix representation of complex variables and obtain the Hessian within this formalism. Together with this fact, we provide a new theoretical analysis of first- and second-order optimality conditions giving criteria such that the Hessian becomes positive definite in a neighborhood of the optimal solution. Because the theoretical analysis is quite involved, for ease of reading we present this analysis at the end while we recall the main results where needed.

The Newton scheme which results taking into consideration all issues mentioned above still may lack of robustness because of non-convexity of the optimization problem. This fact appears less clearly with large values of the regularization parameter and when considering large time intervals for the control. However, in application we need controls that are fast and accurate, i.e. with less regularization. For this purpose, we augment the Newton scheme with a robust linesearch algorithm which exploits a priori estimates and uses continuation techniques to solve our problem with small regularization. Results of numerical experiments demonstrate that the resulting globalized Newton scheme is able to compute fast controls for high-energy transitions with typical second-order convergence.

In the next section, we introduce a dipole quantum control problem and discuss modeling issues concerning the objective and the governing equation. We employ the optimal control framework by formulating a cost to minimize with the equality constraint that the particle dynamics satisfy the time-dependent Schrödinger equation (TDSE). The cost functional is designed in such a way to avoid specification of the

phase of the target function. Further, we review some properties of the TDSE, define the optimality system to be solved, and show that the constrained optimization problem can not have a unique minimizer.

In Section 3.3, a second-order accurate discrete approximation to the Schrödinger equation with dipole control potential is introduced which shares the unitarity for the continuous TDSE. We use a real-valued matrix representation of complex variables for the discretization of the governing equation and of the objective. Hence we derive the discrete optimality system. From this we obtain the reduced objective and correspondingly define the gradient and the reduced Hessian. With this setting, in Section 3.4 we present all details of our Newton method that includes initialization and globalization issues. In particular, we discuss a robust linesearch where the unitarity of the TDSE is used to compute a maximum feasible step length for the linesearch which also provides a useful criteria indicating when a unit step length is feasible.

In Section 3.5, we investigate the ability of the optimal control framework to provide fast and accurate controls for high-energy state transitions and validate our Newton scheme. Results of numerical experiments show that with our approach we are able to obtain controls for very short time intervals and to steer high-energy transition while solving the optimality system to high accuracy, that is, to very small values of the norm of the reduced gradient. In addition, we present a comparison of the performance of the Newton scheme with that of a steepest descent algorithm and of a nonlinear conjugate gradient method, showing that our Newton approach outperforms gradient based schemes.

In the final section, we define our functional setting and discuss existence and uniqueness of solution to the TDSE problem. We use these results to define the reduced optimization problem and illustrate the optimality conditions. Then we prove existence of optimal solutions and provide criteria such that the second-order

sufficient optimality condition holds.

A section of conclusion completes the exposition of our work.

3.2 Model problem and optimal control framework

We illustrate the model of a charged quantum particle subject to a stationary confining potential and a time-dependent electric control field [3]. A dipole approximation of the electric field is considered and we formulate the control problem of steering transitions of the particle among stationary states. In this section, we focus on the physical properties of the model and on the formulation of the control problem, including the main theoretical statements on the optimality system, while in the final section we collect details of our functional analytic setting and present our proofs of the existence of an optimal control solution including necessary and sufficient optimality conditions.

The quantum state of a particle is described by a wavefunction $\psi : Q \to \mathbb{C}$ that is governed by the time-dependent Schrödinger equation (TDSE) as follows

$$i\partial_t \psi(x,t) = \left\{-\partial_x^2 + V(x,t)\right\}\psi(x,t), \qquad (x,t) \in Q = \Omega \times (0,T), \tag{3.1}$$

where Ω is the spatial domain and $(0,T)$ is the time interval, and we choose the scaling of the Planck constant $\hbar = 1$ and the mass $m = 1/2$. The potential $V(x,t)$ consists of a stationary part $V_0(x)$ and a time varying control part.

In the quantum mechanical framework, a dynamically stable system like an atom or a molecule exists in the presence of a stationary confining potential, that is, a potential with a 'well' envelope [14]. In this case one considers the following

eigenproblem

$$\left\{-\partial_x^2 + V_0(x) - \lambda_j\right\}\phi_j(x) = 0, \quad j = 1, 2, ..., \tag{3.2}$$

whose eigenfunctions represent the stationary states and the eigenvalues λ_j represent the energy of the corresponding states. The time-evolution of these states is given by $\psi_j(x,t) = \phi_j(x)\,\exp(-i\lambda_j t)$. A representative stationary potential with various applications in semiconductor nanostructures [19], define on $\Omega = (0,\ell)$, is the infinite barrier well potential where $V_0(x) = 0$ for $x \in (0,\ell)$ and $V_0(0) = +\infty$ and $V_0(\ell) = +\infty$. The infinite barrier condition is equivalent to homogeneous Dirichlet boundary conditions for the wavefunction and thus we have $\lambda_j = \frac{j^2\pi^2}{\ell^2}$ and $\phi_j(x) = \sin(j\pi x/\ell)$.

Although the methodology in this work is not limited to the infinite quantum well potential, in application it is important to consider this case to determine a control function $V(x,t)$ which allows transitions of a charged particle from one stationary state to another of a quantum well over a short time interval. A physically meaningful control mechanism is an electric control field modeling a laser pulse. Using the dipole approximation the total potential results in the form $V(x,t) = V_0(x) + u(t)\,x$, where $u : (0,T) \to \mathbb{R}$ is the modulating control amplitude. Our approach generalizes to n dimensions considering a vector-valued control $\mathbf{u}(t)\cdot\mathbf{x}$ with $\mathbf{x} \in \mathbb{R}^n$ and $\mathbf{u} : (0,T) \to \mathbb{R}^n$.

Next, we discuss some important properties of the solution to the TDSE and report a few results from perturbation theory. We write $\Re e(z)$ and $\Im m(z)$ for the real and imaginary part of a complex $z \in \mathbb{C}$. Moreover, z^* stands for the complex conjugate of z and $|z|_{\mathbb{C}} = \sqrt{z^* z}$ for its absolute value. For our discussion, we define $\mathcal{H} = L^2(\Omega;\mathbb{C})$, the Hilbert space endowed with the inner product

$$(\varphi,\psi)_{\mathcal{H}} = \int_\Omega \varphi(x)^*\psi(x)\,dx \quad \text{for } \varphi,\, \psi \in \mathcal{H},$$

and the induced norm $\|\varphi\|_{\mathcal{H}}$ for $\varphi \in \mathcal{H}$. The Hilbert space $\mathcal{V} = H_0^1(\Omega;\mathbb{C})$ is given by

$$\mathcal{V} = \left\{ \varphi \in \mathcal{H} \,\middle|\, \|\varphi\|_{\mathcal{V}} = \left(\int_\Omega |\varphi'(x)|_{\mathbb{C}}^2 \, dx \right)^{1/2} < \infty, \qquad \varphi = 0 \text{ on } \partial\Omega \right\},$$

supplied with the inner product $(\varphi,\psi)_{\mathcal{V}} = (\varphi',\psi')_{\mathcal{H}}$ for $\varphi,\psi \in \mathcal{V}$ and the induced norm $\|\varphi\|_{\mathcal{V}}$. We also need the Hilbert space

$$\mathcal{W} = L^2(0,T;H_0^1(\Omega;\mathbb{C}) \cap H^2(\Omega;\mathbb{C})) \cap H^1(0,T;L^2(\Omega;\mathbb{C})))$$

For more details on the above Lebesgue and Sobolev spaces and more weaker spaces see the final section and, e.g., [1, 17].

Now, consider the TDSE with an initial state of the quantum system given by $\psi_0(x) \in \mathcal{V}$ at $t = 0$. One recognizes that the Schrödinger evolution operator is time-reversible (non-dissipative) and therefore ψ cannot have better regularity than ψ_0 [10]. We also see that with a time-varying potential there is no energy conservation. In fact we want to change the energy of the system. However, we have mass conservation as stated by the following

Proposition

Let $V(x,t) = V_0(x) + u(t)\,x$ and $\|\psi_0(\cdot)\|_{\mathcal{H}} = 1$, then we have $\|\psi(\cdot,t)\|_{\mathcal{H}} = 1$ for all $t \in [0,T]$.

Proof. The time rate of change of the total probability is

$$\partial_t \|\psi\|_{\mathcal{H}}^2 = (\psi,\psi_t)_{\mathcal{H}} + (\psi_t,\psi)_{\mathcal{H}} = 2\Re e(\psi,\psi_t)_{\mathcal{H}} = 2\Re e(\psi, i\psi_{xx} - iu(t)x\psi)_{\mathcal{H}} \quad (3.3)$$

where

$$(\psi, i\psi_{xx} - iu(t)x\psi)_{\mathcal{H}} = \int_\Omega \psi^* \big(i\psi_{xx} - iu(t)x\psi\big)\, dx = -i\|\psi_x\|_{\mathcal{H}}^2 - iu(t) \int_\Omega \psi^* x\psi \, dx.$$

Since x is a self-adjoint operator (in the sense that $A : \mathcal{H} \to \mathcal{H}$ defined by $(A\psi)(x) = x\psi(x)$ is a self-adjoint operator) with respect to the inner product, it means that we are taking the real part of a purely imaginary quantity in (3.3). It follows that $\partial_t \|\psi\|^2_{\mathcal{H}} = 0$ for all time and so $\|\psi(\cdot, t)\|^2_{\mathcal{H}} = \|\psi_0\|^2_{\mathcal{H}}$. □

We now show that a spatially symmetric potential results in symmetric or anti-symmetric eigenfunctions. Consider $\Omega = (0, \ell)$ and let $\ell_m = \ell/2$.

Proposition

If the stationary Schrödinger equation has a symmetric potential, $V_0(\ell_m + x) = V_0(\ell_m - x)$, then the eigenfunctions must have even or odd parity with respect to ℓ_m.

Proof. Let $\mathcal{P}$ be the parity operator defined $\mathcal{P}f(\ell_m + x) = f(\ell_m - x)$ and $H_0 = -\partial_x^2 + V_0$ be the stationary Hamiltonian with $H_0\phi_j = \lambda_j\phi_j$. We have

$$\mathcal{P}H_0\phi_j(\ell_m + x) = \lambda_j\phi_j(\ell_m - x) = H_0\mathcal{P}\phi_j(\ell_m + x) \;\Rightarrow\; [\mathcal{P}, H_0] = 0. \tag{3.4}$$

Since the operators commute, ϕ_j must be an eigenfunction of the parity operator $\mathcal{P}\phi_j = \mu_j\phi_j$. Given that $\mathcal{P}^2\phi_j = \phi_j$, the parity eigenvalue must be $\mu_j = \pm 1$. Therefore, all eigenfunctions must be either symmetric $\phi_j(\ell_m + x) = \phi_j(\ell_m - x)$ or antisymmetric $\phi_j(\ell_m + x) = -\phi_j(\ell_m - x)$. □

An important result of perturbation theory is that in a long time horizon a time-harmonic control $u(t)$ is able to induce transition between two eigenstates if its frequency equals the difference of energy of the two states [14]. Therefore, it is relatively easy to control state transitions for long time intervals as we show in the example below. However, the problem becomes very difficult if short time intervals

are considered. Here short means that $T \approx 2\pi/\omega$ and in this case the perturbation theory is inapplicable and the control $u(t)$ deviates greatly from an harmonic function. In this case we use an optimal control approach.

To formulate the optimal control problem, we have to decide in which functional space the control is sought. From the previous discussion, it appears that the control space $\mathcal{U} = H_0^1(0, T; \mathbb{R})$ is the most appropriate for dipole controls as it means that the laser pulse cannot change instantaneously and it accommodates sinusoidal functions for long time controls. In the optimal control framework, this choice means that the objective of the optimization has a regularization term of the form $\|u\|_{\mathcal{U}}^2$, where this norm is induced by the following inner product

$$(u, v)_{\mathcal{U}} = \int_0^T \left(u(t)v(t) + \alpha\, \dot{u}(t)\dot{v}(t)\right)\, dt \quad \text{for } u, v \in \mathcal{U},$$

with $0 < \alpha \ll 1$. Notice that with this norm the control is continuous since $H_0^1(0, T)$ is compactly embedded in $C^0([0, T])$ in one dimension. Use of smaller values of α allows for controls with larger rates of change. We have that the control is zero at the beginning and at the end of the time interval which is the maximum time-window for the laser pulse.

Our control problem requires to finding a control $u \in \mathcal{U}$ such that a quantum system initially in the state ψ_0 evolves with (3.1) to a state $\psi(\cdot, T)$ that is as close as possible to a desired target configuration $\tilde{\psi}$. This aim is formulated by requiring to minimize the objective given by the following cost functional

$$\min_{\psi \in \mathcal{W},\, u \in \mathcal{U}} J(\psi, u) := \frac{1}{2}\left(1 - \|P\psi(\cdot, T)\|_{\mathcal{H}}^2\right) + \frac{\gamma}{2}\|u\|_{\mathcal{U}}^2, \tag{3.5}$$

under the constraint given by the TDSE, including the initial condition, denoted as follows

$$e(\psi, u) := \{\partial_t - i\, H(u)\}\ \psi = 0, \tag{3.6}$$

where $H(u) = -\partial_x^2 + V_0(x) + u(t)\,x$ and we introduce the projector $P\psi = (\tilde{\psi}, \psi)_{\mathcal{H}}\tilde{\psi}$. The goal of the first term of the cost functional is to track the given terminal state $\tilde{\psi}$ up to a global phase $e^{i\varphi T}$ which cannot be specified. In the final section, we prove existence of a unique solution to $e(\psi, u) = 0$ for a given $u \in \mathcal{U}$ and discuss the differentiability properties of the operator e and of the objective $J(\psi, u)$ as required for the optimal control formulation.

Before we discuss the solution of this constrained optimization problem, we consider the case of a control of sinusoidal type designed to drive our quantum model from the first eigenstate $\phi_1(x) = \sin(\pi x/2)$ to the second one $\phi_2(x) = \sin(2\pi x/2)$ where we choose $\ell = 2$. We take a control of the form

$$u(t) = u_0 \left[\sin(\omega t) - \sin(\omega T)\frac{t}{T}\right], \quad \omega = \lambda_2 - \lambda_1, \tag{3.7}$$

with $\lambda_2 - \lambda_1 = 3\pi^2/4$ and the linear term is such that $u(0) = 0$ and $u(T) = 0$. With this control in (3.6) and $\psi_0 = \phi_1$, we solve the forward problem and obtain $\psi(\cdot, T)$ which is used in (3.5) together with $\tilde{\psi} = \phi_2$ to determine $J(\psi, u)$. Results with this setting are reported in the two pictures of Figure 3.1. The left picture shows that

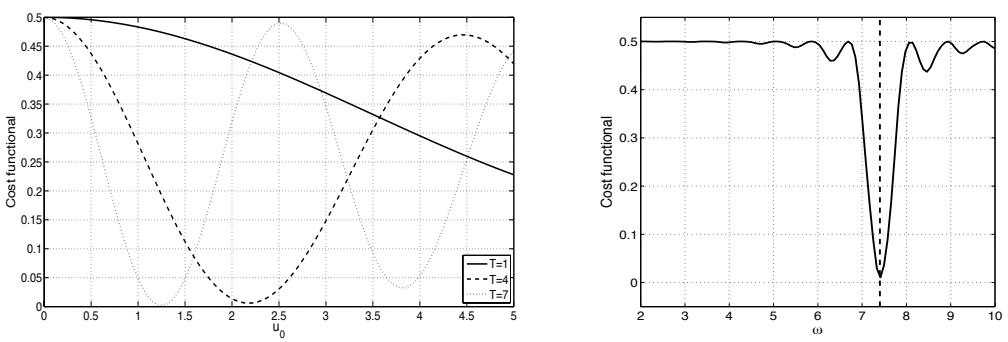

Figure 3.1: *Left*: Values of the objective with nearly time-harmonic control with fixed frequency $\omega = 3\pi^2/4$ and varying amplitude u_0 for three different time horizons T. *Right*: Values of the objective for fixed amplitude $u_0 = 1$ and $T = 8$ for variable frequency.

choosing $\omega = 3\pi^2/4$, smaller amplitudes are required in correspondence to larger

time horizons in order to attain the minimum of the objective. However, with $T = 1$ we have $\omega T \approx 2\pi$ and the objective does not change considerably as we increase the amplitude. On the other hand, in the right picture we see that, choosing T sufficiently large and a fixed amplitude, a clear minimum is obtained for $\omega = 3\pi^2/4$.

We show that a control suitable for fast state transition can be obtained by in the optimal control formulation given by (3.5) and (3.6). To characterize the solution to this problem, we introduce the following Lagrangian

$$L(\psi, u, p) = J(\psi, u) + \Re e \int_0^T \int_\Omega p^*(x,t) e(\psi, u)(x,t)\, dxdt, \tag{3.8}$$

where p is the Lagrange multiplier. We prove in the final section that any minima of (3.5) and (3.6) corresponds to an extremal point of the Lagrangian; see also [23, 24]. Therefore, by taking the Frechét derivatives of $L(\psi, u, p)$ with respect to the optimization variables gives the following first-order optimality system that characterizes the optimal solution, we have

$$\begin{aligned} \left\{ i\partial_t + \partial_x^2 - V_0(x) - u(t)\, x \right\} \psi(x,t) &= 0, \\ \left\{ i\partial_t + \partial_x^2 - V_0(x) - u(t)\, x \right\} p(x,t) &= 0, \\ -\gamma\, u + \gamma\alpha\, \ddot{u} + \Re e \int_\Omega p^*(x,t)\, x\, \psi(x,t)\, dx &= 0 \end{aligned} \tag{3.9}$$

This system consists of the state equation, the adjoint equation, and the optimality condition, respectively, with homogeneous Dirichlet boundary conditions, and initial and terminal conditions given by

$$\begin{aligned} \psi(x,0) &= \psi_0(x), \\ p(x,T) &= i\, (\tilde{\psi}(\cdot), \psi(\cdot,T))_{\mathcal{H}}\, \tilde{\psi}(x), \\ u(0) = 0, \quad u(T) &= 0. \end{aligned} \tag{3.10}$$

In the final section, we prove that there exists at least one solution to (3.9)-(3.10). We also prove that if γ is sufficiently large and the projection $\|P\psi(T)\|^2_{\mathcal{H}}$ is sufficiently small, then the second-order sufficient optimality condition holds and our optimization problem is locally strictly convex.

Notice that the control is a function of time only, and the state and adjoint variables can be seen as implicit functions of the control. Therefore the dimensionality of the optimization problem can be reduced significantly introducing a reduced cost functional $\tilde{J}(u) = J(\psi(u), u)$. In the final section we show that the corresponding gradient is given by

$$\big(\nabla \tilde{J}(u)\big)(t) = \gamma\, u(t) - \gamma\alpha\, \ddot{u}(t) - \Re e \int_{\Omega} p^*(x,t)\, x\, \psi(x,t)\, dx. \tag{3.11}$$

Therefore we have that $\nabla \tilde{J}(u) \in H^{-1}(0,T;\mathbb{R})$ which is problematic with a gradient-based approach because the gradient is not in the same space of the solution and thus neither it provides an update to the control along the descent direction. It has been shown [40], that this problem can be solved by using the Riesz representation of the gradient in the $H^1_0(0,T)$ space as a means of Sobolev smoothing. Although we will ultimately be working with a discrete optimality system, the idea of formulating the gradient in a weighted ℓ^2 space follows analogously.

A main difficulty in the analysis and solution of our quantum control problem is that it may admit multiple solutions (as most bilinear control problems). We prove that this is the case in the following.

Proposition

Let the initial and target states be eigenfunctions and the stationary potential be symmetric, then the reduced cost functional does not have a unique minimizer. In particular, if $u^*(t)$ is a minimizer, then so is $-u^*(t)$ and consequently $\nabla \tilde{J}(u)$ is

non-convex independently of regularization.

Proof. Let $\psi(x,t)$ be a solution to the TDSE with symmetric stationary potential

$$\left[i\partial_t + \partial_x^2 - V_0(x) - u(t)\,x\right]\psi(x,t) = 0$$

and

$$\left[i\partial_t + \partial_x^2 - V_0(-x) - (-u(t))\,(-x)\right]\psi(x,t) = 0.$$

This implies that if a control $u(t)$ yields a solution $\psi(x,t)$, then $-u(t)$ yields a solution which is spatially reversed $\psi(-x,t)$. The projection of the final state onto the target has the value $(\tilde{\psi}(\cdot), \psi(\cdot,T))_{\mathcal{H}}$. Since $\tilde{\psi}(x)$ is an eigenfunction, it has either even or odd parity. The final value of the wavefunction $\psi(x,T)$ is given by the control $u(t)$ and $\mathcal{P}\psi(x,T)$ is given by $-u(t)$. The parity operator is self-adjoint on L^2 ($\mathcal{P} = \mathcal{P}^*$), by virtue of commuting with the self-adjoint Hamiltonian. This gives the relationship

$$\left|\int_\Omega \mathcal{P}\psi^*(x,T)\tilde{\psi}(x)dx\right|^2 = \left|\int_\Omega \psi^*(x,T)\mathcal{P}\tilde{\psi}(x)dx\right|^2 = \left|\int_\Omega \psi^*(x,T)[\pm\tilde{\psi}(x)]dx\right|^2$$

The cost functional depends only on the magnitude of this projection, therefore $\tilde{J}(u) = \tilde{J}(-u)$. The consequence of the above non-uniqueness property is that the cost functional cannot be globally convex, independently of how large the regularization parameter may be. □

3.3 Formulation of the discrete optimal control problem

In a PDE-based optimization problem, there are two possible discretization procedures. One is the optimize-before-discretize approach in which we discretize the optimality system (3.9) choosing appropriate discretization schemes for the forward

equation, for the adjoint equation, and for the optimality equation. The drawback with this approach is the possible inconsistency between the discretized objective and the reduced gradient given by the discrete optimality condition; see [12]. This means discrepancy between the directional derivative $(\nabla \tilde{J}(u), \phi)_{\mathcal{H}}$ and its approximation $\frac{\tilde{J}(u+\epsilon\phi)-\tilde{J}(u-\epsilon\phi)}{2\epsilon}$, which, however, can be controlled at the cost of increasing accuracy of discretization by using finer meshes. The other drawback of the optimize-before-discretize approach is that the Hessian may not be symmetric.

In our experience, gradient inconsistency is usually not negligible in the case of hyperbolic- and Schrödinger-type equations with bilinear controls. For this reason, we pursue the approach of discretize-before-optimize where the consistency between the reduced objective and its gradient is guaranteed. The first step is to discretize the state equation and the Lagrangian and then take derivatives to obtain first- and second-order optimality conditions. The difficulty of this approach is that the approximation scheme resulting for the adjoint equation may be numerically disadvantageous.

In any case, the discretization of the Schrödinger equation must be norm- preserving to ensure a discrete $\partial_t \|\psi(\cdot, t)\|^2_{\mathcal{H}} = 0$. This is essential, otherwise it happens that we may compute a control which attains a minimum of the functional by violating the underlying physical constraint. Moreover, we want a scheme that is second-order accurate also with time-varying potentials.

We know that the classical Crank-Nicolson scheme is norm-preserving and unconditionally stable when solving the Schrödinger equation with stationary potential [32]. However, in quantum control problems, the Hamiltonian between different time steps is different, $H(t_k) \neq H(t_{k-1})$, and in this case the Crank-Nicolson scheme is not norm-preserving. For this reason, we define a modified Crank-Nicolson (MCN) method by first integrating numerically the semigroup operator and then using a Padé approximant.

Consider the semigroup operator $\psi(\delta t) = \exp(\Theta(\delta t))\,\psi(0)$, where $\Theta(t)$ is given by the Magnus expansion [21]. This is an infinite series representation for a time-dependent Hamiltonian. In the case of a dipole control with $H(t) = -\partial_x^2 + V_0(x) + u(t)x$, the Magnus expansion terminates after three terms.

$$\Theta(t) = -i\int_0^t H(\tau)d\tau + \frac{1}{2}\int_0^t \left[\int_0^\tau H(\sigma)d\sigma, H(\tau)\right] d\tau + \cdots \tag{3.12}$$

We choose to approximate $\Theta(t)$ by the first term in the expansion. The analysis of a similar second-order truncation with a midpoint rule is carried out by Hochbruck and Lubich in [20]; see also [38]. In our approach, we approximate the integral in the first term of (3.12) with the trapezoidal rule. The choice of the trapezoidal rule over the midpoint rule results in control and state variables that are defined on the same time step. Since the Magnus formula and the integral are approximated to second order, the overall scheme is second-order accurate also in the case when the potential is time-dependent. In addition, we can prove that our scheme is unconditionally stable.

Now, let N_t be the number of time steps of size $\delta t = \frac{T}{N_t}$ and N_x be the number of intervals of the Ω discretization. The TDSE discretized by our MCN scheme results in the following

$$\psi_k - \psi_{k-1} = -\frac{i\delta t}{4}[H(t_k) + H(t_{k-1})][\psi_k + \psi_{k-1}] \tag{3.13}$$

Spatial discretization of the Hamiltonian $H(t_k)$ is carried out using linear finite elements on a uniform grid which results in a matrix $\mathbf{H}_k$. We have that $\mathbf{H}_k = \mathbf{H}_k^\top$, which is important for preserving unitarity of the time-stepping method. Let $\mathbf{A}_k = \frac{\delta t}{4}[\mathbf{H}_k + \mathbf{H}_{k-1}]$. This gives the desirable property that $\mathbf{A}_k = \mathbf{A}_k^\top$, which is consistent with the infinite-dimensional Hamiltonian operator being Hermitian.

We notice an important fact: While we have no difficulty with the complex-valued variable representation in gradient-based optimization approaches [40], the

real-valued matrix representation of complex variables is necessary for constructing the Hessian; see [39]. Suppose $z_1, z_2 \in \mathbb{C}$ with $z_\ell = x_\ell + i\, y_\ell$ for $\ell = 1, 2$. These can be represented as vectors in $\mathbb{R}^2$ with $Z_\ell = \begin{pmatrix} x_\ell, & y_\ell \end{pmatrix}^\top$. Notice that, considering Z_1 and Z_2 as vectors in $\mathbb{R}^2$, it is not possible to use vector multiplication between them which results equivalent to multiplication between the corresponding complex variables. For this purpose, a matrix representation of one of the two vectors is employed as follows.

$$Z_1 Z_2 = \begin{pmatrix} x_1 & -y_1 \\ y_1 & x_1 \end{pmatrix} \begin{pmatrix} x_2 \\ y_2 \end{pmatrix} = \begin{pmatrix} x_1 x_2 - y_1 y_2 \\ x_1 y_2 + x_2 y_1 \end{pmatrix} \tag{3.14}$$

In this representation, complex conjugacy is performed via the transpose operation. This representation is also valid for matrices and vectors and in such cases leads to block systems. The spatially-discrete form of Equation (3.13) contains a term $-i\,\mathbf{A}_k$, for which therefore a real-valued representation is needed. Including the left-hand side terms, we obtain a block matrix $\mathbf{B}_k$ as follows

$$\mathbf{B}_k = \begin{pmatrix} \mathbf{I} & \mathbf{A}_k \\ -\mathbf{A}_k & \mathbf{I} \end{pmatrix}. \tag{3.15}$$

This gives the following representation of the equality constraint

$$\mathbf{e}_k(\mathbf{y}, \mathbf{u}) = \mathbf{B}_k \mathbf{y}_k - \mathbf{B}_k^\top \mathbf{y}_{k-1}, \quad \mathbf{y}_k = \begin{pmatrix} \Re e[\psi_k] \\ \Im m[\psi_k] \end{pmatrix}, \tag{3.16}$$

where $\mathbf{y}$ is a compact notation for the set of state vectors at each time step $\mathbf{y}_1, \ldots, \mathbf{y}_{N_t}$ and similarly for $\mathbf{u}$.

Given a total number N_x of grid points, the wavefunction at each time step will be a vector in $\mathbb{C}^{N_x - 2}$, therefore the state vector at each step will be in $\mathbb{R}^{2N_x - 4}$. We introduce the matrix operator $\mathbf{S}$ which corresponds, in matrix representation form, to multiplication by i. We have that

$$\mathbf{S} = \begin{pmatrix} \mathbf{0} & -\mathbf{I} \\ \mathbf{I} & \mathbf{0} \end{pmatrix}, \quad (\tilde{\psi}, \psi)_{\mathcal{H}} \text{ corresponds to } \begin{pmatrix} \tilde{\mathbf{y}}^\top \\ \tilde{\mathbf{y}}^\top \mathbf{S} \end{pmatrix} \mathbf{y} \tag{3.17}$$

In this representation, we can rewrite the original cost functional in the form

$$J(\mathbf{y},\mathbf{u}) = \frac{1}{2}\left[1 - \mathbf{y}_{N_t}^\top \begin{pmatrix} \tilde{\mathbf{y}} & -\mathbf{S}\tilde{\mathbf{y}} \end{pmatrix} \begin{pmatrix} \tilde{\mathbf{y}}^\top \\ \tilde{\mathbf{y}}^\top\mathbf{S} \end{pmatrix} \mathbf{y}_{N_t}\right] + \frac{\gamma}{2}\mathbf{u}^\top\mathbf{K}\mathbf{u} \tag{3.18}$$

The matrix $\mathbf{K}$ is symmetric and positive definite and is a linear finite-element discretization of the Helmholtz operator $I - \alpha\partial_x^2$. This means that the weighted inner product $\mathbf{u}^\top\mathbf{K}\mathbf{v}$ is a second-order approximation to $(u,v)_{\mathcal{U}}$.

We consider the Lagrangian

$$\mathbf{L}(\mathbf{y},\mathbf{u},\mathbf{p}) = J(\mathbf{y},\mathbf{u}) + \sum_{k=1}^{N_t} \mathbf{p}_k^\top \mathbf{e}_k(\mathbf{y},\mathbf{u}) \tag{3.19}$$

Differentiating this Lagrangian with respect to its arguments and setting the derivatives to zero gives the discrete first-order optimality system

$$\mathbf{B}_k\mathbf{y}_k = \mathbf{B}_k^\top\mathbf{y}_{k-1}, \tag{3.20}$$

$$\mathbf{B}_k^\top\mathbf{p}_k = \mathbf{B}_{k+1}\mathbf{p}_{k+1}, \tag{3.21}$$

$$\gamma\mathbf{K}\mathbf{u} = \mathbf{f}. \tag{3.22}$$

The control vector $\mathbf{u} = (u_1,\ldots,u_{N_t-1})$ has $N_t - 1$ elements as the control is set to zero at the initial and final times. The elements of the vector $\mathbf{f} = (f_1,\ldots,f_{N_t-1})$ are given as

$$f_j = \mathbf{p}_j^\top\mathbf{V}(\mathbf{y}_j + \mathbf{y}_{j-1}) + \mathbf{p}_{j+1}^\top\mathbf{V}(\mathbf{y}_{j+1} + \mathbf{y}_j), \qquad \mathbf{V} = \frac{\delta t}{4}\begin{pmatrix} \mathbf{0} & -\mathbf{X} \\ \mathbf{X} & \mathbf{0} \end{pmatrix}, \tag{3.23}$$

where $\mathbf{V}$ is the discrete approximation of $\frac{i\delta t}{4}x$ and $\mathbf{X} = \mathrm{diag}(x_1,...,x_{N_x-1})$. The initial and terminal conditions are as follows

$$\mathbf{y}_0 = \begin{pmatrix} \Re e[\psi_0] \\ \Im m[\psi_0] \end{pmatrix} \tag{3.24}$$

$$\mathbf{B}_{N_t}^\top\mathbf{p}_{N_t} = \begin{pmatrix} \tilde{\mathbf{y}} & -\mathbf{S}\tilde{\mathbf{y}} \end{pmatrix} \begin{pmatrix} \tilde{\mathbf{y}}^\top\mathbf{y}_{N_t} \\ \tilde{\mathbf{y}}^\top\mathbf{S}\mathbf{y}_{N_t} \end{pmatrix} \tag{3.25}$$

Notice that our modified Crank-Nicolson scheme results in a unitary time- stepping, while the resulting scheme for the adjoint equation is non-unitary. This situation is reversed in using the standard Crank-Nicolson scheme for the forward problem. We emphasize that because the cost functional depends on the state variable, it is essential to preserve the norm of the state variable.

Now, consider the reduced cost functional $\tilde{J}(\mathbf{u}) = J(\mathbf{y}(\mathbf{u}), \mathbf{u})$. The gradient of this objective function is

$$\nabla \tilde{J}(\mathbf{u}) = \gamma \mathbf{K}\mathbf{u} - \mathbf{f} \tag{3.26}$$

Since the control itself has only $N_t - 1$ degrees of freedom and the state variable has $(N_t - 1)(N_x - 2)$ degrees of freedom, the matrix of the optimality system is very large with $[(2N_x - 3)(N_t - 1)]^2$ elements, albeit sparse. In contrast, the reduced Hessian will be a full matrix with $(N_t - 1)^2$ entries. Because of the structure of the optimal control problem, applying the Hessian to a vector is not significantly more expensive than computing the gradient, so the reduced Hessian approach is suitable for use with a Krylov solver. The application of the Hessian is presented in 2. The reduced Hessian is formulated following [6].

The equality constraint can be written as a block bidiagonal system where $\mathbf{e}(\mathbf{y}, \mathbf{u})$ is a matrix and $\mathbf{y}$ is a column-stacked vector. We have

$$\nabla^2 \tilde{J}(\mathbf{u}) = \mathbf{L_{uu}} + \mathbf{e_u^*} \mathbf{e_y}^{-\top} \mathbf{L_{yy}} \mathbf{e_y}^{-1} \mathbf{e_u} - \mathbf{e_u}^{\top} \mathbf{e_y}^{-\top} \mathbf{L_{yu}} - \mathbf{L_{yu}}^{\top} \mathbf{e_y}^{-1} \mathbf{e_u}. \tag{3.27}$$

Linearizing the system about a control $\mathbf{u}$, the change in the state variable $\mathbf{y}$ due to a change $\delta\mathbf{u}$ is $\delta\mathbf{y} = -\mathbf{e_y}^{-1}\mathbf{e_u}\delta\mathbf{u}$. We have that

$$[\nabla^2 J(\mathbf{u})]\delta\mathbf{u} = \mathbf{L_{uu}}\delta\mathbf{u} + \mathbf{e_u}^{\top}\delta\mathbf{p} + \mathbf{L_{yu}}^{\top}\delta\mathbf{y}, \tag{3.28}$$

where $\delta\mathbf{y} = -\mathbf{e_y}^{-1}\mathbf{e_u}\delta\mathbf{u}$ and $\delta\mathbf{p} = -\mathbf{e_y}^{-\top}[\mathbf{L_{yy}}\delta\mathbf{y} + \mathbf{L_{yu}}\delta\mathbf{u}]$. We can write the lin-

earized equality constraint with the following

$$\mathbf{e_y} = \begin{pmatrix} \mathbf{B}_1 & & & \\ -\mathbf{B}_1^\top & \mathbf{B}_2 & & \\ & \ddots & \ddots & \\ & & -\mathbf{B}_{N_t-1}^\top & \mathbf{B}_{N_t} \end{pmatrix}, \quad \mathbf{e_u} = \begin{pmatrix} \mathbf{c}_1 & & & \\ \mathbf{c}_2 & \mathbf{c}_2 & & \\ & \ddots & \ddots & \\ & & \mathbf{c}_{N_t-1} & \mathbf{c}_{N_t-1} \\ & & & \mathbf{c}_{N_t} \end{pmatrix} \tag{3.29}$$

where $\mathbf{c}_k = \mathbf{V}(\mathbf{y}_k + \mathbf{y}_{k-1})$. The application of ${\mathbf{e_y}}^{-1}$ and ${\mathbf{e_y}}^{-\top}$ follows the two-term recursion form of the forward and adjoint equations given in (3.20) and (3.21). The matrix $\mathbf{L_{uu}}$ is given by $\gamma\mathbf{K}$ and $\mathbf{L_{yu}}$ has the form

$$\mathbf{L_{yu}} = \begin{pmatrix} \mathbf{V}^\top(\mathbf{p}_1 + \mathbf{p}_2) & \mathbf{V}^\top\mathbf{p}_2 & & \\ \mathbf{V}^\top\mathbf{p}_2 & \mathbf{V}^\top(\mathbf{p}_2 + \mathbf{p}_3) & \mathbf{V}^\top\mathbf{p}_3 & \\ & \ddots & \ddots & \\ & & \mathbf{V}^\top\mathbf{p}_{N_t-1} & \mathbf{V}^\top(\mathbf{p}_{N_t-1} + \mathbf{p}_{N_t}) \\ & & & \mathbf{V}^\top\mathbf{p}_{N_t} \end{pmatrix} \tag{3.30}$$

It is the $\mathbf{L_{yy}}$ block that necessitates the real variable formulation, because the Lagrangian is not analytic in ψ. $\mathbf{L_{yy}}$ is a block matrix of $N_t - 1 \times N_t - 1$ blocks, each of size $N_x - 2 \times N_x - 2$. However, since the cost depends only on final-time observation, these blocks are all zero except for the lowest right-most block. This block contains the projection matrix of at least rank 2, i.e. $\mathbf{P} = \begin{pmatrix} \tilde{\mathbf{y}} & -\mathbf{S}\tilde{\mathbf{y}} \end{pmatrix} \begin{pmatrix} \tilde{\mathbf{y}} & -\mathbf{S}\tilde{\mathbf{y}} \end{pmatrix}^\top$. Writing this explicitly in real and imaginary parts, results in the matrix

$$\mathbf{P} = \begin{pmatrix} \psi_r\psi_r^\top + \psi_i\psi_i^\top & 0 \\ 0 & \psi_r\psi_r^\top + \psi_i\psi_i^\top \end{pmatrix} \tag{3.31}$$

There is no way to form this operator utilizing the dyadic product of a complex-valued vector with itself. Indeed, the fact that a rank-2 matrix is needed instead of a rank-1 matrix indicates the lack of an equivalent complex representation.

We have completed the formulation of the discrete optimal control problem that has been tailored to guarantee a consistent gradient and an appropriate construction of the Hessian.

3.4 A globalized Newton method

In this section, we discuss our globalized Newton approach focusing on two issues. First, we discuss the problem of starting the Newton procedure which arises due to the fact that, in a quantum control setting, the starting configuration and the target are usually orthogonal functions. In particular, it is meaningful to require to reach the target state exactly, which is possible if the weight of the regularization terms goes to zero. However, in this case it is difficult to argue positive definiteness of the Hessian. The second issue arises from the lack of convexity of our optimization problem and the need of a robust and efficient linesearch procedure.

Our numerical experience shows that the initialization of the minimizing iteration is a delicate step. Guessing an initial control to be nearly harmonic as in equation (3.7) can be a viable strategy when $\omega T \gg 1$. However, for short time intervals, a more robust initialization is required. Clearly, an initial guess of a zero control does not work. As the initial and target states are both eigenfunctions, they are orthogonal and the projection onto the target will be zero in the absence of a non-zero control function. Then the particle remains in the initial state and, $P\psi = (\tilde{\psi}, \psi)_{\mathcal{H}}\tilde{\psi} = 0$ which makes the adjoint variable and consequently the gradient identically zero. We have that the cost functional has a local maximum. If one were to modify the target state to be some $\hat{\psi} \in \text{span}(\psi_0, \tilde{\psi})$, then the projection onto the modified target will be non-zero, which in turn gives a non-zero gradient.

An additional difficulty arises from the parity of the eigenstates. In particular, if ψ_0 and $\tilde{\psi}$ are either both even or both odd, then the integral term in (3.11) will vanish

due to an antisymmetric integrand. For this reason, we recommend modifying the target state to $\hat{\psi} \in \text{span}(\psi_0, \tilde{\psi}, x\tilde{\psi})$. Once a control is computed for the transition $\psi_0 \to \hat{\psi}$, it may be used as a starting guess for the transition $\psi_0 \to \tilde{\psi}$. This approach mimics an homotopy method. For very fast controls and large energy transitions, we use a sequence of intermediate targets $\hat{\psi}_1, \hat{\psi}_2, ...$ which approach $\tilde{\psi}$ in L^2.

The choice of regularization parameters plays an important role in the initialization as well. It is desirable to start having a large regularization, that gives faster convergence in computing the Newton direction with `symmlq`. At the same time, a large weight of the cost will compromise the goal of attaining the target as close as possible. Therefore we employ successive reductions of the regularization parameter. We have found that halving γ whenever $\|\nabla \tilde{J}(u)\|_{\mathcal{U}}$ reaches a given tolerance provides robust convergence to optimal controls corresponding to very small regularization.

We start the discussion of our globalized Newton scheme giving the workflow of the main Algorithm 1, followed by the illustration of the linesearch procedure given by Algorithm 3. To improve readability, we use the notation of the continuous formulation. Their discrete counterpart is discussed in the previous section.

Notice that in Algorithm 3 we anticipate the possible lack of positive definiteness, while still exploiting the symmetry of the Hessian, by using the Krylov-type symmetric LQ method [31]. In our experience, `symmlq` consistently computes search directions in less time than other Krylov methods, such as GMRES or BiCG. If the Hessian has negative eigenvalues, `symmlq` may compute an ascent direction. Whether the direction is an ascent or descent can be determined from the sign of its projection onto the gradient. In the cases where $\delta\mathbf{u}$ is an ascent direction, $-\delta\mathbf{u}$ is a descent direction and thus it is used instead.

We have shown in Proposition 3.2 that the objective is nonconvex and therefore a linesearch is required to globalize the Newton method. Once a search direction $\mathbf{d}$ is

Data: Given ψ_0, $\tilde{\psi}$, γ, α, T, $u = 0$

Choose $\hat{\psi}$;

while $||\nabla \tilde{J}(\mathbf{u})|| > tol$ **do**

  Compute search direction δu with Algorithm 3;

  Compute a^* with Algorithm 4;

  $\mathbf{u} \leftarrow \mathbf{u} + a^* \delta \mathbf{u}$;

end

$\hat{\psi} \leftarrow \tilde{\psi}$;

$iter \leftarrow 0$;

while $iter < maxit$ **do**

  while $\|\nabla \tilde{J}(\mathbf{u})\| > tol$ **do**

    Compute search direction δu with Algorithm 3 ;

    Compute a^* with Algorithm 4;

    $\mathbf{u} \leftarrow \mathbf{u} + a^* \delta \mathbf{u}$;

  end

  $\gamma \leftarrow \gamma/2$;

  $iter \leftarrow iter + 1$;

end

Algorithm 1: Complete minimization program

computed by the Krylov-Newton solver, the aim is to compute a step length a such that it satisfies the strong Wolfe conditions (SWC) given by

$$\tilde{J}(\mathbf{u} + a\,\mathbf{d}) \leq \tilde{J}(\mathbf{u}) + c_1 a \mathbf{d}^\top \nabla \tilde{J}(\mathbf{u}), \quad 0 < c_1 \ll 1, \tag{3.32}$$

$$|\mathbf{d}^\top \nabla \tilde{J}(\mathbf{u} + a\,\mathbf{d})| \leq c_2 |\mathbf{d}^\top \nabla \tilde{J}(\mathbf{u})|, \quad c_1 < c_2 < 1. \tag{3.33}$$

When using a linesearch with a Newton-type method, it is often recommended that one begins with $a = 1$; see, e.g., [29]. This is an excellent choice when the functional is locally quadratic. However, in our optimization problem, the desired step length can be orders of magnitude smaller which happens when the higher order derivatives

Data: Given a control $\mathbf{u}$, state variable $\mathbf{y}$ and adjoint variable $\mathbf{p}$

Solve $\mathbf{e_y}\delta\mathbf{y} = -\mathbf{e_u}\delta\mathbf{u}$;

Solve $\mathbf{e_y}^\top\delta\mathbf{p} = -[\mathbf{L_{yy}}\delta\mathbf{y} + \mathbf{L_{yu}}\delta\mathbf{u}]$;

$[\nabla^2\tilde{J}(\mathbf{u})]\,\delta\mathbf{u} = \mathbf{L_{uu}}\delta\mathbf{u} + \mathbf{e_u}^\top\delta\mathbf{p} + \mathbf{L_{yu}}^\top\delta\mathbf{y}$

Algorithm 2: Applying the reduced Hessian to a test vector $\delta\mathbf{u}$

Data: Given a control $\mathbf{u}$, make an initial guess of search direction

$\delta\mathbf{u} = -\mathbf{L_{uu}}^{-1}\nabla\tilde{J}(\mathbf{u})$

Use Algorithm 2 to apply the Hessian, iteratively solve $\nabla^2\tilde{J}(\mathbf{u})\delta\mathbf{u} = -\nabla\tilde{J}(\mathbf{u})$ with `symmlq`;

if $\delta\mathbf{u}^\top\nabla\tilde{J}(\mathbf{u}) > 0$ **then**

  $\delta\mathbf{u} \leftarrow -\delta\mathbf{u}$;

end

Algorithm 3: Computing the search direction

of $J(\mathbf{u} + a\,\mathbf{d})$ with respect to a are large compared to the first and second-order derivatives.

We use our knowledge of the model to define the initial step length. In our case, the tracking part of the cost functional is bounded between 0 and 1 for all controls by virtue of the unitarity of the state equation; see Proposition 3.2. On the other hand, the cost functional is bounded from below by the regularization term. This amounts to a quadratic polynomial and we can write

$$\tilde{J}(\mathbf{u} + a\,\mathbf{d}) \geq m_2 a^2 + m_1 a + m_0,$$

where the coefficients are $m_0 = \frac{\gamma}{2}\mathbf{u}^\top\mathbf{K}\mathbf{u} - J(\mathbf{u}) \leq 0$, $m_1 = \gamma\mathbf{u}^\top\mathbf{K}\mathbf{d}$, and $m_2 = \frac{\gamma}{2}\mathbf{d}^\top\mathbf{K}\mathbf{d}$. Since $m_0 \leq 0$, the equation $m_2a^2 + m_1a + m_0 = 0$ admits real roots and we can establish an upper bound on the maximum feasible step length as follows

$$a_{\max} = \frac{\sqrt{m_1^2 - 4m_0m_2} - m_1}{2m_2}. \tag{3.34}$$

In addition, this upper bound provides a valuable metric in the sense that if $a_{\max} \ll 1$ occurs, it means that a locally quadratic model is not valid. We have the following new result:

Proposition

For sufficiently small $c_1 > 0$, there exits at least one step length a^* which satisfies the SWC condition in the interval $(0, a_{max}]$

Proof. Because $\tilde{J}(\mathbf{u} + a_{\max}\,\mathbf{d}) \geq \tilde{J}(\mathbf{u})$ and $\mathbf{d}^\top \nabla \tilde{J}(\mathbf{u}) < 0$, by the intermediate value theorem, there must be at least one value of $a^* \in (0, a_{\max}]$ such that $\tilde{J}(\mathbf{u} + a^*\,\mathbf{d}) < 0$ and $\mathbf{d}^\top \nabla \tilde{J}(\mathbf{u} + a^*\,\mathbf{d}) = 0$. □

In order to have a robust and efficient linesearch scheme we combine two methods. First, we apply the Algorithm 4 that, for a given a descent direction $\mathbf{d}$, computes the maximum feasible step length. If $a = 1$ satisfies the SWC condition, it is accepted. Otherwise, it is assumed that the functional is locally approximated by a cubic polynomial and for this purpose we construct a cubic Hermite interpolant on $[0, 1]$. The minimum a_m of this polynomial function is tested for the SWC condition. If this condition is not satisfied, we apply a more robust scheme represented by the bisection method of Algorithm 5 given below. At the end a minimizer will be bracketed by $[0, a_{amax}]$.

We have implemented a modified bisection method to compute a minimum of a C^2 function. For this purpose, we write a set of criteria which ensure that a twice continuously differentiable function $f(x)$ must have at least one local minimizer $x^* \in (x_l, x_r)$. We have the following

Proposition

Suppose that f is continuously differentiable. If $f'(x_l) < 0$ and $f'(x_r) > 0$, then there must be at least one point in $\tilde{x} \in (x_l, x_r)$ such that $\tilde{x}$ is a local minimum.

Proposition

Suppose that f is continuously differentiable. If $f'(x_l) < 0$ and $f(x_r) > f(x_l)$ ($f'(x_l) > 0$, $f(x_r) < f(x_l)$), then there must be at least one point in $\tilde{x} \in (x_l, x_r)$ such that $\tilde{x}$ is a local minimum.

These two propositions give the guideline for the formulation of the following minimization algorithm. If for any reason, Algorithm 5 returns a critical point a^* which does not satisfy the SWC condition, then we can use the fact that for sufficiently small value of c_1 there exists a point that does satisfy the SWC and lies between 0 and any critical point which does not. We can then use a^* as an upper bound and apply the bisection scheme on the interval $(0, a^*)$.

3.5 Numerical Results

In this section, we are concerned with the evaluation of the optimal control formulation for dipole control of a quantum system and with the investigation of the computational performance of the proposed Newton scheme. We consider the cost for state transitions for different choices of the regularization parameters and we compare the convergence behavior of the Krylov-Newton scheme with that of gradient-type schemes. We work in the discrete H^1 space; see [40]. We focus on fast state transitions and we compare results with T ranging from very small to moderate values. Unless otherwise stated, we take a spatial domain $\Omega = [0, 2]$ with $N_x = 100$ grid

points and consider the time interval $(0, T)$ subdivided in $N_t = 100$ time steps.

In Figure 3.2, we report the values of the objective at the optimum of state transition $1 \rightarrow 2$ for different values of the regularization parameters. We notice that for a given γ, the objective value increases while increasing the value of α, that is, penalizing highly varying controls. We see that our scheme can explore a large range of values of γ such that good tracking of the target function can be guaranteed. In Figure 3.2, we also plot the optimal controls corresponding to a given α for a range of γ values. We notice that, as the weight of the cost reduces, the control acquires more structure and we obtain an improved tracking.

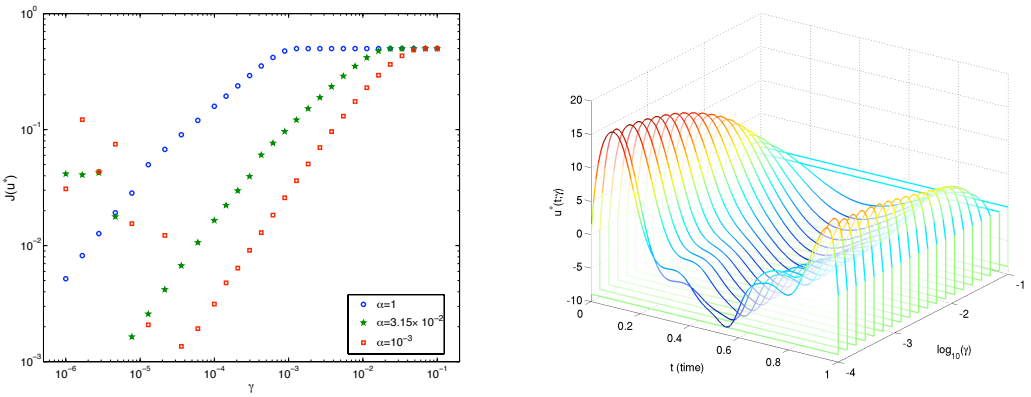

Figure 3.2: *Left:* The cost for the state transition $1 \rightarrow 2$ given an optimal control u^* for different choices of the regularization parameters, γ and α. *Right:* The optimal control for the state transition $1 \rightarrow 2$ as a function of time with $\alpha = 10^{-3}$ for a range of fixed values of γ.

The results shown in Figure 3.2, suggest that the resulting optimal control are not simple harmonic functions. This fact appears more clearly in the plot of Figure 3.3 where optimal controls for different state transitions are depicted.

In correspondence to the control of the transition $1 \rightarrow 2$, we provide in Figure 3.4 a picture of the corresponding time evolution of $|\psi(x,t)|^2$. We can clearly see the transition occurring for the state.

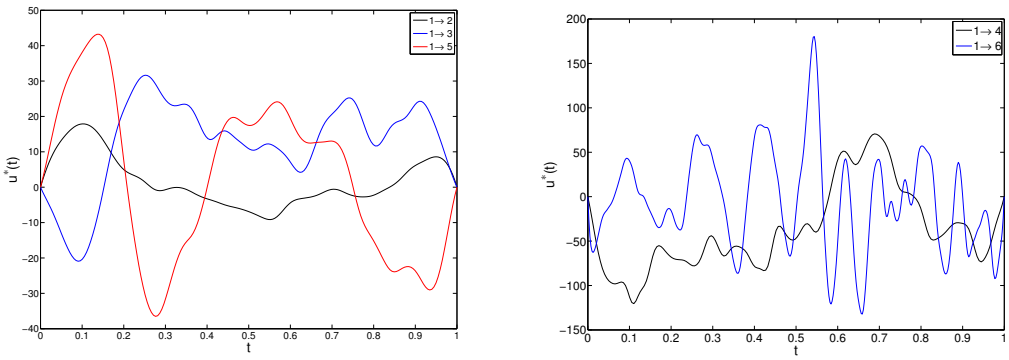

Figure 3.3: *Left:* Optimal controls for transitions from the first state to the second, the third, and the fifth states. *Right:* Optimal controls for transitions from the first state to the fourth and the sixth states.

We remark that large differences are obtained between optimal controls corresponding to different time horizons. In Figure 3.5, we see that as the terminal time T increases from the very small value $T = 0.75$ to the moderate value $T = 4$, the amplitude of the control decreases of two orders of magnitude and becomes less oscillating. This result points out the difficulty of solving for short terminal times.

Next, we investigate the computational performance of our optimal control solver. We start with Table 3.1, where we compare the convergence behavior of the Krylov-Newton (KN) scheme, of the steepest descent (SD) scheme, and of the nonlinear conjugate gradient (NCG) scheme. We use the NCG method proposed by Hager and Zhang [53] which in our case appears to be the most competitive among NCG schemes.

For these experiments, we choose the initial state $\psi_0(x) = \sin(\pi x)$ and the target state is $\tilde{\psi}(x) = \frac{1}{\sqrt{2}}[\sin(\pi x)+\sin(2\pi x)]$. We take $T = 1$. The regularization parameters are $\gamma = 10^{-1}$ and $\alpha = 10^{-3}$. Results with this setting are reported in Table 3.1 that provides the convergence history of the iterative schemes along nine iterations. We

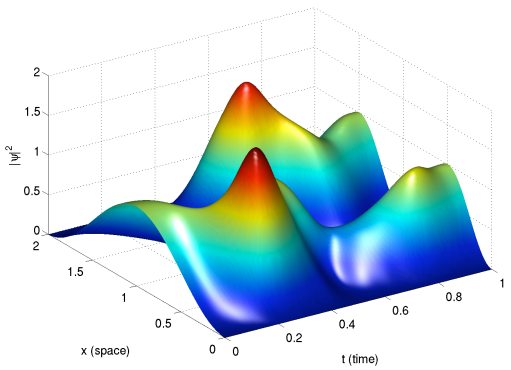

Figure 3.4: Optimal control transition of $|\psi(x,t)|^2$ from first to second eigenstate.

can see that the Krylov-Newton scheme does not descend as rapidly in the first steps followed by accelerate convergence in the subsequent steps thus outperforming the SD scheme and the NCG scheme.

Table **??** gives the decrease of the norm of the gradient for the method of steepest descent and the present Krylov-Newton method for successive iterations. For this test, 400 time steps and 200 spatial grid points were used with $T = 1$, $\alpha = 10^{\cdot 2}$, $\gamma = 10^{-3}$, $\psi_0(x) = \sin(\pi x)$, $\tilde{\psi}(x) = \frac{1}{\sqrt{10}}[\sin(\pi x) + 3\sin(2\pi x)]$. The `symmlq` solver was required to have a residual bounded by 10^{-12} for each Newton solve. For the first few iterations the norm of the gradient is about the same for the two methods, but ultimately, the Krylov-Newton method attains a gradient which is zero to machine precision in just 8 steps. The steepest descent approach had not achieved this by the 50th iteration. These results indicate that the Krylov-Newton method is exhibiting superlinear convergence.

A useful metric of computational performance of the schemes discussed here is a comparison of CPU times to reduce the value of the norm $||\nabla \tilde{J}(u)||$, representing the error in solving the optimality condition. We consider the initial state as $\phi_1(x)$ and the target as $\tilde{\psi} = \frac{1}{\sqrt{2}}(\phi_1 + \phi_2)$, $T = 1$, and fixed regularization parameter $\alpha = 10^{-2}$.

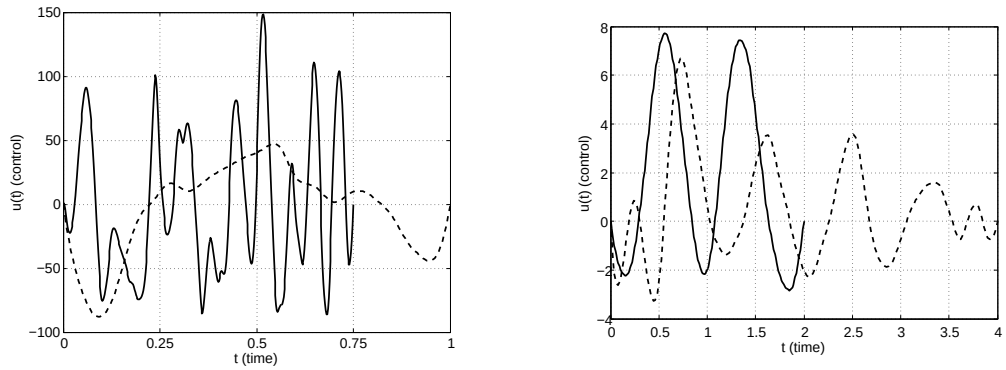

Figure 3.5: *Left*: The optimal control u for the state 1-to-2 transition with $T = 0.75$ in solid line. The dashed line is the optimal control, multiplied by factor of 5, for $T = 1$ so that it can be shown on the same scale. *Right*: The optimal controls for $T = 2$ and $T = 4$ with solid and dashed lines respectively.

We compare for two different values $\gamma = 10^{-1}$ and $\gamma = 10^{-4}$ to show the influence of regularization on the convergence of the control problem. In Figure 3.6, we plot the values of $||\nabla \tilde{J}(u_k)||$ for a sequence of iterations $k = 1, 2, ...$, as a function of CPU time to illustrate the relative performance of the KN method compared to the NCG scheme. In both cases, the MATLAB Krylov solver, `symmlq` is used with a tolerance of 10^{-5} and the $\mathbf{L_{uu}}$ block is used as a preconditioner. The plots in Figure 3.6 show that the NCG scheme provides comparable computational performance to the KN scheme when choosing larger values of γ. However, as γ is taken smaller, the KN method converges significantly faster to the optimal control solution.

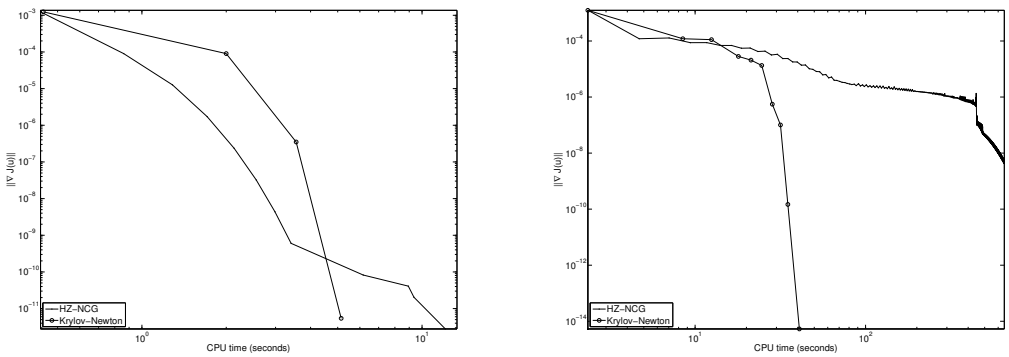

Figure 3.6: Convergence results for $\gamma = 10^{-1}$ (left) and $\gamma = 10^{-4}$ (right) with the KN scheme and the NCG scheme; $\alpha = 10^{-2}$.

3.6 Analysis of the dipole quantum control problem

We present all details of our functional analytic setting and present our results on the existence of an optimal control solution including necessary and sufficient optimality conditions. For ease of presentation, in this section we repeat a few definitions concerning functional spaces. To the best of our knowledge, this is the first systematic and complete analysis of first- and second-order necessary and sufficient optimality conditions for the dipole quantum control problem.

Let $\Omega = (0, \ell)$ be an open interval with $\ell > 0$. Recall that for $q \in [1, \infty)$ the Lebesgue space $L^q(\Omega; \mathbb{C})$ is defined as

$$L^q(\Omega;\mathbb{C}) = \left\{ \varphi : \Omega \to \mathbb{C} \,\middle|\, \varphi \text{ measurable and } \|\varphi\|_{L^q(\Omega;\mathbb{C})} = \left(\int_\Omega |\varphi(x)|_{\mathbb{C}}^q \, dx \right)^{\frac{1}{q}} < \infty \right\}.$$

In particular, we set $\mathcal{H} = L^2(\Omega; \mathbb{C})$, which is a Hilbert space endowed with the inner product

$$(\varphi, \psi)_{\mathcal{H}} = \int_\Omega \varphi(x)^* \psi(x) \, dx \quad \text{for } \varphi,\, \psi \in \mathcal{H}$$

and the induced norm $\|\varphi\|_{\mathcal{H}}$ for $\varphi \in \mathcal{H}$. The Hilbert space $\mathcal{V} = H_0^1(\Omega;\mathbb{C})$ is given by

$$\mathcal{V} = \left\{ \varphi \in \mathcal{H} \,\middle|\, \|\varphi\|_{\mathcal{V}} = \left(\int_\Omega |\varphi'(x)|_{\mathbb{C}}^2 \, dx \right)^{1/2} < \infty \right\}$$

supplied by the inner product

$$(\varphi, \psi)_{\mathcal{V}} = (\varphi', \psi')_{\mathcal{H}} \quad \text{for } \varphi, \psi \in \mathcal{V}$$

and the induced norm $\|\varphi\|_{\mathcal{V}} = \sqrt{(\varphi,\varphi)_{\mathcal{V}}}$ for $\varphi \in \mathcal{V}$. For more details on Lebesgue and Sobolev spaces we refer to [1, 17], for instance.

For $T > 0$ let $Q = \Omega \times (0,T)$. If Y is a Banach space, we define the Bochner space $L^2(0,T;Y)$ as the space of all measurable functions $\varphi : [0,T] \to Y$ satisfying

$$\|\varphi\|_{L^2(0,T;Y)} = \left(\int_0^T \|\varphi(t)\|_Y^2 \, dt \right)^{1/2},$$

where we write $\varphi(t)$ for the function on Y only; see, e.g., [1, 17]. Analogously, the spaces $H_0^1(0,T;Y)$ and $H^1(0,T;Y)$ are defined. In particular, we write $L^2(0,T)$, $H_0^1(0,T)$ or $H^1(0,T)$ if $Y = \mathbb{R}$.

Let us introduce the Hilbert space

$$W(0,T) = \left\{ \varphi \in L^2(0,T;\mathcal{V}) \,\middle|\, \frac{d\varphi}{dt} \in L^2(0,T;\mathcal{V}') \right\},$$

where $\mathcal{V}' = H^{-1}(\Omega;\mathbb{C})$ denotes the dual space of $\mathcal{V} = H_0^1(\Omega;\mathbb{C})$. The space $W(0,T)$ is endowed with the inner product

$$(\varphi, \psi)_{W(0,T)} = \int_0^T (\varphi_t(t), \psi_t(t))_{\mathcal{V}'} + (\varphi(t), \psi(t))_{\mathcal{V}} \, dt \quad \text{for } \varphi, \psi \in W(0,T)$$

and the associated induced norm.

3.6.1 The state equation

Let $u : (0,T) \to \mathbb{R}$ be a given control input function. We suppose that our potential V has the form

$$V(x,t) = V_0(x) + u(t)\, x \quad \text{for } (x,t) \in Q \tag{3.35}$$

where $V_0 : \Omega \to \mathbb{R}$ is fixed. Then, the wave function $\psi : Q \to \mathbb{C}$ is governed by the time-dependent Schrödinger equation:

$$i\,\psi_t(x,t) = -\psi_{xx}(x,t) + V(x,t)\psi(x,t) \qquad \text{for } (x,t) \in Q, \tag{3.36a}$$

$$\psi(0,t) = \psi(L,t) = 0 \qquad \text{for } t \in (0,T), \tag{3.36b}$$

$$\psi(x,0) = \psi_0(x) \qquad \text{for } x \in \Omega, \tag{3.36c}$$

where i is the imaginary unit and $\psi_0 : \Omega \to \mathbb{C}$ is a given initial wave function distribution. We say that ψ is a weak solution to (3.36) if $\psi \in W(0,T)$ holds with $\psi(0) = \psi_0$ in $\mathcal{H}$ and

$$\int_0^T (i\,\psi_t, \varphi)_{\mathcal{V}',\mathcal{V}}\, dt = \int_0^T \int_\Omega \psi_x \varphi_x^* + V\psi\varphi^*\, dxdt \quad \text{for all } \varphi \in L^2(0,T;\mathcal{V}) \tag{3.37}$$

is satisfied, where $(\cdot\,,\cdot)_{\mathcal{V}',\mathcal{V}}$ denotes the dual pairing between $\mathcal{V}$ and $\mathcal{V}'$.

Proposition

Let $\psi_0 \in \mathcal{H}$, $V_0 \in L^2(\Omega)$ and $V(x,t) = V_0(x) + u(t)x$ for $(x,t) \in Q$. Then, there exists a unique weak solution ψ to (3.35) satisfying $\|\psi(t)\|_{\mathcal{H}} = \|\psi_0\|_{\mathcal{H}}$ for all $t \in [0,T]$. If, in addition, $\psi \in L^\infty(\Omega)$ holds, then

$$\|\psi\|_{W(0,T)} \le C\,\left(1 + \|u\|_{L^\infty(0,T)}\right). \tag{3.38}$$

Proof. For the existence of a weak solution to (3.35) we refer the reader to [41]. From (3.37) we infer that

$$(i\,\psi_t(t), \psi(t))_{\mathcal{V}',\mathcal{V}} = \int_\Omega \left|\psi_x(t)\right|_{\mathbb{C}}^2 + V(\cdot\,,t)\left|\psi(t)\right|_{\mathbb{C}}^2 dx \quad \text{for almost all (f.a.a.) } t \in (0,T).$$

Recall that for $\psi \in W(0,T)$ we have

$$(i\,\psi_t(t), \psi(t))_{\mathcal{V}',\mathcal{V}} = \frac{i}{2}\,\frac{d}{dt}\,\|\psi(t)\|_{\mathcal{H}}^2 \quad \text{f.a.a. } t \in (0,T).$$

see, e.g., [17]. By assumption, $V(x,t) \in \mathbb{R}$ f.a.a. $(x,t) \in Q$. Thus,

$$\frac{d}{dt}\,\|\psi(t)\|_{\mathcal{H}}^2 = -2i \int_\Omega \big|\psi_x(t)\big|_{\mathbb{C}}^2 + V(\cdot\,,t)\big|\psi(t)\big|_{\mathbb{C}}^2\,dx \quad \text{f.a.a. } t \in (0,T). \tag{3.39}$$

The left-hand side of 3.39 is purely real, whereas the right-hand side of 3.39 is purely imaginary. Thus, (3.39) can only be satisfied both sides are zero. Consequently, $\|\psi(t)\|_{\mathcal{H}}^2$ is constant, i.e.,

$$\|\psi(t)\|_{\mathcal{H}} = \|\psi_0\|_{\mathcal{H}} \quad \text{f.a.a. } t \in [0,T]. \tag{3.40}$$

Moreover,

$$\begin{aligned}
\|\psi\|_{L^2(0,T;\mathcal{V})}^2 &= -\int_0^T \int_\Omega \big(V_0(x) + u(t)x\big)\big|\psi(x,t)\big|_{\mathbb{C}}^2\,dxdt \\
&\le \big(\|V_0\|_{L^\infty(\Omega)} + \|u\|_{L^\infty(0,T)}\big)\,\|\psi\|_{L^2(0,T;\mathcal{H})}^2 \\
&\le \big(\|V_0\|_{L^\infty(\Omega)} + \|u\|_{L^\infty(0,T)}\big)\,\|\psi_0\|_{\mathcal{H}}^2
\end{aligned}$$

and (3.38) imply (3.36a). □

Next we introduce the control space $\mathcal{U} = H_0^1(0,T)$ supplied with the inner product

$$(u,v)_{\mathcal{U}} = \int_0^T u(t)v(t) + \alpha\dot{u}(t)\dot{v}(t)\,dt \quad \text{for } u,v \in \mathcal{U}$$

with $0 < \alpha \ll 1$ and the induced norm $\|u\|_{\mathcal{U}} = \sqrt{(u,u)_{\mathcal{U}}}$ for $u \in \mathcal{U}$. Use of small values of α allows for controls with larger rate of changes. Since the aim of the optimal control problem will be to drive a particle from one eigenstate to another, it is required that the control is zero at the beginning and the end of the time interval.

Let us define the Hilbert spaces

$$\mathcal{Z} = W(0,T) \times \mathcal{U} \quad \text{and} \quad \mathcal{Y} = L^2(0,T;\mathcal{V}) \times \mathcal{H}$$

endowed with their natural product topology. We identify the dual $\mathcal{Y}'$ of $\mathcal{Y}$ with $L^2(0,T;\mathcal{V}') \times \mathcal{H}$.

To formulate the Schrödinger equation as an abstract operator equation we define the nonlinear operator $e = (e_1, e_2) : \mathcal{Z} \to \mathcal{Y}'$ by

$$(e(z), \varphi)_{\mathcal{Y}',\mathcal{Y}} = \int_0^T \Big((i\,\psi_t, p)_{\mathcal{V}',\mathcal{V}} - \int_\Omega \psi_x p_x^* - V\psi p^*\,dx \Big) dt + (\psi(0) - \psi_0, p_0)_{\mathcal{H}}$$

for $z = (\psi, u) \in \mathcal{Z}$ and $\varphi = (p, p_0) \in \mathcal{Y}$. Recall that the potential V given by (3.35) depends on the control u. For given $u \in \mathcal{U}$ the function ψ is a weak solution to (3.36) if and only if $e(\psi, u) = 0$ in $\mathcal{Y}'$.

Lemma

The operator $e : \mathcal{Z} \to \mathcal{Y}'$ is twice Fréchet-differentiable and its Fréchet derivatives at $\bar{z} = (\bar{\psi}, \bar{u}) \in \mathcal{Z}$ are given by

$$\begin{aligned}(e'(\bar{z})z, \varphi)_{\mathcal{Y}',\mathcal{Y}} &= \int_0^T \Big((i\,\psi_t, p)_{\mathcal{V}',\mathcal{V}} - \int_\Omega \psi_x p_x^* - \big(u(t)x\bar{\psi} + (V_0 + \bar{u}(t)x)\psi\big)p^*\,dx \Big) dt \\ &\quad + (\psi(0), p_0)_{\mathcal{H}}, \\ (e''(\bar{z})(z,\tilde{z}), \varphi)_{\mathcal{Y}',\mathcal{Y}} &= \int_0^T \int_\Omega \big(u(t)x\tilde{\psi} + \tilde{u}(t)x\psi\big)p^*\,dxdt\end{aligned}$$

for any directions $z = (\psi, u)$, $\tilde{z} = (\tilde{\psi}, \tilde{u}) \in \mathcal{Z}$ and for $\varphi = (p, p_0) \in \mathcal{Y}$. In particular, the second Fréchet derivative is Lipschitz-continuous on $\mathcal{Z}$.

Proof. Let $\bar{z} = (\bar{\psi}, \bar{u}) \in \mathcal{Z}$ be arbitrary. Then, by the Sobolev embedding theorem [1, 17] we have $\bar{u} \in C([0,T])$ so that the claim follows by using standard arguments. □

To ensure existence of Lagrange multiplier we will make use of the next result.

Proposition

The linear operator $e_\psi(\bar{z}) : \mathcal{Z} \to \mathcal{Y}'$ is bijective for every $\bar{x} \in \mathcal{Z}$, where e_ψ denotes the partial Fréchet derivative of e with respect to ψ.

Proof. Let $\bar{z} = (\bar{\psi}, \bar{u}) \in \mathcal{Z}$ be chosen arbitrary. The operator $e_\psi(\bar{z})$ is bijective, if the equation $e_\psi(\bar{z})\psi = (F, \phi_0)$ possesses a unique solution $\psi \in \mathcal{Z}$ for any $F \in L^2(0,T;\mathcal{V}')$ and $\phi_0 \in \mathcal{H}$. Thus, ψ solves

$$(i\,\psi_t(t), \varphi)_{\mathcal{V}',\mathcal{V}} + a(t;\psi,\varphi) = (F(t),\varphi)_{\mathcal{V}',\mathcal{V}} \qquad \text{for all } \varphi \in \mathcal{V}, \tag{3.41a}$$

$$\psi(\cdot\,,0) = \phi_0 \qquad \text{in } \Omega, \tag{3.41b}$$

where the time-dependent bilinear form $a(t;\cdot\,,\cdot) : \mathcal{V} \times \mathcal{V} \to \mathbb{C}$ is defined as

$$a(t;\phi,\varphi) = \int_\Omega \phi'(x)\varphi'(x)^* + \big(V_0(x) + \bar{u}(t)x\big)\phi(x)\varphi(x)^*\,dx \text{ for } \phi,\varphi \in \mathcal{V} \text{ and } t \in [0,T].$$

Since $\bar{u} \in H^1(0,T)$ holds and $H^1(0,T)$ is continuously embedded in $C([0,T])$, there exists a constant $c_1 > 0$ such that

$$|\bar{u}(t)| \le c_1 \|u\|_{\mathcal{U}} \quad \text{for all } t \in [0,T]. \tag{3.42}$$

Moreover, $\mathcal{V}$ is embedded into $L^4(\Omega;\mathbb{C})$. Thus, there exists a constant $c_2 > 0$ satisfying $\|\varphi\|_{L^4(\Omega;\mathbb{C})} \le c_2 \|\varphi\|_{\mathcal{V}}$ for all $\varphi \in \mathcal{V}$. Hence,

$$\begin{aligned}\big|a(t;\phi,\varphi)\big| &\le \|\phi\|_{\mathcal{V}}\|\varphi\|_{\mathcal{V}} + \big(\|V_0\|_{L^2(\Omega)} + c_1\|u\|_{\mathcal{U}}\big)\|\phi\|_{L^4(\Omega;\mathbb{C})}\|\varphi\|_{L^4(\Omega;\mathbb{C})} \\ &\le \Big(1 + c_2\big(\|V_0\|_{L^2(\Omega)} + c_1\|u\|_{\mathcal{U}}\big)\Big)\|\phi\|_{\mathcal{V}}\|\varphi\|_{\mathcal{V}} \quad \text{for } \phi,\varphi \in \mathcal{V}.\end{aligned}$$

so that the bilinear form a is bounded. Using Agmon's inequality [37]

$$\|\varphi\|_{L^\infty(\Omega;\mathbb{C})} \le c_3 \|\varphi\|_{\mathcal{H}}^{1/2}\|\varphi\|_{\mathcal{V}}^{1/2} \quad \text{for } \varphi \in \mathcal{V}$$

and Young's inequality [2]

$$ab \le \frac{1}{\varepsilon^p}\frac{a^p}{p} + \varepsilon^q\frac{b^q}{q}$$

with $a = c_3(\|V_0\|_{L^2(\Omega)} + c_1\|u\|_{\mathcal{U}})\|\varphi\|_{\mathcal{H}}$, $b = \|\varphi\|_{\mathcal{V}}$, $\varepsilon = 1$, $p = 4/3$, $q = 4$ we find

$$\begin{aligned} a(t;\varphi,\varphi) &\geq \|\varphi\|_{\mathcal{V}}^2 - \big(\|V_0\|_{L^2(\Omega)} + c_1\|u\|_{\mathcal{U}}\big)\|\varphi\|_{\mathcal{H}}\|\varphi\|_{L^\infty(\Omega;\mathbb{C})} \\ &\geq \|\varphi\|_{\mathcal{V}}^2 - c_3\big(\|V_0\|_{L^2(\Omega)} + c_1\|u\|_{\mathcal{U}}\big)\|\varphi\|_{\mathcal{H}}^{3/2}\|\varphi\|_{\mathcal{V}}^{1/2} \geq c_4\|\varphi\|_{\mathcal{V}}^2 - c_5\|\varphi\|_{\mathcal{H}}^2, \end{aligned}$$

where $c_4 = 3/4$ and $c_4 = 3(c_3(\|V_0\|_{L^2(\Omega)} + c_1\|u\|_{\mathcal{U}}))^{4/3}/4$. Now the claim follows from a complex variant of classical results for linear evolution problems; see, e.g., [15]. □

Remark

It follows from Proposition 3.6.1 that the operator $e'(\bar{z})$ is surjective for every $\bar{z} = (\bar{\psi}, \bar{u}) \in \mathcal{Z}$. This implies that every point $\bar{z}$ is a regular point. ◊

Let $\bar{z} = (\bar{\psi}, \bar{u}) \in$ be arbitrary. By $ker\, e'(\bar{z}) \subset \mathcal{Z}$ we denote the null space of the operator $e'(\bar{z})$. Suppose that $z = (\psi, u) \in ker\, e'(\bar{z})$ is given. Then, ψ satisfies

$$\begin{aligned} i\,\psi_t(x,t) &= -\psi_{xx}(x,t) + \big(V_0(x) + \bar{u}(t)x\big)\psi(x,t) \\ &\quad + u(t)x\bar{\psi}(x,t) && \text{f.a.a. } (x,t) \in Q, && \text{(3.43a)} \\ \psi(0,t) &= \psi(L,t) = 0 && \text{f.a.a. } t \in (0,T), && \text{(3.43b)} \\ \psi(x,0) &= 0 && \text{f.a.a. } x \in \Omega. && \text{(3.43c)} \end{aligned}$$

Multiplying (3.43a) by $\psi(x,t)^*$ and integrating over Ω imply that

$$\begin{aligned} &\frac{1}{2}\frac{d}{dt}\|\psi(t)\|_{\mathcal{H}}^2 + i\,\|\psi(t)\|_{\mathcal{V}}^2 \\ &\qquad = i\int_\Omega \big(V_0(x) + \bar{u}(t)x\big)|\psi(x,t)|^2 + u(t)x\bar{\psi}(x,t)\psi(x,t)^*\,dx. \end{aligned} \tag{3.44}$$

The real part of (3.44) reads

$$\frac{1}{2}\frac{d}{dt}\|\psi(t)\|_{\mathcal{H}}^2 = -u(t)\int_\Omega x\Im m\big(\bar{\psi}(x,t)\psi(x,t)^*\big)\,dx. \tag{3.45}$$

where we have used that $V_0(x)$ as well as $u(t)$ are real-valued. We infer from (3.43) and Young's inequality [2] that

$$\frac{1}{2}\frac{d}{dt}\|\psi(t)\|_{\mathcal{H}}^2 \leq |u(t)|\|\bar{\psi}(t)\|_{\mathcal{H}}\|\psi(t)\|_{\mathcal{H}} \leq \frac{1}{2}\left(|u(t)|^2\|\bar{\psi}(t)\|_{\mathcal{H}}^2 + \|\psi(t)\|_{\mathcal{H}}^2\right).$$

Using Gronwall's inequality we find that

$$\|\psi(t)\|_{\mathcal{H}}^2 \leq e^{t/2}\left(\|\psi(0)\|_{\mathcal{H}}^2 + \frac{1}{2}\int_0^t |u(s)|^2\|\bar{\psi}(s)\|_{\mathcal{H}}^2 ds\right) \tag{3.46}$$

Combining (3.42), (3.43c), and (3.46) we obtain

$$\|\psi(t)\|_{\mathcal{H}}^2 \leq c_2\|u\|_{\mathcal{U}}^2 \quad \text{f.a.a. } t \in [0,T]. \tag{3.47}$$

with the constant $c_2 = c_1 e^{T/2}\|\bar{\psi}\|_{L^2(0,T;\mathcal{H})}^2/2$.

Now we consider the imaginary part of (3.44). Using (3.47) Hölder's and Young's inequality we find

$$\begin{aligned}\|\psi(t)\|_{\mathcal{V}}^2 &= \int_\Omega \big(V_0(x) + \bar{u}(t)x\big)|\psi(x,t)|^2 + u(t)x\Re e\,\left(\bar{\psi}(x,t)\psi(x,t)^*\right) dx \\ &\leq \big(\|V_0\|_{L^\infty(\Omega)} + |\bar{u}(t)|\big)\|\psi(t)\|_{\mathcal{H}}^2 + \frac{1}{2}\left(|u(t)|^2 + \|\bar{\psi}(t)\|_{\mathcal{H}}^2\|\psi(t)\|_{\mathcal{H}}^2\right) \\ &\leq c_2\big(\|V_0\|_{L^\infty(\Omega)} + |\bar{u}(t)|\big)\|u\|_{\mathcal{U}}^2 + \frac{1}{2}\left(|u(t)|^2 + c_2\|\bar{\psi}(t)\|_{\mathcal{H}}^2\|u\|_{\mathcal{U}}^2\right).\end{aligned} \tag{3.48}$$

Estimate (3.48) implies

$$\|\psi\|_{L^2(0,T;\mathcal{V}}^2 \leq \left(c_2\big(T\|V_0\|_{L^\infty(\Omega)} + \|\bar{u}\|_{L^1(0,T)}\big) + \frac{1}{2} + \frac{c_2}{2}\|\bar{\psi}\|_{L^2(0,T;\mathcal{H}}^2\right)\|u\|_{\mathcal{U}}^2. \tag{3.49}$$

Setting

$$c_3 = \sqrt{\max\left(c_2 T, c_2\big(T\|V_0\|_{L^\infty(\Omega)} + \|\bar{u}\|_{L^1(0,T)}\big) + \frac{1}{2} + \frac{c_2}{2}\|\bar{\psi}\|_{L^2(0,T;\mathcal{H}}^2\right)}$$

we conclude from (3.47) and (3.49) that

$$\|\psi\|_{L^2(0,T;\mathcal{H})} + \|\psi\|_{L^2(0,T;\mathcal{V})} \leq c_3\|u\|_{\mathcal{U}}. \tag{3.50}$$

Proposition

Suppose that $\bar{z} \in Z$ and that $V_0 \in L^\infty(\Omega)$. Then,

$$\|\psi\|_{W(0,T)} \leq C_{ker} \|u\|_{\mathcal{U}} \quad \textit{for all } z = (\psi, u) \in ker\, e'(\bar{z})$$

for a constant $C_{ker} > 0$.

Proof. We have already derived an estimate in the $L^\infty(0,T;\mathcal{H})$ and the $L^2(0,T;\mathcal{V})$-norms; see (3.50). Recall that

$$\|\psi_t\|_{L^2(0,T;\mathcal{V}')} = \sup_{\|\varphi\|_{L^2(0,T;\mathcal{V})}=1} \int_0^T (\psi_t(t), \varphi(t))_{\mathcal{V}',\mathcal{V}}\, dt.$$

Now, the proof follows directly from (3.43a) and (3.50). □

3.6.2 The minimization problem

Given an initial wave function ψ_0, we wish to find a control $u \in \mathcal{U}$ such that $\psi(T) \in \mathcal{H}$ is in some sense close to a given desired target wave function $\tilde{\psi} \in \mathcal{H}$. This is to say that the aim of the optimal control problem is to minimize the cost functional $J : \mathcal{Z} \to \mathbb{R}$ given by

$$J(z) = \frac{1}{2}\left(1 - \|P\psi(T)\|_{\mathcal{H}}^2\right) + \frac{\gamma}{2}\|u\|_{\mathcal{U}}^2, \quad z = (\psi, u) \in \mathcal{Z}, \tag{3.51}$$

where the linear and bounded projection operator $P : \mathcal{H} \to \mathcal{H}$ is defined as

$$P\phi = (\tilde{\psi}, \phi)_{\mathcal{H}}\tilde{\psi} \quad \text{for } \phi \in \mathcal{H}$$

and $\gamma > 0$ is a regularization parameter.

Lemma

The cost functional J is twice Fréchet-differentiable. Its Fréchet derivatives at $\bar{z} = (\bar{\psi}, \bar{u}) \in \mathcal{Z}$ are

$$J'(\bar{z})z = -(P\bar{\psi}(T), P\psi(T))_{\mathcal{H}} + \gamma\,(\bar{u}, u)_{\mathcal{U}},$$
$$J''(\bar{z})(z, \tilde{z}) = -(P\tilde{\psi}(T), P\psi(T))_{\mathcal{H}} + \gamma\,(\tilde{u}, u)_{\mathcal{U}}$$

for any directions $z = (\psi, u)$, $\tilde{z} = (\tilde{\psi}, \tilde{u}) \in \mathcal{Z}$ and for $\varphi = (p, p_0) \in \mathcal{Y}$. In particular, the second Fréchet derivative is Lipschitz-continuous on $\mathcal{Z}$.

Proof. The claim follows by standard arguments so that the proof is omitted here. □

The set of admissible solutions of the optimal control problem that will be introduced now is given by

$$\mathcal{F}(\mathbf{P}) = \left\{ z \in \mathcal{Z} \,\middle|\, e(z) = 0 \text{ in } \mathcal{Y}' \right\}.$$

Then, the optimal control problems reads

$$\min J(z) \quad \text{subject to (s.t.)} \quad z \in \mathcal{F}(\mathbf{P}). \tag{$\mathbf{P}$}$$

Theorem

There exists at least one optimal solution $z^\circ = (\psi^\circ, u^\circ)$ to $(\mathbf{P})$.

Proof. By Proposition 3.6.1 the set $\mathcal{F}(\mathbf{P})$ is nonempty. Let $\{z^n\}_{n\in\mathbb{N}}$, $z^n = (\psi^n, u^n)$, be a minimizing sequence in $\mathcal{F}(\mathbf{P})$. Then, $\|u^n\|_{\mathcal{U}}$ is bounded. Recall that $\mathcal{U}$ is (compactly) embedded into $L^\infty(\Omega)$; see [1, p. 144]. By (3.38) the sequence $\{\psi^n\}_{n\in\mathbb{N}}$ is bounded in $W(0,T)$. Thus, there exist a subsequence $\{z^{n_k}\}_{k\in\mathbb{N}}$, $z^{n_k} = (\psi^{n_k}, u^{n_k})$,

and an element $z^\circ = (\psi^\circ, u^\circ) \in \mathcal{Z}$ such that

$$\psi^{n_k} \rightharpoonup \psi^\circ \qquad \text{as } k \to \infty \qquad \text{in } W(0,T), \tag{3.52a}$$

$$u^{n_k} \rightharpoonup u^\circ \qquad \text{as } k \to \infty \qquad \text{in } \mathcal{U}. \tag{3.52b}$$

Since $\mathcal{U}$ is compactly embedded into $C([0,T])$ we conclude from (3.52b) that

$$u^{n_k} \to u^\circ \text{ as } k \to \infty \text{ in } C([0,T]). \tag{3.53}$$

Combining $z^{n_k} \in \mathcal{F}(\mathbf{P})$ for all k, (3.52a) and (3.53) we have

$$0 = \lim_{k\to\infty} (e(z^{n_k}), \varphi)_{\mathcal{Y}',\mathcal{Y}} = (e(x^\circ), \varphi)_{\mathcal{Y}',\mathcal{Y}} \quad \text{for all } \varphi \in \mathcal{Y}.$$

Since the cost functional is weakly lower semicontinuous [35, p. 377] the claim follows directly. □

3.6.3 The reduced problem

Let $u \in \mathcal{U}$ be given. Then, by Proposition 3.6.1 there exists a unique weak solution to (3.35). Thus, the solution operator $\mathcal{S} : \mathcal{U} \to W(0,T)$ is well-defined. Boundedness of $\mathcal{S}$ follows from (3.38). We introduce the so-called reduced cost functional

$$\tilde{J}(u) = J(\mathcal{S}(u), u) \quad \text{for } u \in \mathcal{U}$$

and the reduced problem

$$\min \tilde{J}(u) \quad \text{s.t.} \quad u \in \mathcal{U} \tag{$\tilde{\mathbf{P}}$}$$

which is, in contrast to ($\mathbf{P}$), an unconstrained optimal control problem. If $u^\circ \in \mathcal{U}$ is a solution to ($\tilde{\mathbf{P}}$), then $z^\circ = (\mathcal{S}(u^\circ), u^\circ)$ solves ($\mathbf{P}$).

From Lemmas 3.6.1 and 3.6.2 it follows that $\tilde{J}$ is twice continuously Fréchet-differentiable. In particular, we have at $\bar{u} \in \mathcal{U}$ and

$$(\tilde{J}'(\bar{u}), u)_{\mathcal{U}} = (J_\psi(\mathcal{S}(\bar{u}), \bar{u}), \mathcal{S}'(\bar{u})u)_{W(0,T)} + (J_u(\mathcal{S}(\bar{u}), \bar{u}), u)_{\mathcal{U}} \tag{3.54}$$

for a direction $u \in \mathcal{U}$. We derive from $e(\mathcal{S}(\bar{u}), \bar{u}) = 0$ that

$$0 = e_\psi(\mathcal{S}(\bar{u}), \bar{u})\mathcal{S}'(\bar{u})u + e_u(\mathcal{S}(\bar{u}), \bar{u})u$$

for a direction $u \in \mathcal{U}$. By Proposition 3.6.1 the operator $e_\psi(\mathcal{S}(\bar{u}), \bar{u})$ is invertible. Thus, setting $\bar{z} = (\mathcal{S}(\bar{u}), \bar{u}) \in \mathcal{Z}$ and $\psi = \mathcal{S}'(\bar{u})u \in W(0,T)$ we derive

$$\psi = -e_\psi(\bar{z})^{-1} e_u(\bar{z})u. \tag{3.55}$$

Inserting (3.55) into (3.54) we obtain

$$\begin{aligned}(\tilde{J}'(\bar{u}), u)_{\mathcal{U}} &= -(J_\psi(\bar{z}), e_\psi(\bar{z})^{-1} e_u(\bar{z})u)_{W(0,T)} + (J_u(\bar{z}), u)_{\mathcal{U}} \\ &= (J_u(\bar{z}), u)_{\mathcal{U}} - (e_\psi(\bar{z})^{-\star} J_\psi(\bar{z}), e_u(\bar{z})u)_{\mathcal{Y}'} \\ &= (J_u(\bar{z}) - e_u(\bar{z})^\star e_\psi(\bar{z})^{-\star} J_\psi(\bar{z}), u)_{\mathcal{U}}\end{aligned} \tag{3.56}$$

for a direction $u \in \mathcal{U}$, where $e_\psi(\bar{z})^{-\star} : W(0,T) \to \mathcal{Y}'$ and $e_u(\bar{z})^\star : \mathcal{Y}' \to \mathcal{U}$ denote the adjoint operators of $e_\psi(\bar{z})^{-1} : \mathcal{Y}' \to W(0,T)$ and $e_u(\bar{z}) : \mathcal{U} \to \mathcal{Y}'$, respectively, satisfying

$$\begin{aligned}(e_\psi(\bar{z})^{-\star}\varphi, G)_{\mathcal{Y}'} &= (\varphi, e_\psi(\bar{z})^{-1} G)_{W(0,T)} && \text{for all } (\varphi, G) \in W(0,T) \times \mathcal{Y}', \\ (e_u(\bar{z})^\star F, v)_{\mathcal{Y}'} &= (F, e_u(\bar{z})v)_{\mathcal{Y}'} && \text{for all } (F, v) \in \mathcal{Y}' \times \mathcal{U}.\end{aligned}$$

It follows from (3.56) that the gradient of the reduced cost functional is given by

$$\tilde{J}'(\bar{u}) = J_u(\bar{z}) - e_u(\bar{z})^\star e_\psi(\bar{z})^{-\star} J_\psi(\bar{z}) \quad \text{in } \mathcal{U}.$$

3.6.4 Optimality conditions

Let $u^\circ \in \mathcal{U}$ be a solution to $(\tilde{\mathbf{P}})$. We write $\psi^\circ = \mathcal{S}(u^\circ)$ and $x^\circ = (\psi^\circ, u^\circ)$. To investigate first-order necessary optimality conditions for $(\tilde{\mathbf{P}})$ or $(\mathbf{P})$ we introduce the Lagrange functional $L : \mathcal{Z} \times \mathcal{Y} \to \mathbb{R}$ by

$$L(z, \lambda) = J(z) + \Re e\,(e(z), \lambda)_{\mathcal{Y}',\mathcal{Y}} \quad \text{for } z = (\psi, u) \in \mathcal{Z} \text{ and } \lambda = (p, p_0) \in \mathcal{Y}.$$

It follows from Proposition 3.6.1, Remark 3.6.1 that there exists a unique Lagrange multiplier $\lambda^\circ = (p^\circ, p_0^\circ)$ satisfying together with the optimal solution z° the system

$$L_\psi(z^\circ, \lambda^\circ)z = 0 \qquad \text{for all } z \in \mathcal{Z}, \tag{3.57a}$$

$$L_u(z^\circ, \lambda^\circ)u = 0 \qquad \text{for all } u \in \mathcal{U}, \tag{3.57b}$$

$$e(z^\circ) = 0 \qquad \text{in } \mathcal{Y}'; \tag{3.57c}$$

see, e.g., [24, 28]. We derive from (3.57a) that p° is a weak solution to

$$i\,p_t^\circ(x,t) = -p_{xx}^\circ(z,t) + \big(V_0(x) + u^\circ(t)x\big)p^\circ(x,t) \qquad \text{f.a.a. } (x,t) \in Q, \tag{3.58a}$$

$$p^\circ(0,t) = p^\circ(L,t) = 0 \qquad \text{f.a.a. } t \in (0,T), \tag{3.58b}$$

$$p^\circ(x,T) = i\,\big(P\psi^\circ(T)\big)(x) \qquad \text{f.a.a. } x \in \Omega, \tag{3.58c}$$

in particular, p° lies in $W(0,T)$ and $p_0^\circ = p^\circ(T) \in \mathcal{H}$. Using (3.57b) we obtain that $u^\circ \in \mathcal{U}$ is a weak solution to

$$-\alpha\gamma\ddot{u}^\circ(t) + \gamma u^\circ(t) = -\Re e\bigg(\int_\Omega x\psi^\circ(x,t)p^\circ(x,t)^*\,dx\bigg) \qquad \text{f.a.a. } t \in (0,T), \tag{3.59a}$$

$$u^\circ(0) = u^\circ(T) = 0. \tag{3.59b}$$

Finally, (3.57c) implies that ψ° satisfies the state equation (3.36) with control input $u = u^\circ$.

Remark

Analogously to the proof of Proposition 3.6.1 we obtain that $\|p^\circ(t)\|_{\mathcal{H}} = \|p^\circ(T)\|_{\mathcal{H}}$ f.a.a. $t \in [0,T]$. Thus, using (3.58c) we have $\|p^\circ\|_{L^2(0,T;\mathcal{H})} = \sqrt{T}\,\|P\psi^\circ(T)\|_{\mathcal{H}}$. $\lozenge$

Notice that the gradient of the reduced cost functional is given by

$$\tilde{J}'(u^\circ) = L_u(z^\circ, \lambda^\circ) \quad \text{in } \mathcal{U}.$$

To investigate second-order sufficient optimality conditions we derive from Lemmas 3.6.1 and 3.6.2 that the second Fréchet derivative of the Lagrangian at an optimal solution $z^\circ = (\psi^\circ, u^\circ) \in \mathcal{F}(\mathbf{P})$ and at its associated dual variable $\lambda^\circ = (p^\circ, p_0^\circ) \in \mathcal{Y}$ satisfies

$$L_{zz}(z^\circ, \lambda^\circ)(z, z) = \Re e \int_0^T \int_\Omega 2u(t)x\psi(x,t)p^\circ(x,t)^* \, dxdt - \|P\psi(T)\|_{\mathcal{H}}^2 + \|u\|_{\mathcal{U}}^2 \quad (3.60)$$

for any direction $z = (\psi, u) \in \mathcal{Z}$.

Theorem

Suppose that $z^\circ = (\psi^\circ, u^\circ) \in \mathcal{F}(\mathbf{P})$ is an optimal solution to $(\mathbf{P})$ and that $\lambda^\circ = (p^\circ, p_0^\circ) \in \mathcal{Y}$ is the associated dual variable. If γ is sufficiently large, if $\|p^\circ\|_{L^2(0,T;\mathcal{H})}$ is sufficiently small and if

$$\|P\psi(T)\|_{\mathcal{H}}^2 \le \frac{\gamma}{4} \|u\|_{\mathcal{U}}^2 \quad \textit{for all } z \in \ker e'(z^\circ), \quad (3.61)$$

then the second-order sufficient optimality condition holds, i.e., there exists a constant $\kappa > 0$ such that

$$L_{zz}(z^\circ, \lambda^\circ)(z, z) \ge \kappa \|z\|_{\mathcal{Z}}^2 \quad \textit{for all } z \in \ker e'(z^\circ). \quad (3.62)$$

Proof. We derive from (3.42), (3.50), Proposition 3.6.1, and (3.60) that

$$\begin{aligned} L_{zz}(z^\circ, \lambda^\circ)(z, z) &\ge -\|u\|_{C([0,T])} \|\psi\|_{L^2(0,T;\mathcal{H})} \|p^\circ\|_{L^2(0,T;\mathcal{H})} - \|P\psi(T)\|_{\mathcal{H}}^2 + \gamma \|u\|_{\mathcal{U}}^2 \\ &\ge -c_1 \|u\|_{\mathcal{U}} \|\psi\|_{L^2(0,T;\mathcal{H})} \|p^\circ\|_{L^2(0,T;\mathcal{H})} - \|P\psi(T)\|_{\mathcal{H}}^2 \\ &\quad + \frac{\gamma}{4} \|u\|_{\mathcal{U}}^2 + \frac{\gamma}{2C_{ker}} \|\psi\|_{W(0,T)}^2 \\ &\ge \left(\frac{\gamma}{2} - \frac{c_1}{2} - \frac{c_1 c_3}{2} \|p^\circ\|_{L^2(0,T;\mathcal{H})} \right) \|u\|_{\mathcal{U}}^2 + \frac{\gamma}{2C_{ker}} \|\psi\|_{W(0,T)}^2. \end{aligned}$$

If

$$\kappa = \min\left(\frac{\gamma}{2C_{ker}}, \frac{\gamma}{2} - \frac{c_1}{2} - \frac{c_1 c_3}{2}\|p^\circ\|_{L^2(0,T;\mathcal{H})}\right) > 0 \tag{3.63}$$

holds, then we obtain (3.62). □

Remark

Utilizing Remark 3.6.4 we have the following sufficient condition for Theorem 3.6.4:

If

$$\|P\psi^\circ(T)\|_{\mathcal{H}} < \frac{\gamma}{2c_1 c_3\sqrt{T}} \quad \text{nd} \quad \gamma > 2c_1$$

hold, condition (3.63) is satisfied. ◊

Data: Given a descent direction p and the function $f(a) = \tilde{J}(\mathbf{u} + a\,\mathbf{d})$ and
$f'(a) = \mathbf{d}^\top \nabla \tilde{J}(\mathbf{u} + a\,\mathbf{d})$

Compute a_{max} based on equation 3.34

if $a_{max} > 2$ **then**
- Evaluate $f(1)$ and $f'(1)$;
- **if** $a = 1$ *satisfies SWC* **then**
  - $a^* \leftarrow 1$;
- **else**
  - Construct cubic model on $[0, 1]$ and compute its minimum a_m;
  - Evaluate $f(a_m)$ and $f'(a_m)$
  - **if** $a = a_m$ *satisfies SWC* **then**
    - $a^* \leftarrow a_m$;
  - **else**
    - **if** $[0, a_m]$ *brackets a minimum* **then**
      - $a_r \leftarrow a_m$;
    - **else if** $[0, 1]$ *brackets a minimum* **then**
      - $a_r \leftarrow 1$;
    - **else**
      - $a_r \leftarrow a_{max}$;
    - **end**
    - $a^* \leftarrow bisect(0, a_r)$.
  - **end**
- **end**

else
- $a^* \leftarrow bisect(0, a_{max})$

end

Algorithm 4: Linesearch algorithm

Data: a_l and a_r which bracket a minimum point. $L = a_r - a_l$.

$$f(a) = \tilde{J}(\mathbf{u} + a\,\mathbf{d}) \text{ and } f'(a) = \mathbf{d}^\top \nabla \tilde{J}(\mathbf{u} + a\,\mathbf{d})$$

while $L > tol$ **do**

Compute the midpoint $a_m = \frac{1}{2}(a_l + a_r)$ and evaluate $f(a_m)$ and $f'(a_m)$

if a_m *satisfies SWC* **then**

$a^* \leftarrow a_m$;

end

if $f'(a_l) < 0$ *and either* $f'(a_r) > 0$ *or* $f(a_r) > f(a_l)$ **then**

$a_r \leftarrow a_m$;

else if $f'(a_l) > 0$ *and* $f'(a_r) < 0$ *or* $f(a_r) < f(a_l)$ **then**

$a_r \leftarrow a_m$;

else

$a_l \leftarrow a_m$;

end

$L \leftarrow (a_r - a_l)$

end

Algorithm 5: Bisection minimizer

Table 3.1: Convergence of the SD scheme, the NCG scheme, and the KN scheme to reach the optimal cost $\tilde{J}^* = \tilde{J}(u^*)$.

Iteration	$\tilde{J}_{SD} - \tilde{J}^*$	$\tilde{J}_{NCG} - \tilde{J}^*$	$\tilde{J}_{KN} - \tilde{J}^*$
1	2.4969×10^{-1}	2.4969×10^{-1}	2.4969×10^{-1}
2	1.3070×10^{-2}	1.3070×10^{-2}	1.5346×10^{-2}
3	6.4184×10^{-3}	6.4184×10^{-3}	5.1099×10^{-3}
4	5.5337×10^{-3}	5.3438×10^{-3}	2.2381×10^{-4}
5	4.8170×10^{-3}	3.1011×10^{-3}	1.8383×10^{-4}
6	4.2081×10^{-3}	2.3384×10^{-3}	1.6253×10^{-5}
7	3.6768×10^{-3}	1.2475×10^{-3}	2.7534×10^{-6}
8	3.2177×10^{-3}	9.1869×10^{-5}	3.3921×10^{-7}
9	2.8141×10^{-3}	5.9258×10^{-5}	4.7022×10^{-9}

Table 3.2: Convergence of the SD scheme and the KN scheme with respect to $||\nabla \tilde{J}(u)||$

Iteration	$\|\|\nabla \tilde{J}_{SD}(u)\|\|$	$\|\|\nabla \tilde{J}_{KN}(u)\|\|$
1	1.8615×10^{-4}	1.8615×10^{-4}
2	6.5263×10^{-5}	6.5263×10^{-5}
3	6.0031×10^{-5}	2.4732×10^{-5}
4	2.3535×10^{-5}	1.5557×10^{-5}
5	2.8106×10^{-5}	1.2316×10^{-6}
6	1.5703×10^{-5}	1.0977×10^{-8}
7	1.7062×10^{-5}	3.5480×10^{-13}
8	1.0322×10^{-5}	2.0009×10^{-17}
9	1.3312×10^{-5}	0
50	1.9114×10^{-7}	0

Chapter 4

Control of open quantum systems

The principal aim of quantum control is to bring about a desired change in the state of the system through the use of a control such as an electric or magnetic field. Since non-relativistic quantum dynamics are described by the solution to the time-dependent Schrödinger equation, a linear homogeneous partial differential equation, any control function must appear within the Hamiltonian operator, giving the control problem a bilinear structure. In the last twenty years there has been a increasing body of literature on the application of the optimal control framework to quantum mechanical problems with an emphasis on closed quantum systems and systems with two or three states. Recently, Pechen[67] et. al. have investigated the control landscapes for open quantum systems with two states and Roloff[68] have considered a number of approaches for the control of an open system with applications to quantum bits and gates. This chapter considers optimal control of open quantum systems with a single particle in the context of a PDE-constrained optimization to obtain high-yield controls.

Quantum systems may be either open or closed. A closed quantum system is understood to be isolated from its environment and exhibits conservation laws, such

as the a conserved total number of particles; this typically does not apply in open systems. Even when the physical processes being modeled can not influence the total number of particles, it may be advantageous to use an open system model for computational efficiency. If one wishes to model the dynamics of an atom, for example, there is the possibility of photoionization and dissociation which results when a control field excites an electron to the point where it has sufficient energy to escape its localized state about the nucleus. In such a situation, the electron does not cease to exist, but it may computationally inefficient to model the atom and the proportionally much larger domain which contains it. The open system approach allows one to truncate the domain to only the region of interest and incorporate an interaction between the system and an environment. In the case of photoionization, a loss mechanism would be included in the model to characterize the escape of the electron from the influence of the nuclear potential.

Semiconductor quantum wells are formed by the epitaxial growth of two or more materials with different conduction or valence band energies. Considering electrons, the structure will consist of a well layer sandwiched between barrier layers with a larger conduction band energy. An electron may be confined within the well region if it lacks the necessary energy to move about in the surrounding barrier region, however, the potential difference is finite, and an excitation may promote the electron to a higher energy state where it may escape the well. Because such quantum wells typically have a width on the order of 30-150Å, while the thickness of the semiconductor wafer is on the order of hundreds of microns, it is not computationally efficient to model the entire structure, when one is only interested in transitions within the well region.

There are varied approaches to modeling an open system. Since it is not possible to completely discretize unbounded domains, typically one models the global system as a local one interacting with an environment. Although matter is not created

or destroyed, the total number of particles in the local system is no longer a fixed constant as they may be lost to the environment by some escape mechanism. As such open quantum systems exhibit two characteristics which are dissimilar to closed systems. First, the semigroup operator is not unitary because the continuity equation will contain sink or source terms which couple the local system to the environment. Second, open systems no longer have a purely real point spectrum, but in general have a real continuous spectrum and can also have discrete complex eigenvalues called *resonances*.

To model the coupling of the local system to the environment, it is necessary to introduce a loss mechanism such that $||\psi(\cdot, t)||$ is monotonically decreasing in time. One approach is to truncate the computational domain and impose an absorbing boundary condition. The fundamental idea is to impose a condition at the boundary which either gives the exact or approximate behavior that would be exhibited if the domain were to be extended indefinitely. The method of Jiang [71] accomplishes this by formulating a convolution integral in time which relates the value of the wavefunction to its derivative. When the potential is not asymptotically constant and is varying in time, as is the case of the present work, this approach is does not appear to be tractable. Instead we employ the method of complex exterior scaling, which was first introduced by Simon[69]. Subsequently, it was shown that perfectly matched layers[70] could be implemented based on this idea. The principle is to deform the spatial coordinates from an interval on the real line to a contour in the complex plane along which the wavefunction exhibits asymptotic decay. The domain may then be truncated as outward propagating waves will be absorbed by the PML.

Here we consider as a model problem, a particle confined by the Morse potential. The Morse potential is a one-dimensional model for, among other things, the potential energy of a diatomic molecule. Since it is possible dissociate a diatomic molecule with sufficiently intense fields, it is a finite potential and therefore there exists both

discrete and continuous spectrum. The discrete spectrum corresponds physically to a bound state, which means that the diatomic molecule is bound together an will not dissociate without provocation. The continuous spectrum corresponds to unbound states and indicate that the two atoms are no longer bound to one another although may still influence each other's behavior, they are free to move apart from one another in this regime.

The Morse potential has the form

$$V(x) = V_0(1 - e^{a(x_{eq}-x)})^2, \quad 0 \leq x < \infty$$

where V_0 is the depth of the potential well, x_0 is called the equilibrium bond distance and is the location of the minimum of the potential. The factor a determines the width of the potential well and also the height at the origin $x = 0$.

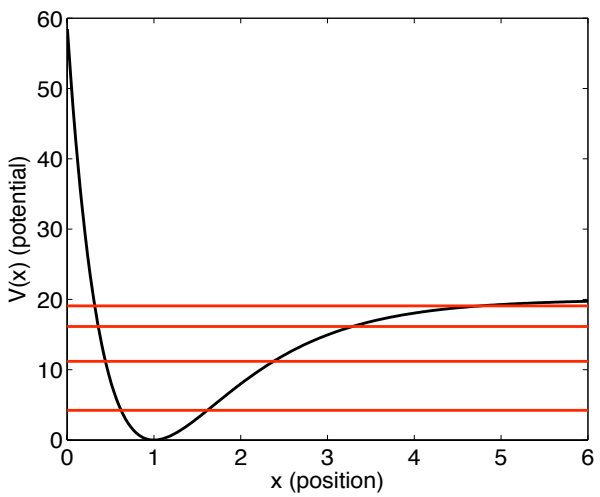

Figure 4.1: Sample Morse potential for the parameters $V_0 = 20$, $a = 1$, and $x_0 = 1$. The red lines indicate the locations of the bound states.

The Morse potential is an interesting example as it is one of the few potentials for which closed form expressions are known for the eigenfunctions and eigenvalues, however, these expressions are complicated and are expressed in terms of Laguerre

polynomials and Gamma functions. Instead of employing the analytical solutions, we will rely here on high order spectral element methods for approximately computing eigenpairs.

To form the PMLs with the method of complex exterior scaling, we deform the spatial coordinate from the real line to a continuous contour C in the complex plane. The complex-valued spatial coordinate becomes

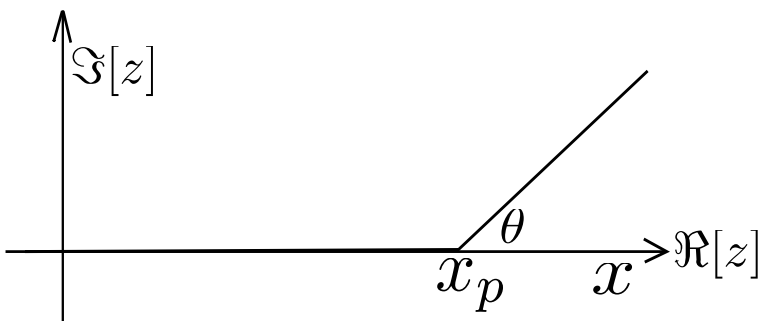

Figure 4.2: Perfectly matched layer using the method of complex exterior scaling.

$$z(x) = \begin{cases} x & \text{if} \quad 0 < x \leq x_p \\ x + (x - x_p)e^{i\theta} & \text{if} \quad x_p < x < x_{max} \end{cases} \tag{4.1}$$

When using the complex coordinate, $z(x)$ will replace x. The state equation becomes

$$i\partial_t \psi(z,t) = \{-\partial_z^2 + V(z) + u(t)z\}\psi(z,t) \tag{4.2}$$

In the undeformed region where $x \leq x_p$, this is exactly identical to the original state equation, however, inside a PML layer, $z \to x^{i\theta}$ and $\partial_z \to e^{-i\theta}\partial_x$. The state equation becomes

$$i\partial_t\psi(x,t) = \{-e^{-i2\theta}\partial_x^2 + V(xe^{i\theta}) + u(t)xe^{i\theta}\}\psi(x,t) \tag{4.3}$$

In general the potential term $V(xe^{i\theta})$ could be a cause for concern for transcendental $V(x)$, however, the Morse potential rapidly approaches a constant for increasing x and if the point x_p is chosen be sufficiently large that $V(x) \approx V_0$, the state equation in the PML reduces to

$$i\partial_t\psi(x,t) = \{-e^{-i2\theta}\partial_x^2 + V_0 + u(t)xe^{i\theta}\}\psi(x,t) \tag{4.4}$$

Since the deformation of the spatial coordinate is continuous, $\psi(x,t)$ will also be globally continuous, however, discontinuity in $\frac{dz}{dx}$ at the point x_p will lead to a discontinuity in $\partial_x\psi$ at this points as well.

Now that we have an open quantum system, there are two sorts of objectives one may consider for the control problem. In the presence of multiple bound states, we can again try to compute a control which drives the state of the system between bound states, with the added difficulty now that as the control amplitude becomes large, there is the possibility of losing the particle to the environment via tunneling or field-assisted thermionic emission [76]. In the finite potential case, there are finitely many bound states which are represented by eigenfunction $\phi_1, ..., \phi_n$ and the cost functional for maximizing the probability of finding a particle in a state k would correspond to minimizing the term $-\|\mathcal{P}_k\psi\|^2$, where $\mathcal{P}_k$ is the orthogonal projection operator onto the kth eigenstate and its action is defined as

$$\mathcal{P}_k\psi(x,t) = \phi(x)\int_\Omega \bar{\phi}_k(x)\psi(x,t)d\Omega \tag{4.5}$$

where $\phi_k(x)$ is the kth eigenfunction. If the eigenfunctions are bound states, they may are real functions and $\phi_k(x) = \bar{\phi}_k(x)$.

An alternate objective might be to intentionally drive the particles apart by inducing a transition from a bound state into the continuum. Ideally we would like to avoid dealing with the complicated nature of the continuous spectrum since the wavefunctions which satisfy $\mathcal{H}\psi = \lambda\psi$ where $\lambda > V_0$ are not elements of L^2 and we will need a more sophisticated framework than that of Hilbert spaces to work with them.

We do know that if the wavefunction is not localized in the confining potential, part of it will reach the PML and be attenuated and the total probability $\|\psi(\cdot, t)\|^2$ will become smaller than unity and since this is an observable quantity, we could attempt to minimize it. Another reasonable choice is the use the fact that the bound eigenfunctions span a subspace $\Phi_B = \{\phi_1, ..., \phi_n\}$ and we can define an orthogonal projection onto Φ_B with the operator

$$\mathcal{P}_B\psi(x,t) = \sum_{k=1}^{n} \phi_k(x) \int_\Omega \bar{\phi}_k(x)\psi(x,t)d\Omega \tag{4.6}$$

With this operator, we do not need to know the generalized eigenfunctions which correspond to the continuous spectrum or how to properly normalize them; it suffices to know that if ϕ_c is a such a function, that $\phi_c \perp \Phi_B$. Since $\mathcal{P}_B$ is an orthogonal projector it follows that $I - \mathcal{P}_B = \mathcal{P}_{B^\perp}$. Thus if we want to drive the state of the system into the continuum, that this can be achieved by minimizing the functional $\|\mathcal{P}_B\psi\|^2$.

4.1 Regularity and discretization

An L^2 control regularization term is most commonly used in the literature and although the space L^2 admits discontinuous controls, the standard problem formulation only allows discontinuities at the end times $t = 0, T$. In a gradient-based optimization scheme, the control function at any iteration is in the span of the the initial

guess of the control and the gradient at each step. It has been proven by Degani et al[83] that a piecewise constant optimal control is globally constant. This follows from the fact that a bounded control yields a continuous gradient on the open interval $(0, T)$. Discontinuities in the optimal control can and usually do occur at the initial and final times. Their proposed solution is to write the control in a suitable basis functions. Their motivation for time-discontinuous controls is that they can be produced by laser pulse shapers. An important consequence of their proof, however, is that the optimal control in L^2 is, in fact a $C^\infty([0, T])$.

Two commonly used methods for integrating the Schrödinger equation in time are the Crank-Nicolson and Strang splitting methods as used in chapter 2. These are both second-order accurate in time, but unitary provided the discretized Hamiltonian is symmetric. These two schemes are, however, not commutative in the sense of optimal control problems. By this, we mean that the discretized optimality system is not the same as the optimality conditions of the discretized cost as was observed for the Crank-Nicolson method in the preceding chapter.

In the current work, we consider arbitrarily high-order time integration via the DG discretization; this method is detailed in appendix C. It has been shown [85, 86], that DG time discretization of parabolic equations is indeed commutative in time. This is convenient in the sense that we can simply discretize the optimality system with DG in time and continuous Galerkin (CG) methods in space and not incur any discretization error in the gradient and Hessian.

DG time discretization does not inherently preserve the spatial L^2 norm of the wavefunction as the Crank-Nicolson and Strang-Splitting methods do. A potential consequence of this can be that an optimal control is computed which reduces the cost functional in an aphysical way with numerical dissipation. This can be expected with controls that are either very large or are too rapidly changing in time. It should be remarked that this is mostly a problem for closed quantum systems which are

inherently non-dissipative. In the lossy open system case, the loss to the environment tends to be the dominant mechanism and we generally do not need to worry about numerical dissipation. For purposes of completeness we nonetheless present an approach to restricting numerical dissipation.

One possible approach to preventing this behavior would be to carry out a numerical analysis on the DG-discretized Schrödinger equation and establish appropriate constraints on the control function such that the state variable reasonably satisfies conservation of probability. As an alternative, we provide a discretization-independent strategy of imposing a constraint on the state itself. Ideally, the total probability should be exactly 1 at all times, but this may be relaxed slightly with the point-wise time constraint that $1 - \rho \leq (\bar{\psi}, \psi) \leq 1 + \rho$ where ρ is chosen to be small positive number.

This inequality constraint is introduced approximately by adding a penalty term to the cost functional. Let

$$f_{\min}(t) := \min(0, (\bar{\psi}, \psi) - 1 + \rho), \quad f_{\max}(t) := \max(0, (\bar{\psi}, \psi) - 1 - \rho) \tag{4.7}$$

Including these terms gives the cost functional

$$J(\psi, \bar{\psi}, u) = \int_0^T \frac{\gamma}{2} u^2 + (\bar{\psi}, \mathcal{A}\psi) + \frac{c}{2}[f_{\min}^2 + f_{\max}^2] dt \tag{4.8}$$

where c is chosen to be large and the formulation of the operator $\mathcal{A}$ is discussed in appendix A.

We wish to minimize this cost functional over all ψ and u subject to the equality constraint

$$(\partial_t + i\mathcal{H}(u))\psi(x,t) = 0, \quad \psi(x,0) = \psi^0(x)$$

The complex conjugate of the state equation must also hold by construction and so for a real-valued Lagrangian, two Lagrange multipliers are necessary, although they

are simply conjugates of one another. The Lagrangian is

$$L(\psi, \bar{\psi}, u, p, \bar{p}) = J(\psi, \bar{\psi}, u) + \int_0^T (p, (\partial_t + i\mathcal{H})\psi) + (\bar{p}, (\partial_t - i\mathcal{H})\bar{\psi})dt \tag{4.9}$$

Taking first variations with respect to the state and control and setting the resulting equations to zero gives the first order optimality system. As a point of comparison, we give here the equation for the Lagrange multiplier and the reduced gradient for the reduced form $\tilde{J}(u) = J(\psi(u), \bar{\psi}(u), u)$ of the original cost functional A.4 and the new cost A.19. The adjoint equation is

$$(\partial_t - i\mathcal{H})p = \mathcal{A}^*\bar{\psi} + c[f_{\min} + f\max]\bar{\psi}, \quad p(x, T) = 0 \tag{4.10}$$

and the corresponding reduced gradient is

$$\nabla\tilde{J}(u) = \gamma u + 2\Im[(\mathcal{P}_\varphi \mathcal{H}_u \bar{\psi} - \mathcal{H}_u p, \psi)] \tag{4.11}$$

It is interesting to note that although the two formulations produce completely different Lagrange multipliers, given a control u, the reduced gradient will be identical and as with the cost itself, the reduced gradient is independent of the trajectory function.

To take second variations, the Wirtinger calculus tells us to compute the Jacobian of the Hermitian conjugate of the gradient. This gives rise to a Hermitian KKT Hessian. Writing out the full second-order optimality conditions gives the following system, where the blocks are specified in appendix B.

$$\begin{pmatrix} L_{\psi\psi} & L_{\psi\bar{\psi}} & L_{\psi u} & 0 & L_{\psi\bar{p}} \\ L_{\bar{\psi}\psi} & L_{\bar{\psi}\bar{\psi}} & L_{\bar{\psi}u} & L_{\bar{\psi}p} & 0 \\ L_{u\psi} & L_{u\psi} & L_{uu} & L_{up} & L_{u\bar{p}} \\ 0 & L_{p\bar{\psi}} & L_{pu} & 0 & 0 \\ L_{\bar{p}\psi} & 0 & L_{\bar{p}u} & 0 & 0 \end{pmatrix} \begin{pmatrix} \delta\psi \\ \delta\bar{\psi} \\ \delta u \\ \delta p \\ \delta\bar{p} \end{pmatrix} = - \begin{pmatrix} 0 \\ 0 \\ L_u^\dagger \\ 0 \\ 0 \end{pmatrix} \tag{4.12}$$

Using the Schur reduction on the second-order optimality conditions, we can express find governing equations for the variation in state and adjoint variables and also the action of the reduced Hessian on a test function. The differential change in the wave function given a differential change in the control δu satisfies and inhomogeneous Schrödinger-like equation.

$$(\partial_t + i\mathcal{H})\delta\psi = -i\mathcal{H}_u\delta u\psi, \quad \delta\psi(x,0) = 0, \quad \delta\psi(\partial\Omega,t) = 0 \tag{4.13}$$

Much like the wave function itself, the variation of the wave function is identical to the one obtained for the standard cost functional. The differential change in the adjoint variable satisfies the PDE

$$\begin{aligned}(\partial_t - i\mathcal{H})\delta p = \; & i\mathcal{H}_u\delta u p + (\mathcal{A}^* + c[f_{\max} + f_{\min}])\delta\bar{\psi} \\ & +(\mathcal{A}_u^*\delta u + 2c[\chi_{\max} + \chi_{\min}]\Re(\psi,\delta\bar{\psi}))\bar{\psi} \\ & p(x,T) = 0, \quad p(\partial\Omega,t) = 0\end{aligned} \tag{4.14}$$

Where the characteristic functions are defined by

$$\chi_{\max} = \begin{cases} 1 & \text{if } (\bar{\psi},\psi) > 1+\rho \\ 0 & \text{else} \end{cases} \qquad \chi_{\min} = \begin{cases} 1 & \text{if } (\bar{\psi},\psi) < 1-\rho \\ 0 & \text{else} \end{cases} \tag{4.15}$$

The action of the reduced Hessian on a test function δu is most compactly expressed as

$$[\nabla^2\tilde{J}(u)]\delta u = \gamma u + 2\Re[(i\mathcal{H}_u p - \mathcal{A}_u^\dagger\bar{\psi},\delta\psi) + i(\mathcal{H}_u\psi,\delta p)] \tag{4.16}$$

This allows the use of an iterative solver such as a Krylov method to approximately compute the δu which satisfies the equation $[\nabla^2\tilde{J}(u)]\delta u = -\nabla\tilde{J}(u)$.

For the potential depicted in figure 4.1, an optimal control was computed for the bound–to–bound and bound–to–continuum transition. Figure 4.1 shows the control for driving the ground state to the first excited state in time $T = 2$ in the left panel. In the right panel, the green curve shows the initial state and the blue the state at

the final time. The surface of $|\psi(x,t)|^2$ is shown in 4.1 and one may clearly see the single mode of the ground state being split into the two modes of the excited state.

The problem of computing controls for a bound–to–continuum transition is, in some sense, much easier than bound–to–bound, since there are infinitely many acceptable target states. Simply applying a sufficiently intense static field would eventually be sufficient to cause the state to leak out of the confining potential. Nonetheless, we consider the optimal control problem where we wish to minimize the projection onto the bound states at the final time and see a suitable control function in the left panel of figure 4.1 and the corresponding final time behavior of the state in the right panel. The sharp kink in the blue curve occurs at the PML boundary as this region is highly lossy. The interface can also be seen clearly as the wavefunction impinges on the PML at $x = 10$ in the space-time plot in figure 4.1.

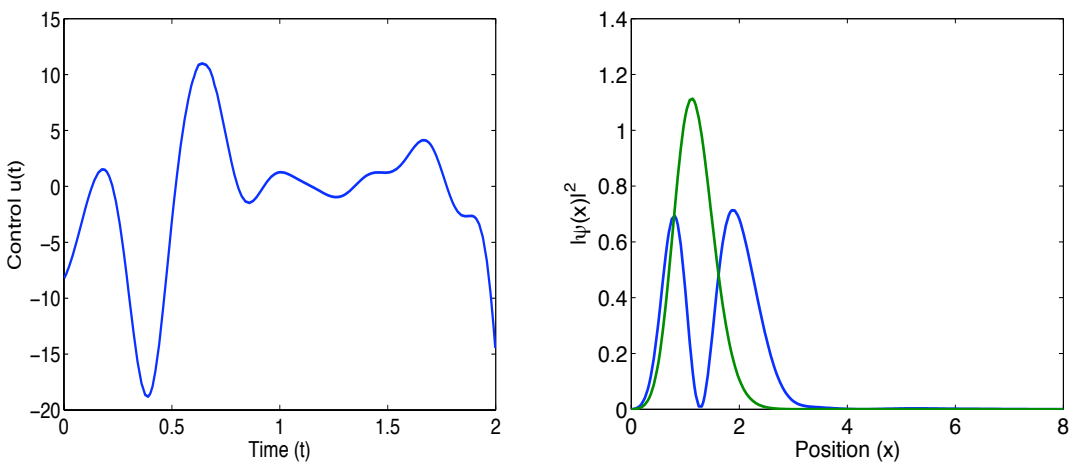

Figure 4.3: *Left:* Optimal control function $u^*(t)$ which drives the ground state to the first excited state. *Right:* Final time state behavior corresponding to the control.

One observation should be made regarding the use of high-order time discretization for the optimal control problem. Although it is possible to capture more high frequency oscillations with the discontinuous Galerkin schemes than it is with Crank-Nicolson, there is an unfortunate consequence of high order methods. As the Hessian

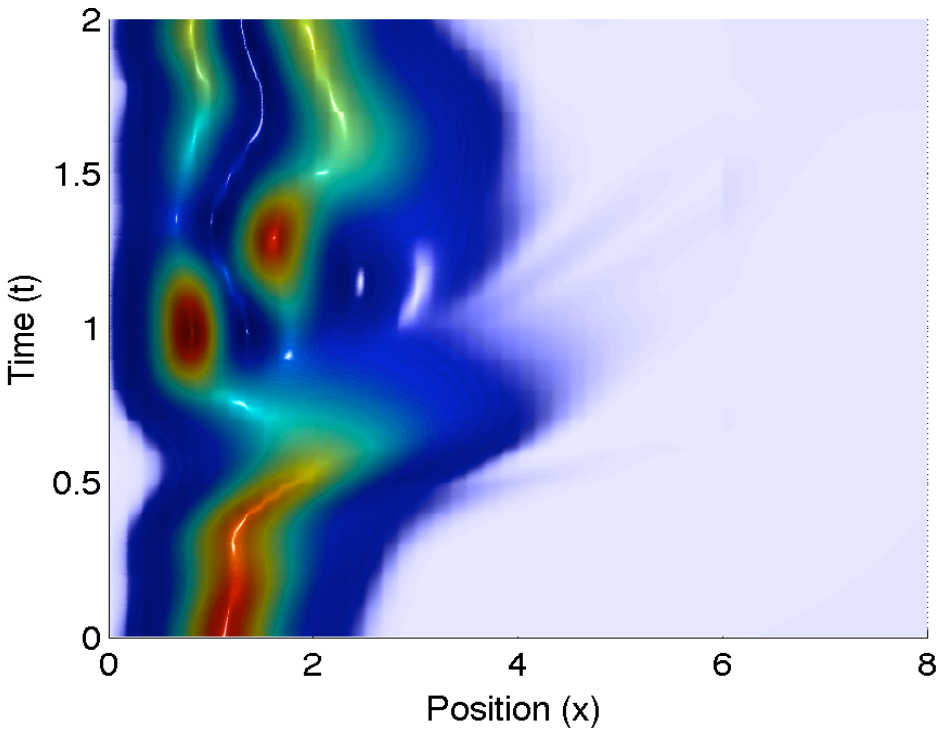

Figure 4.4: Space-time behavior of $|\psi(x,t)|^2$ as it is driven by the optimal control.

of the optimality system is essentially an integro-differential operator, its spectral radius will tend to be quite large for high-order discretizations. As such, the convergence rate of Krylov methods to compute the Newton search direction will be greatly diminished. From numerical experiments with DG time discretization, it usually takes far longer to compute a single Newton step than it does to compute a suitable minimizer with a NCG method with linesearches.

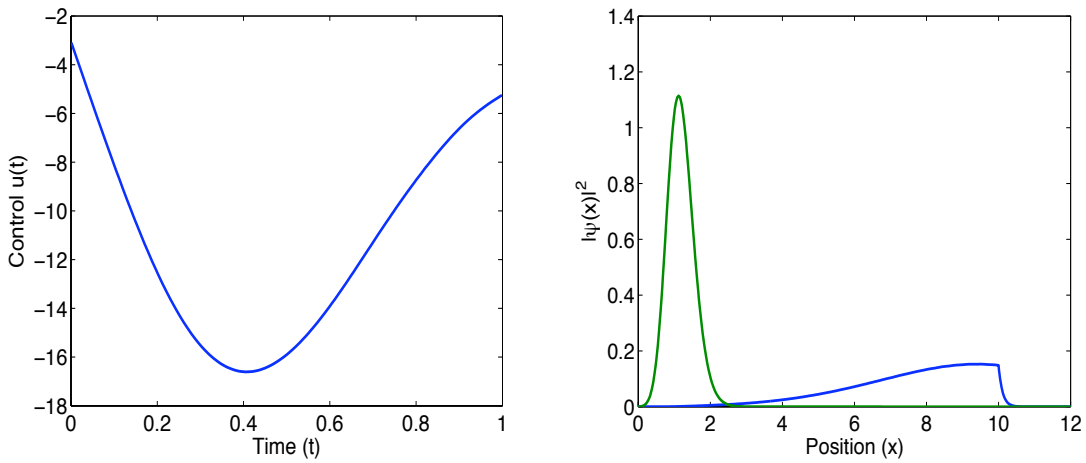

Figure 4.5: *Left:* Optimal control function $u^*(t)$ which drives the ground state to the continuum. *Right:* Final time state behavior corresponding to the control.

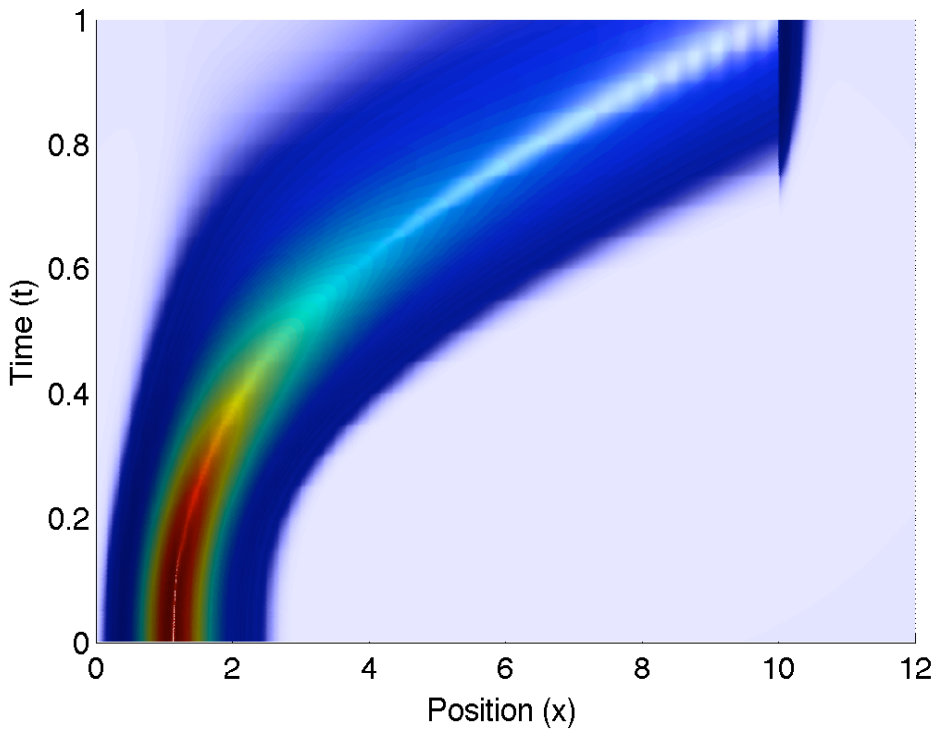

Figure 4.6: Space-time behavior of $|\psi(x,t)|^2$ as it is driven by the optimal control.

Chapter 5

Control of higher-dimensional systems

In higher spatial dimensions, generally the control is not simply scalar valued amplitude, but is rather some vector valued function. Generalizing the dipole control problem to the situation $\mathbf{x} \in \mathbb{R}^n$, the control will be a time–varying vector–valued function $\mathbf{u} : [0, T] \to \mathbf{R}^n$. This can be written as $\mathbf{u}(t) = [\ u_1(t) \quad \cdots \quad u_n(t)\ ]$.

$$\{i\partial_t + \Delta - V_0(\mathbf{x}) - \mathbf{u}(t) \cdot \mathbf{x}\}\, \psi(\mathbf{x}, t) = 0, \quad \psi(\mathbf{x}, t) = \psi_0(\mathbf{x}) \tag{5.1}$$

A suitable cost functional in this situation is

$$J(\psi, \bar{\psi}, \mathbf{u}) = 1 - (\bar{\psi}, \mathcal{P}\psi)_T + \frac{\gamma}{2} \sum_{j=1}^{n} \|u_j\|^2_{H_0^1} \tag{5.2}$$

The spatial discretization is carried out by first partitioning the domain into a simplex mesh and then using a nodal Galerkin approximation on each element.

Figure 5.3 shows the vector control function for driving the first state to the

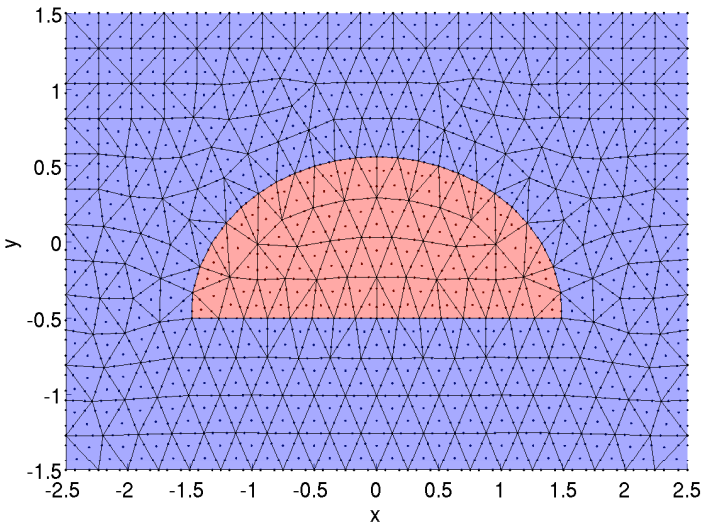

Figure 5.1: Simplex mesh for the quantum dot control problem. Grid points are depicted for cubic trial functions.

second state in time $T = 4$. The time evolution of the level sets of $|\psi(x, y, t)|^2$ are plotted in the corresponding right panel.

The parity of the potential imposes some restrictions on the types of controls that can induce certain state–to–state transitions. For the sample structure shown, the first, third, and fourth states are all symmetric in the x-direction and the second state is the only bound state which is anti-symmetric in the x direction. As a consequence, it is not possible to drive a particle into the second state from any of the other bound states without a control component in the x-direction. Moreover, one can generalized this to the following proposition.

Proposition

Supposing a piecewise smooth control, the probability of a particle occupying the second eigenstate can not be influenced by controls with only a y-component.

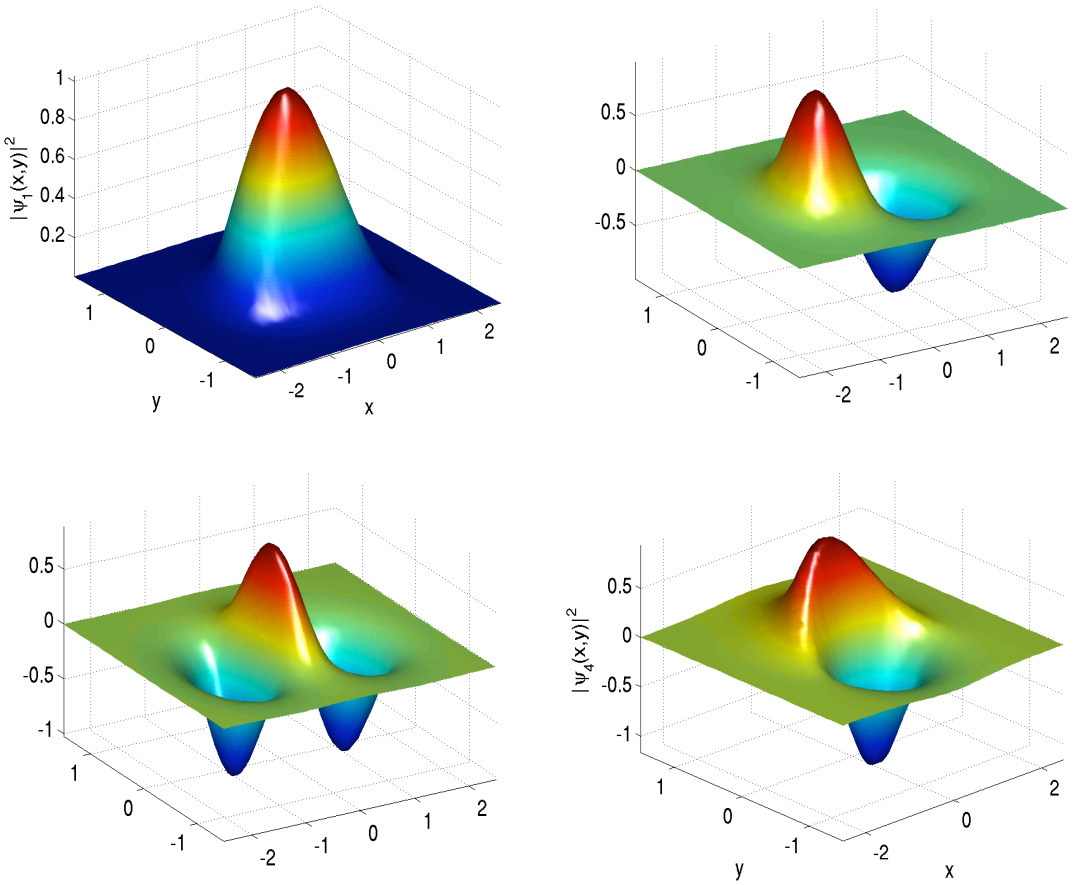

Figure 5.2: The first four bound states of the lens-shaped quantum dot.

Proof. Let $|r(t)|^2 = |(\psi, \phi_2)|^2$ be the probability of finding the particle in second state ϕ_2 corresponding to eigenvalue λ_2 and let $\psi(0)$ have no projection onto ϕ_2. Then we can write

$$\begin{aligned} r(t) &= (\psi, \phi_2) \\ \dot{r}(t) &= (\dot{\psi}, \phi_2) = -i\lambda_2 r(t) - iu(t)(\psi, y\phi_2) \end{aligned} \tag{5.3}$$

If we evaluate $r(0)$, we see that it is zero due to the orthogonality of the initial state and the target state. Similarly, $\dot{r}(0) = 0$ because the first term is zero and in the second term we have a the product of functions in the integrand are antisymmetric in x, so the inner product is zero. Each time we differentiate, new terms are introduced

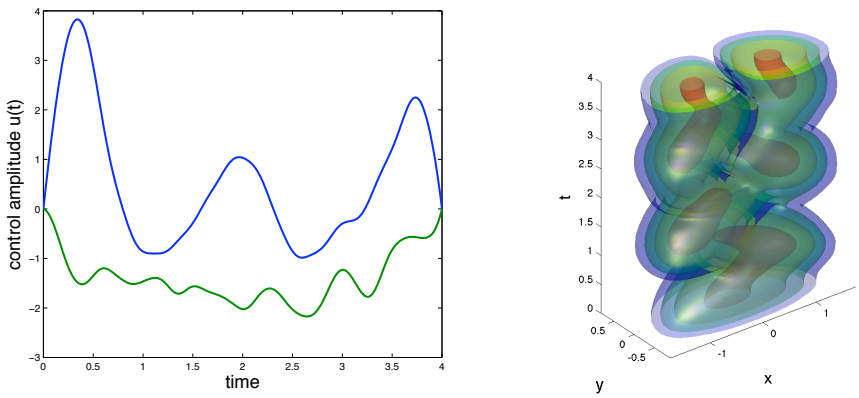

Figure 5.3: Optimal control from for state $1 \rightarrow 2$ transition

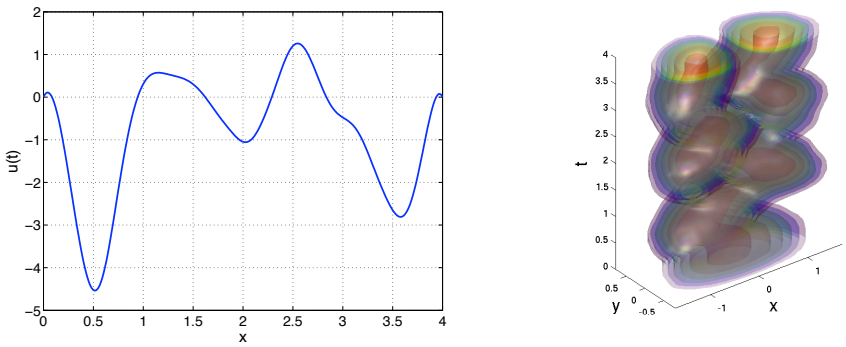

Figure 5.4: Optimal control from for state $1 \rightarrow 2$ transition

in the inner product, however, in every case, the resulting integrand is antisymmetric in x and consequently $r^{(k)}(0) = 0$ for all k. Since all coefficients in the Taylor series are zero, it must be identically zero. □

It is, however, possible to induce a transition from the first state to the second state using a control which has only an x-component. This is shown in figure 5.4. This would correspond to a state transition in a quantum dot that is induced by normally incident light, as the electric field would then be polarized in the x-direction.

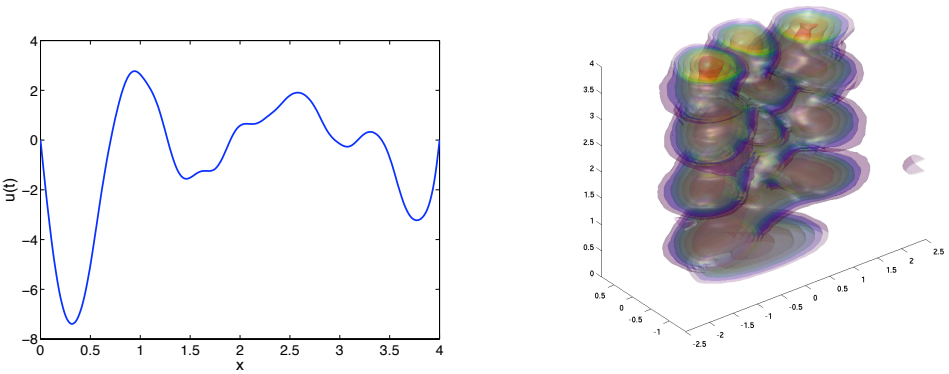

Figure 5.5: Optimal control from for state $1 \rightarrow 3$ transition

Chapter 6

An efficient solver for quantum control problems

In most of the literature involving numerical solution of the TDSE, various spatial discretizations ranging from second-order differences to full global spectral expansions have been used, however, the typically low order methods such as Crank-Nicolson or Strang splitting are used for the time discretization. This is somewhat counter-intuitive when one considers the structure of the TDSE. If we simply consider the evolution equation for a free particle, we have

$$i\partial_t \psi(\mathbf{x}, t) = -\Delta\psi(\mathbf{x}, t) \tag{6.1}$$

for which the solution on the infinite space-time domain has the form of the complex exponential

$$\psi(\mathbf{x}, t) \sim \exp(i\mathbf{k} \cdot \mathbf{x} - i\omega t) \tag{6.2}$$

Plugging this ansatz function into the TDSE gives us the relationship $\omega = \mathbf{k} \cdot \mathbf{k}$ which indicates that the frequency of oscillations in time scales as the square of the frequency of oscillations in space and that the disparity becomes greater with higher

spatial dimensions. As a consequence, it is quite reasonable to expect that the for comparable order discretizations in space and time, a much finer grid will be needed in time than in space. A very fine time grid in turn means needing a high number of degrees of freedom for the control function in the optimal control problem and with it slower convergence. Finally, it has been established [83] that the optimal control should be a C^∞ function. This motivates the use of a global spectral discretization in time as it is well-known that a spectral discretization will provide an optimal approximation to a smooth function with the fewest terms.

In the optimal control problem, we are concerned with a more general state equation than the free particle TDSE above. We are primarily interested in developing efficient, spectrally-accurate solvers for equations of the form

$$i\partial_t\psi(\mathbf{x},t) = \{-\Delta + V_0(\mathbf{x}) + \mathbf{u}(t)\cdot\mathbf{x}\}\psi(\mathbf{x},t), \quad \psi(x,0) = \psi_0(x) \tag{6.3}$$

For purposes of simple illustration, however, we consider a single spatial dimension and zero confining potential. We are interested in pure initial states so $\psi_0(x)$ will be an eigenfunction of the stationary Hamiltonian operator $\mathcal{H}_0 = -\partial_x^2 + V_0(x)$ which satisfies the relationship $\mathcal{H}_0\phi_j(x) = \lambda_j\phi_j(x)$. In the absence of a control function, the solution to the TDSE is simply $\psi(x,t) \sim \phi_j(x)\exp(-i\lambda_j t)$. For reasons of efficient Krylov methods to be discussed later, we carry out a change of dependent variable such that the PDE we solve always has homogeneous initial and boundary conditions. As a consequence, a forcing term is introduced. Let $y = \psi(x,t) - \phi_j(x)\exp(-i\lambda_j t)$ be the deviation between the controlled and uncontrolled solutions with the same initial and boundary conditions. The PDE for the new variable is then

$$\{i\partial_t y + \partial_x^2 - V_0(x) - u(t)x\}y(x,t) = u(t)x\phi_j(x)\exp(-i\lambda_j t), \quad y(x,0) = 0 \tag{6.4}$$

There exist numerous spectral methods which give sparse operators in modal or nodal bases for special cases, however, since the above TDSE contains an arbitrary time-dependent function $\mathbf{u}(t)$, it is reasonable to expect that any basis will lead to full matrices.

Since full matrices are unavoidable, we instead consider a discretization with a mind toward iterative system solvers so that no matrices need ever be explicitly constructed, but rather their action on given vectors can be performed rapidly. To solve the optimality system, typically an enormous number of PDE solves is needed and if the PDE solver itself is iterative, many matrix–vector products must be computed and indeed the speed of this operation will dominate the CPU time. Given this fact, a discretization based on fast transforms is ideal.

6.1 Chebyshev Pseudospectral Discretization

The Fast Fourier Transform (FFT) is, in many respects, the paradigm of a good numerical method. The operation count scales as $O(n \log n)$, parallelizes well, and it is numerically robust. On a finite non–periodic interval, however, trigonometric functions no longer provide optimal approximations. Instead, we make use of the related basis consisting of Chebyshev polynomials of the first kind. These polynomials are defined by the three-term recurrence

$$T_{k+1}(x) = 2xT_k(x) - T_{k-1}(x), \quad T_0(x) = 1, \quad T_1(x) = x \tag{6.5}$$

and also the trigonometric formula

$$T_k(x) = \cos\left(k \cos^{-1}(x)\right) \tag{6.6}$$

The space of algebraic polynomials of order n, $\mathbb{P}_n$ is spanned by the first n Chebyshev polynomials as they are linearly independent, therefore every nth order polynomial

has the *modal* expansion.

$$p_n(x) \in \mathbb{P}_n \;\Rightarrow\; p_n(x) = \sum_{k=0}^{n} \hat{p}_k T_k(x) \tag{6.7}$$

Assuming the standard domain $x \in [-1, 1]$, we can also define a *nodal* representation of $p_n(x)$ based on its values at $n+1$ distinct points.

$$p_n(x) = \sum_{j=0}^{n} p_n(x_j)\ell_j(x) \tag{6.8}$$

In this representation the $\ell_j(x)$ are the Lagrange polynomials which satisfy the condition $\ell_j(x_k) = \delta_{jk}$. With appropriate choice of the nodal set $\{x_0, x_1, ..., x_\}$ it is possible to construct a bijective mapping between the modal and nodal representations which can be carried out numerically very quickly. We use the Chebyshev–Gauss–Lobatto nodes for this set. These nodes are defined as

$$x_j = \cos\left(\frac{\pi j}{N}\right), \quad j = 0, ..., N \tag{6.9}$$

and they are the critical points of $T_n'(x)$ plus the end points ± 1. The matrix which transforms between the modal and nodal representations is the Chebyshev Vandermonde matrix V, where $V_{jk} = T_j(x_k) = T_k(x_j)$.

$$V \begin{pmatrix} \hat{p}_0 \\ \vdots \\ \hat{p}_n \end{pmatrix} = \begin{pmatrix} p_n(x_0) \\ \vdots \\ p_n(x_n) \end{pmatrix} \tag{6.10}$$

Unlike the Vandermonde matrix based on monomials at uniform grid points, a classic example of an ill-conditioned matrix, the Chebyshev Vandermonde matrix is very well-conditioned. It is never necessary to construct this matrix, however, as the Fast Chebyshev Transform (FCT), allows conversion between modal and nodal representations almost as quickly as the FFT on which it is based.

Let $\mathcal{F}(\xi)$ be the FFT and $\mathcal{F}^{-1}(\xi)$ be its inverse. MATLAB gives very efficient implementations of these algorithms in the functions `fft` and `ifft` respectively. The FCT from nodal to modal representation is a fast algorithm which is analogous to multiplication by V^{-1}. Given a vector of nodal values $z \in \mathbb{C}^{n+1}$, the FCT is a the two–step process

$$w = \mathcal{F} \begin{pmatrix} z_0 \\ \frac{1}{2}z_1 \\ \vdots \\ \frac{1}{2}z_{n-1} \\ z_n \\ \frac{1}{2}z_{n-1} \\ \vdots \\ \frac{1}{2}z_1 \end{pmatrix}, \quad \hat{z} = \begin{pmatrix} w_0 \\ \vdots \\ w_n \end{pmatrix} \tag{6.11}$$

The inverse operation (IFCT) is analogous to multiplication by V. Given the set of Chebyshev expansion coefficients $\hat{z} \in \mathbb{C}^{n+1}$, the nodal value as obtained from the two–step process

$$w = \mathcal{F}^{-1} \begin{pmatrix} \hat{z}_0 \\ \vdots \\ \hat{z}_{n-1} \\ \hat{z}_n \\ \hat{z}_{n-1} \\ \vdots \\ \hat{z}_1 \end{pmatrix}, \quad z = \begin{pmatrix} w_0 \\ 2w_1 \\ \vdots \\ 2w_{n-1} \\ w_n \end{pmatrix} \tag{6.12}$$

Both the FCT and IFCT can be performed on a number of vectors simultaneously with no added difficulty in practice.

For our model problem of dipole control, the state equation is defined on a tensor product space–time domain, so we will use global pseudospectral discretizations in space and time, however, in some applications, the geometry of the structure may preclude a global expansion in space. Nonetheless, we present the method for constructing both first and second order difference operators in the nodal basis, where the basis functions are the Lagrange polynomials based on the Chebyshev–Gauss–Lobatto nodes.

Let $\hat{D}$ be the *modal* differentiation operator and D be the *nodal* differentiation operator. These two operators are similar, and the similarity matrix which relates them is none other than the Chebyshev Vandermonde matrix T, where $T_{jk} = T_k(x_j)$.

$$D = T\hat{D}T^{-1} \tag{6.13}$$

The elements of the nodal differentiation matrix are the derivatives of the Lagrange polynomials at each of the grid points

$$D_{ij} = \ell'_j(x_i) \tag{6.14}$$

The simplest first–order problem to solve is the boundary value problem on the standard interval $[-1, 1]$

$$u'(x) = f(x), \quad u(-1) = 0 \tag{6.15}$$

Since the boundary condition is at the left endpoint, x_n, one uses only the first n equations to obtain the system

$$\begin{pmatrix} \ell'_0(x_0) & \ell'_1(x_0) & \cdots & \ell'_{n-1}(x_0) \\ \ell'_0(x_1) & \ell'_1(x_1) & \cdots & \ell'_{n-1}(x_1) \\ \vdots & \vdots & \ddots & \vdots \\ \ell'_0(x_{n-1}) & \ell'_1(x_{n-1}) & \cdots & \ell'_{n-1}(x_{n-1}) \end{pmatrix} \begin{pmatrix} u(x_0) \\ u(x_1) \\ \vdots \\ u(x_{n-1}) \end{pmatrix} = \begin{pmatrix} f(x_0) \\ f(x_1) \\ \vdots \\ f(x_{n-1}) \end{pmatrix} \tag{6.16}$$

with the boundary condition $u(x_n) = 0$. The reduced differentiation matrix can be denoted as D_r. Unlike the original nodal differentiation matrix D, which was rank one deficient, due to its null–space of constant–valued functions, the matrix D_r is nonsingular and moreover, one may obtain an explicit formula for its inverse.

At this point, it should be mentioned that pseudospectral discretizations are well–studied and has been reported that the spectral radius of differential operators grows as $O(n^2)$ and $O(n^4)$ for first- and second–order operators respectively and tend to have large extremal eigenvalues[89]. For this reason, Krylov solvers for PDEs discretized with pseudospectral methods can be expected to exhibit extremely poor convergence behavior in the absence of suitable preconditioning.

The earliest preconditioning strategies involved constructing finite difference approximations on the same grid and reasonably good results have been reported for second–order operators, with relatively little literature on first–order operators, see [89] and references therein.

Another approach based on the modal form of integration operators[88] was introduced by Hesthaven[90]. The idea behind this method is that the modal integration matrix $\hat{B}$ is a sort of pseudo–inverse of the modal differentiation matrix $\hat{D}$, however, it is rank–deficient, a disastrous property for a preconditioner. Hesthaven addresses this shortcoming by introducing some parametric modifications to $\hat{B}$.

The principle of matrix preconditioning is that, when confronted with a problem $Ax = b$, one would like to find a matrix $M \approx A^{-1}$, such that the the preconditioned problem $MAx = Mb$ can be solved more rapidly with an iterative solver. In the case of Krylov solvers, the property that is sought is that MA has a clustered spectrum and, ideally, is as close to the identity as possible. To this end, we will use preconditioning matrices which are the exact inverses of the first- and second–order pseudospectral differentiation matrices with Dirichlet boundary conditions.

To do so, first we decompose the modal differentiation matrix into the block representation

$$\hat{D} = \left(\begin{array}{c|c} 0 & \hat{D}_r \\ \hline 0 & 0 \end{array}\right), \quad \hat{D}_r = \left(\begin{array}{cccccc|c} 1 & 0 & 3 & 0 & 5 & 0 & \cdots \\ 0 & 4 & 0 & 8 & 0 & 12 & \\ 0 & 0 & 6 & 0 & 10 & 0 & \\ 0 & 0 & 0 & 8 & 0 & 12 & \\ 0 & 0 & 0 & 0 & 10 & 0 & \\ 0 & 0 & 0 & 0 & 0 & 12 & \\ \hline \vdots & & & & & & \ddots \end{array}\right) \tag{6.17}$$

The matrix $\hat{D}$ has a known inverse as it is obtained from the recurrence relation for Chebyshev polynomials. Loosely following the notation of Coutsias, *et al*[88], the matrix $\hat{B}_r = \hat{D}_r^{-1}$ is a banded integration–type operator.

$$[\hat{B}_r]_{jk} = [\hat{D}_r^{-1}]_{jk} = \begin{cases} 1 & \text{if} \quad k = j = 1 \\ \frac{1}{2j} & \text{if} \quad k = j, j > 1 \\ -\frac{1}{2j} & \text{if} \quad k = j + 2 \\ 0 & \text{otherwise} \end{cases} \tag{6.18}$$

We can write out the reduced differentiation operator as the product

$$D_r = T_a \hat{D}_r T_b^{-1} \tag{6.19}$$

where the matrices T_a and T_b^{-1} are $n \times n$ blocks of T and T^{-1} respectively.

$$T = \left(\begin{array}{c|c} T_a & * \\ \hline * & * \end{array}\right), \quad PT^{-1} = \left(\begin{array}{c|c} T_b^{-1} & * \\ \hline * & * \end{array}\right), \quad P = \left(\begin{array}{c|c} 0 & I \\ \hline 1 & 0 \end{array}\right) \tag{6.20}$$

Where P is a permutation matrix that performs a shift. The Sherman–Morrison–Woodbury (SMW) formula allows one to compute T_a^{-1} and T_b based on knowledge

of T and T^{-1}. In general, supposing we have a block matrix $M \in \mathbb{R}^{n\times n}$ of the form

$$M = \left(\begin{array}{c|c} A & B \\ \hline C & D \end{array}\right), \quad A \in \mathbb{R}^{m\times m},\ D \in \mathbb{R}^{p\times p} \tag{6.21}$$

where $n = m + p$, the block matrix may be split in the following way

$$M = \left(\begin{array}{c|c} A & O \\ \hline O & D \end{array}\right) + UV, \quad U = \left(\begin{array}{c|c} B & O \\ \hline O & I \end{array}\right), \quad V = \left(\begin{array}{c|c} O & I \\ \hline C & O \end{array}\right) \tag{6.22}$$

With this choice of slipping, $U \in \mathbb{R}^{n\times 2p}$ and $V \in \mathbb{R}^{2p\times n}$. Let the block–diagonal part of of M be called M_d so that $M = M_d + UV$. Now we wish develop a formula for M_d^{-1} based on knowledge of how to apply M^{-1} to given vectors. The SMW formula gives the inverse of M_d as

$$M_d^{-1} = M^{-1} + M^{-1}U(I - VM^{-1}U)^{-1}VM^{-1} \tag{6.23}$$

The SMW requires solving a reduced 2×2 system for the rank–2 correction. The matrix which appears both in computing T_a^{-1} and T_b is nonsingular and has a determinant of $\frac{1}{2n}$.

Given that the reduced differentiation operator is $D_r = T_a\hat{D}_rT_b^{-1}$, its exact inverse is

$$B_r = D_r^{-1} = (T_a\hat{D}_rT_b^{-1})^{-1} = T_b\hat{B}_rT_a^{-1} \tag{6.24}$$

In the case where $M = T$ and $n + 1$ CGL points are used, we are trying to obtain a formula for the action of T_a^{-1} and we can obtain explicit forms of the terms appearing in the SMW formula.

$$T^{-1}U = \frac{1}{2n}\left(\begin{array}{cc} -(-1)^n & 1 \\ \hline 2(-1)^n & -2 \\ -2(-1)^n & 2 \\ 2(-1)^n & -2 \\ \vdots & \vdots \\ \hline 2n-1 & (-1)^n \end{array}\right), \quad VT^{-1} = \begin{pmatrix} 0 & 1 \\ 1 & 0 \end{pmatrix} U^\top T^{-1} \tag{6.25}$$

$$(I - VT^{-1}U)^{-1} = \begin{pmatrix} 1 & (-1)^n \\ (-1)^n(1-2n) & 1 \end{pmatrix} \tag{6.26}$$

To apply T_a^{-1} to a vector $x \in \mathbb{C}^n$, we append a zero element to the end to get a vector in $\mathbb{C}^{n+1}$, then apply the SMW formula for M_d^{-1} and extract the first n elements. The end result is $T_a^{-1}x$.

Matters are slightly more complicated in determining the action of T_b since T_b^{-1} is not a diagonal block in T^{-1}, but this is remedied via multiplication with a permutation matrix. Following the generic block labeling from above, we have a block matrix decomposition $PM = M_d + UV$, so the SMW formula for M_d^{-1} in this situation is

$$M_d^{-1} = M^{-1}P^\top - M^{-1}P^\top U(I - VM^{-1}P^\top U)^{-1}VM^{-1}P^\top \tag{6.27}$$

To determine the action of T_b, we have that $M = T^{-1}$, and the terms appearing in the analogous SMW formula again have explicit forms

$$TP^\top U = \begin{pmatrix} \frac{-1}{2n} & 1 \\ \frac{-1}{2n} & 1 \\ \vdots & \vdots \\ \frac{-1}{2n} & 1 \\ \frac{2n-1}{2n} & 1 \end{pmatrix}, \quad (VT)^\top = \begin{pmatrix} 1 & \frac{2n-1}{2n} \\ -1 & \frac{1}{2n} \\ 1 & \frac{-1}{2n} \\ -1 & \frac{1}{2n} \\ \vdots & \vdots \end{pmatrix} \tag{6.28}$$

$$(I - VTP^{\top}U)^{-1} = \begin{pmatrix} 1 & 2n \\ \frac{1-2n}{2n} & 1 \end{pmatrix} \tag{6.29}$$

We now have an exact formula for the inverse of the first derivative operator with a homogeneous Dirichlet condition at the left boundary. The boundary value problem can be solved using only matrix multiplication as $u = B_r f$ and no numerical inversion of a matrix is needed. The solution requires one call each to FCT and IFCT and a few sparse matrix multiplications.

Now we consider the second–order problem

$$u''(x) = f(x), \quad u(\pm 1) = 0 \tag{6.30}$$

and discretize again using the Chebyshev pseudospectral method. Writing out the discretized system explicitly, we have

$$\begin{pmatrix} \ell_1''(x_1) & \ell_2''(x_1) & \cdots & \ell_{n-1}''(x_1) \\ \ell_1''(x_2) & \ell_2''(x_2) & \cdots & \ell_{n-1}''(x_2) \\ \vdots & \vdots & \ddots & \vdots \\ \ell_1''(x_{n-1}) & \ell_2'(x_{n-1}) & \cdots & \ell_{n-1}''(x_{n-1}) \end{pmatrix} \begin{pmatrix} u(x_1) \\ u(x_2) \\ \vdots \\ u(x_{n-1}) \end{pmatrix} = \begin{pmatrix} f(x_1) \\ f(x_2) \\ \vdots \\ f(x_{n-1}) \end{pmatrix} \tag{6.31}$$

with the boundary conditions $u(x_0) = u(x_n) = 0$. The full second–order pseudospectral differentiation matrix is $D^2 = T\hat{D}^2T^{-1}$ and we aim to find expressions for the interior $(n-1) \times (n-1)$, which we will denote as $D_r^{(2)}$ and its inverse $B_r^{(2)}$. The superscript in parenthesis is intended to distinguish these matrices from the square of D_r and B_r respectively. As before, we can express the reduced matrix as

$$D_r^{(2)} = T_a \hat{D}_r^{(2)} T_b^{-1} \tag{6.32}$$

where the $T_a, T_b^{-1} \in \mathbb{R}^{(n-1)\times(n-1)}$ are different from the first–order case and are

related to T and T^{-1} in the following way

$$T = \left(\begin{array}{c|cc} * & * & * \\ \hline T_a & * & * \\ \hline * & * & * \end{array}\right), \quad T^{-1} = \left(\begin{array}{cc|c} * & * & * \\ * & * & * \\ \hline * & T_b^{-1} & * \end{array}\right) \tag{6.33}$$

The matrix $\hat{D}_r^{(2)}$ is the upper right block of the matrix $\hat{D}^2$.

$$\hat{D}^2 = \hat{D}\hat{D} = \left(\begin{array}{cc|c} 0 & 0 & \hat{D}_r^{(2)} \\ \hline 0 & 0 & 0 \\ 0 & 0 & 0 \end{array}\right) \tag{6.34}$$

The block $\hat{D}_r^{(2)}$ has the exact inverse $\hat{B}_r^{(2)}$ for which the elements are

$$[\hat{B}_r^{(2)}]_{jk} = \begin{cases} \frac{1}{4} & \text{if} \quad j = k = 1 \\ \frac{1}{4j(j+1)} & \text{if} \quad j = k \neq 1 \\ \frac{1}{2-2(j+1)^2} & \text{if} \quad k = j+2 \\ \frac{1}{4(j+1)(j+2)} & \text{if} \quad k = j+4 \\ 0 & \text{otherwise} \end{cases} \tag{6.35}$$

The exact inverse of $D_r^{(2)} = T_a \hat{D}_r^{(2)} T_b^{-1}$ is $B_r^{(2)} = T_b \hat{B}_r^{(2)} T_a^{-1}$. As before, the SMW formula allows one to determine the action of T_a^{-1} and T_b in terms of T^{-1} and T with help of the permutation matrix P. To obtain the desired diagonal block form, the following permutations are used

$$PT = \left(\begin{array}{c|cc} T_a & * & * \\ \hline * & * & * \\ * & * & * \end{array}\right), \quad T^{-1}P = \left(\begin{array}{cc|c} * & * & * \\ * & * & * \\ \hline * & * & T_b^{-1} \end{array}\right) \tag{6.36}$$

To obtain the formula for The SMW formula for the inverse of the block diagonal part is

$$M_d^{-1} = T^{-1}P^{-1} + T^{-1}P^{-1}U(I - VT^{-1}P^{-1}U)^{-1}VT^{-1}P^{-1} \tag{6.37}$$

For both computing T_a^{-1} and T_b, we must solve a reduced 4×4 system. The matrix to be inverted in both cases is guaranteed to be nonsingular and, in fact, its determinant is $\frac{2}{n^2}$. As before, constituent matrices can be written in exact form.

$$T^{-1}P^{-1}U = \frac{1}{n}\left(\begin{array}{cccc} \frac{(-1)^n-1}{2} & \frac{-(1+(-1)^n)}{2} & \frac{1}{2} & \frac{1}{2} \\ \hline -2 & 0 & -1 & 1 \\ 0 & -2 & 1 & 1 \\ -2 & 0 & -1 & 1 \\ \vdots & \vdots & \vdots & \vdots \\ \hline n-2 & 0 & (-1)^{n-1} & 1 \\ 0 & n-1 & \frac{(-1)^n}{2} & \frac{1}{2} \end{array}\right) \tag{6.38}$$

$$(I - VT^{-1}P^{-1}U)^{-1} = \begin{pmatrix} 1 & 0 & \frac{-(-1)^n}{2} & \frac{1}{2} \\ 0 & 1 & \frac{(-1)^n}{2} & \frac{1}{2} \\ \frac{(-1)^n(n-2)}{2} & (-1)^n(1-n) & 1 & 0 \\ \frac{2-n}{2} & 1-n & 0 & 1 \end{pmatrix} \tag{6.39}$$

Unfortunately, we do not have a clean and simple expression for the $4 \times (n+1)$ matrix $VT^{-1}P^{-1}$ since it contains sums of cosine terms. Nonetheless, the matrix can be numerically computed quickly by taking the FCT of the V matrix and permuting the result column–wise.

The block T_b^{-1} appears as the lower right block in T^{-1}, so we modify the block decomposition as follows

$$M = \left(\begin{array}{c|c} A & B \\ \hline C & D \end{array}\right) = \left(\begin{array}{c|c} A & 0 \\ \hline 0 & D \end{array}\right) + \left(\begin{array}{c|c} I & 0 \\ \hline 0 & C \end{array}\right)\left(\begin{array}{c|c} 0 & B \\ \hline I & 0 \end{array}\right) \tag{6.40}$$

which we denote as $M = M_d + UV$ again and if $M = T^{-1}P$, then the D block is T_b^{-1}. To compute the inverse of this matrix T_b, we use the SMW formula to get

$$M_d^{-1} = P^\top T + P^\top TU(I - VP^\top TU)^{-1}VP^\top T \tag{6.41}$$

and extract the lower right block of size $(n-1)\times(n-1)$. We have explicit formulas for the $VP^\top T$ and $(I-VP^\top TU)^{-1}$ matrices, but as with computing T_a^{-1}, one of the terms, $P^\top TU$, defies a concise representation due to sums of cosines. It can, however, be quickly computed with the IFCT. The known terms are

$$(VP^\top T)^\top = \left(\begin{array}{cccc} \frac{n-1}{n} & 0 & 1 & 1 \\ 0 & \frac{n-2}{n} & -1 & 1 \\ \hline \frac{-1}{n} & 0 & 1 & 1 \\ 0 & \frac{-2}{n} & -1 & 1 \\ \frac{-1}{n} & 0 & 1 & 1 \\ \vdots & \vdots & \vdots & \vdots \end{array}\right) \tag{6.42}$$

$$(I-VP^\top TU)^{-1} = \left(\begin{array}{cccc} 1 & 0 & \frac{1-n}{2n} & \frac{1-n}{2n} \\ 0 & 1 & \frac{n-2}{2n} & \frac{2-n}{2n} \\ n & \frac{-n}{2} & 1 & 0 \\ n & \frac{n}{2} & 0 & 1 \end{array}\right) \tag{6.43}$$

6.2 Discretizing the TDSE and preconditioning

The pseudospectral method of the preceding section can now be applied to a discretizing the modified TDSE in equation 6.4. Discretizing in space and time on an $(n_x+1)\times n_t$ rectangular grid, one obtains the system

$$(iD_r^{(1)}\otimes I + I\otimes D_r^{(2)} - V)y = \mathrm{vec}(F_r) \tag{6.44}$$

where $y\in\mathbb{C}^{(n_x-1)(n_t)}$ is the column–stacked solution to the initial boundary value problem on the interior grid points $x_1,...,x_{n_x-1}$ and $t_0,...,t_{n_t-1}$, I is the identity

matrix of the appropriate size, V is a diagonal matrix containing the nodal values of the stationary potential function $V_0(x,t)$ plus the dipole control $u(t)x$ on the interior points, $F_r \in \mathbb{C}^{(n_x-1)\times(n_t-1)}$ is the forcing function on the interior points, and $D_r^{(1)}$ and $D_r^{(2)}$ are the pseudospectral discretizations of the first and second derivative operators with row elimination corresponding to the homogeneous Dirichlet conditions.

We do not have an explicit formula for the two–dimensional operator appearing in the left–hand–side of 6.44, nonetheless, we can make a sensible choice for a preconditioner by, in a sense, integrating the system once in time and twice in space. This is carried out by multiplying from the left with the operator $B_r^{(1)} \otimes B_r^{(2)}$. The preconditioned system is

$$(iI \otimes B_r^{(2)} + B_r^{(1)} \otimes I - [B_r^{(1)} \otimes B_r^{(2)}]V_0)y = \mathrm{vec}(B_r^{(2)} F_r [B_r^{(1)}]^\top) \tag{6.45}$$

While $B_r^{(1)} \otimes B_r^{(2)}$ is certainly not the optimal preconditioner as it is not the inverse of the original matrix, we can expect favorable convergence behavior with Krylov methods due to the more clustered spectrum. As an example, consider the case where $V = 0$, $n_t = 60$, and $n_x = 20$. The eigenvalues of the original matrix, $iD_r^{(1)} \otimes I + I \otimes D_r^{(2)}$, and the preconditioned matrix $iI \otimes B_r^{(2)} + B_r^{(1)} \otimes I$ are compared in figure 6.2. The distribution of eigenvalues is mostly clustered along the real axis without preconditioning as the second–order derivative matrix dominates the behavior of the spectrum. In contrast, the preconditioned matrix exhibits more clustering about the imaginary axis owing to the fact that the first–order integral is dominating the eigenvalue distribution. The preconditioned matrix shows better eigenvalue clustering overall and this gives good reason to expect improved convergence with a Krylov solver.

A better preconditioner for the space–time operator can be obtained by combining spectral integration preconditioning in time and finite difference preconditioning in

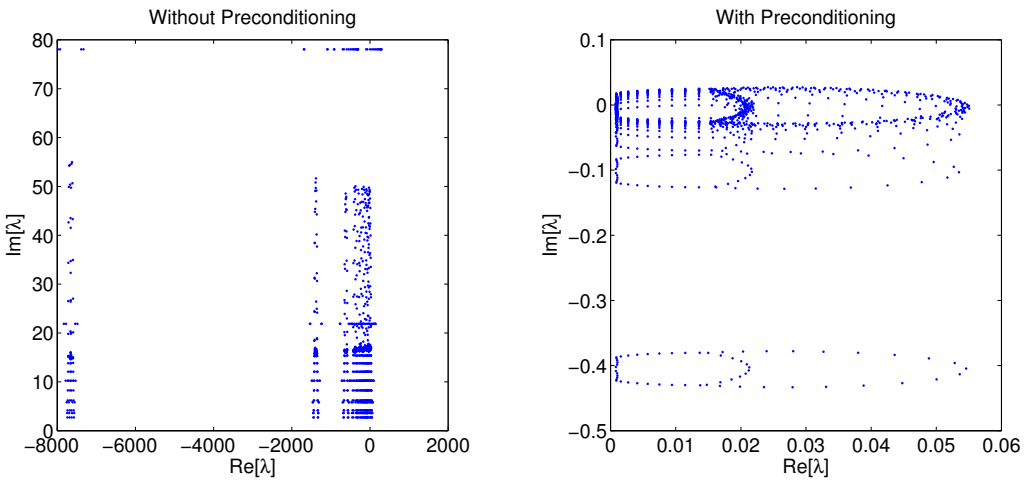

Figure 6.1: *Left:* $\sigma(D_r^{(1)} \otimes I + I \otimes D_r^{(2)})$ for $n_x = 20$, $n_t = 60$.
Right: $\sigma(iI \otimes B_r^{(2)} + B_r^{(1)} \otimes I)$ for $n_x = 20$, $n_t = 60$.

space. We begin by writing the operator in derivative form with a swapped (t, x) ordering. The r subscript is dropped as it is implicit and instead we specify t or x depending on which dimension the matrix operates.

$$(iI_x \otimes D_t^{(1)} + D_x^{(2)\otimes I_t} - V)y = \mathrm{vec}(F_r) \tag{6.46}$$

Now we precondition the system in time by multiplying through by $I_x \otimes B_t^{(1)}$

$$(iI_x \otimes I_t + D_x^{(2)} \otimes B_t^{(1)} - (I_x \otimes B_t^{(1)})V)y = \mathrm{vec}(B_t^{(1)} F_r) \tag{6.47}$$

The pseudospectral second derivative matrix $D_x^{(2)}$ is approximated by a second–order finite difference matrix $\tilde{D}_x^{(2)}$ on the same CGL grid as described in [89]. The space–time precondition matrix is then the block tridiagonal matrix

$$M = iI_x \otimes I_t + \tilde{D}_x^{(2)} \otimes B_t^{(1)}$$

The potential term $(I_x \otimes B_t^{(1)})V$ can be safely neglected when forming the preconditioner since it is lower order in space and time than the other part of the solution operator. The preconditioner M can be used repeatedly for solving the modified

Schrödinger equation as is needed for solving the optimal control problem. We can further economize on speed by storing the LU factors of the preconditioner to a data file to be used by a Krylov solver. The computational cost of solving systems with the LU factors scales linearly with the number of spatial grid points and quadratically with the number of time grid points. With a sparse banded representation of the operator $B_r^{(1)}$ it should be possible to reduce the costs to scaling linearly with the number of time grid points as well.

6.3 Numerical Results

Let the model problem be the dipole–driven square well on the domain $(x,t) \in [0,2] \times [0,2]$. The sample control is the sinusoidal amplitude $u(t) = 2\sin(3\pi t)$. Using a pseudospectral discretization with n_x+1 spatial grid points in space and n_t+1 grid points in time, aim to solve the modified TDSE 6.4 with three different approaches: without preconditioning (none), with space–time integration preconditioning (B), and with the hybrid preconditioning of finite–differences in space and integration in time (hybrid). First we compare the condition number of the matrix approximation to the solution as a function of n_t and n_x.

n_t	n_x	none	B	hybrid
10	10	7.6×10^2	1.4×10^2	1.1×10^1
10	30	5.6×10^4	1.4×10^2	1.2×10^1
10	50	4.3×10^5	1.3×10^2	1.2×10^1
30	10	1.2×10^3	1.3×10^3	6.4×10^1
30	30	6.0×10^4	1.3×10^3	1.3×10^1
30	50	4.6×10^5	1.3×10^3	1.5×10^1
50	10	2.3×10^3	4.3×10^3	7.2×10^2
50	30	6.0×10^4	4.3×10^3	1.9×10^1
50	50	4.6×10^5	4.3×10^3	2.2×10^1

Table 6.1: Condition number of the matrix approximation to the solution operator.

To compare performance of the three methods, we a approximately solve the discretized equations using the GMRES method without restarting and record how many iterations are required to reduce the residual to below 10^{-5}.

n_t	n_x	none	B	hybrid
10	10	65	46	9
10	30	199	46	8
10	50	332	46	8
30	10	182	125	16
30	30	546	130	6
30	50	913	130	6
50	10	266	136	27
50	30	771	140	6
50	50	1289	140	6

Table 6.2: Number of GMRES iterations needed to reduce the residual to below 10^{-5}.

The argument in favor of high–order methods in time and relatively low–order methods in space is supported by plotting the relative magnitude of the space–time Chebyshev expansion coefficients of a typical wavefunction controlled with sinusoidal dipole potential.

Figure 6.3 demonstrates the typical behavior of numerous test cases. The expansion coefficients in the spatial dimension decay very rapidly and only a few Chebyshev polynomials in space are needed to accurately approximate the true wavefunction, however, the expansion coefficients decay much more slowly in the temporal dimension, owing to the highly oscillatory behavior of the wavefunction in time. The initial data is the ground state in a square quantum well.

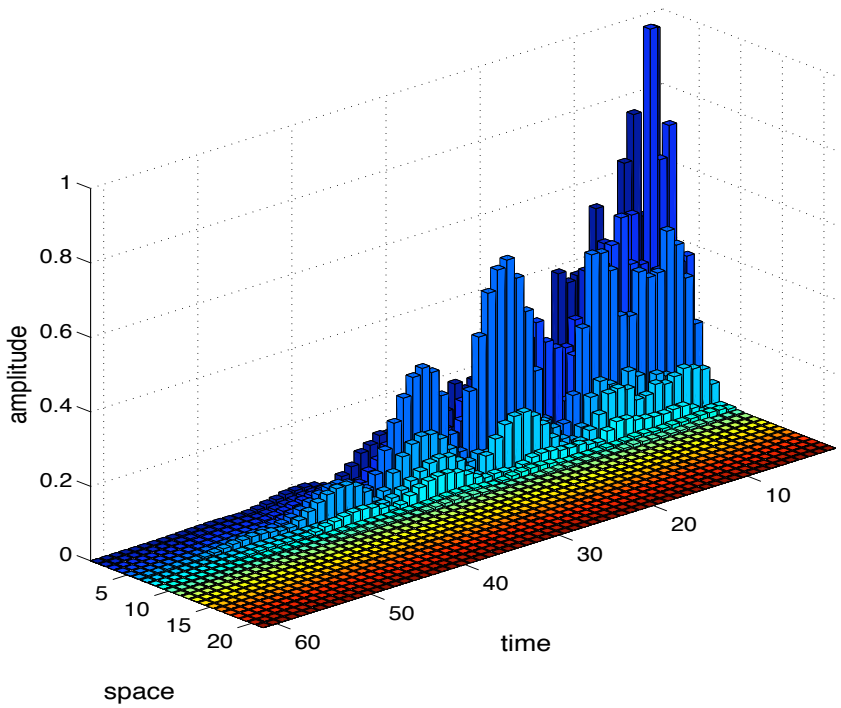

Figure 6.2: Normalized Chebyshev expansion coefficients of a time–harmonic dipole–driven wavefunction.

6.4 A sparse spectral time discretization

This discretization and preconditioning strategy of the preceding sections is clearly well–suited to resolving the highly oscillatory behavior in time and keeping the number of Krylov iterations needed to approximately solve the system quite modest. Additionally, the solution operator can be applied rapidly via FCTs. The one drawback to discretization is that while the time needed to solve systems with the preconditioner scales linearly with respect to the order in spatial discretization, it scales quadratically with the order of the time discretization because the $B_r^{(}1)$ matrix is full.

Ideally, a discretization would have a sparse banded preconditioner M so that the cost of solving systems of the form $Mx = b$ scales linearly with the order in space and time. To that end, we finally suggest a modal Chebyshev Petrov–Galerkin basis in time such that the temporal mass and stiffness matrices have minimal bandwidth. The trial functions $\phi_k(t)$ should have a convenient representation in terms of Chebyshev polynomials and they must satisfy the homogeneous Dirichlet condition at the initial time, i.e. $\phi_k(-1)$. Conversely, test functions $\varphi_j(t)$ are desired to span a dual space and satisfy a similar boundary condition at the final time, $\varphi_j(+1) = 0$. Such a basis has been recently suggested by Shen and Wang [92].

$$\begin{array}{l}\phi_k(t) = c_k(1-t)T_k(t) \\ \varphi_k(t) = c_k(1+t)T_k(t)\end{array} \qquad c_k = \begin{cases} \frac{1}{2\sqrt{2}} & \text{if} \quad k = 0 \\ \frac{1}{2} & \text{if} \quad k \geq 1 \end{cases} \tag{6.48}$$

With the standard Chebyshev–weighted inner–product $(u, v)_w = \int_{-1}^{1} u(t)v(t)(1 - t^2)-1/2dt$, these trial and test functions give rise to a tridiagonal stiffness matrix and pentadiagonal mass matrix.

$$(\varphi_j, \phi_k)_w = \begin{cases} \frac{1}{2} & \text{if} \quad j = k \neq 1 \\ \frac{1}{4} & \text{if} \quad j = k = 1 \\ \frac{-1}{2\sqrt{2}} & \text{if} \quad j = 2, k = 0 \\ \frac{-1}{2\sqrt{2}} & \text{if} \quad j = 0, k = 2 \\ \frac{-1}{4} & \text{if} \quad j \geq 1, k = j \pm 2 \\ 0 & \text{else} \end{cases} \tag{6.49}$$

$$(\varphi_j, \dot{\phi}_k)_w = \begin{cases} 1 & \text{if} \quad j = k \\ \frac{-1}{2\sqrt{2}} & \text{if} \quad j = 1, k = 0 \\ \frac{j}{2} & \text{if} \quad k = j + 1 \\ \frac{-j}{2} & \text{if} \quad j \geq 2, k = j - 1 \\ 0 & \text{else} \end{cases} \tag{6.50}$$

If we choose the Chebyshev–Gauss points $t_k = \cos(\frac{(2k+1)\pi}{2(n+1)})$ for $k = 0..n$ in time, then the discrete cosine transform can be used to transform between nodal and modal representation. This can be carried out quickly via the MATLAB functions `dct` and `idct` for example.

Chapter 7

Current and future work

The ongoing and continuing work consists of two areas of focus: improving computational method for quantum control problems and tackling more complicated problems involving multiple particles and spin.

The challenge of designing faster algorithms for solving the quantum optimality system, as mentioned in the introduction, is two-fold. PDE–constrained optimization requires solving a very large number of PDEs to evaluate the cost at various points in the search space and also to compute gradients and Newton search directions. To reduce the computational time, one must either develop faster PDE solvers, make better use of the information from each PDE solve, or ideally both.

The space–time spectral discretization of the TDSE discussed in chapter 6 relies on the application of spectral approximations of differential and integral operations through the use of Fast Fourier Transforms. The total number of transformations between the nodal and modal representations could be reduced be applying the matrices to blocks of vectors in parallel. This could be exploited by replacing the standard Krylov solver with a block Krylov solver.

In particular the Block GMRES algorithm[93, 94] is an attractive candidate for solving the state equation as sets of Arnoldi vectors are added to the Krylov space simultaneously and it is possible to choose an intelligent set of seed vectors to start the algorithm. The nature of PDE–constrained optimization is such that we must solve the state equation many times and often with input controls that are only slightly perturbed from earlier iterations. This means one could store information about the the state variable during the optimization process and use old solutions to make guesses of new solutions. This could be a significant cost–saving measure when performing a line–search.

Suppose that we have computed a search direction v and wish to find a step length α which satisfies appropriate criteria, such as the Wolfe–Powell conditions. To find the α, we must repeatedly solve a PDE of the form

$$\{i\partial_t + \partial_x^2 - V_0(x) - [u(t) + \alpha v(t)]\}\psi(x,t) = 0, \quad \psi(x,0) = \psi^0(x) \tag{7.1}$$

For small changes in α, we can expect small changes in ψ, which means if we take a series of steps $\alpha = \alpha_0, \alpha_1, \alpha_2, ...$ and compute corresponding solutions $\psi_0, \psi_1, \psi_2, ...$, selected Arnoldi vectors used to compute the solutions could be recycled to decrease the number of GMRES iterations needed to compute subsequent ψ.

Another approach would be to view the linesearch problem as a case of solving a multiple shift system

$$(A + \alpha_k B)x = b$$

for a number of values of α_k. The structure of the quantum control problem is attractive because the shift factor occurs in the lowest order term of the operator $A + \alpha B$ in the sense that A contains all the derivative terms and B contains only a variable coefficient. The solution of multiple shifted systems with Block–GMRES is discussed in the general sense [94], but has also been used in applications such as the solution of multiple Helmholtz equations of differing frequencies [95].

Newton's method for PDE–constrained optimization usually relies on a Krylov solver which applies the Hessian to a sequence of vector iterates. As seen in chapter 3, application of the Hessian requires the solution of a state and adjoint equation for each iterate. If the state equation is itself solved iteratively, then nested Krylov methods are needed. In this situation is makes considerably more sense to use block method for both the inner and outer loop to decrease computational work.

While we have demonstrated fast and efficient methods for a single particle, many practical problems of interest involve multiple particles. Of particular interest is controlling the state of a collection of fermions confined to a quantum well. The idea follows from that of the control of a single particle in a straightforward way, however, the dimensionality of the multiparticle system leads to many more degrees of freedom even in a single spatial dimension.

For example, in one spatial dimension with N particles, $\psi(\mathbf{x}, t)$ denotes the multi-electron wavefunction as a short-hand for $\psi(x_1, \ldots, x_N, t)$ and the Laplace operator is $\Delta = \partial_{x_1}^2 + \cdots \partial_{x_N}^2$. The time-dependent Schrödinger equation for N particles with Coulomb interaction and dipole control field is then

$$i\partial_t \psi(\mathbf{x}, t) = \left\{ -\Delta + \sum_{j=1}^{N} \left(u(t) x_j + \sum_{k \neq j}^{N} \frac{q}{|x_j - x_k|} \right) \right\} \psi(\mathbf{x}, t)$$

where q is the charge carried by an electron. The obvious question is how to devise a formulation for an optimal control problem which is still tractable in the case of multiple particles. One point to exploit is that using nodal discretizations of the Hamiltonian, although the size of the matrix grows tremendously with number of particles, the multi-particle Laplacian becomes progressively more diagonally dominant. An investigation is needed to develop fast algorithms in particular for problems with only a few particles, where approximations for many particle systems such as Hartree Fock and multi-configurational methods may be very inaccurate, but the dimensionality of the full problem is already unwieldy.

Finally, spintronics holds great potential for significantly faster devices since only the spin state of a particle is altered and it is not required to physically move a charge. Incorporating spin effects leads to the Pauli equation

$$i\hbar\dot{\psi} = \left\{ \frac{1}{2m}(\sigma \cdot (p - qA))^2 + q\phi \right\}$$

where m and q are the mass and charge of the particle, σ is the spin tensor, p is the momentum operator, A is the magnetic vector potential, and ϕ is the electric scalar potential. The wavefunction itself now takes values in $\mathbb{C}^2$.

From a control standpoint, time-dependent electric and magnetic fields are the way in which the state of the system is altered, so some combination of A and ϕ would be control functions, giving rise again to a multilinear control problem. A particular problem of interest here would be that of computing a time-optimal control for switching the spin state of a particle as this is fundamentally what is needed for a single bit of memory. Then, continuing to interpret the spin of particles as logic states, we will need to find control functions for switching simple logic devices either quickly or with constraints on the amount of energy spent.

Chapter 8

Conclusions

The control of physical systems at the quantum scale is a challenging problem due to its nonlinear structure, but holds much promise for the development of future technologies. The computational cost of computing an optimal control tends to become quite large due to the fact that the many PDE solves are needed to evaluate the cost functional or solve first– and second–order optimality equations.

We observed that choice of function space for the control can have a significant impact on the convergence of NCG and BFGS methods, that these methods could be modified to utilize the corresponding inner products, and that convergence could be expedited further by using cascadic implementations.

The first true Newton method applied to quantum optimal control was introduced as well. It was illustrated that because the cost functional is not an analytic function of the quantum mechanical wavefunction, difficulties in deriving the second order optimality conditions can arise and one must either employ a real variable formulation, or the Wirtinger calculus. It was shown that the approaches of optimize–before–discretize and discretize–before–optimize can produce differing results and that a modification of the Crank–Nicolson method will restore unitarity

for time–dependent potentials. A robust line–search method was presented based on the underlying physics which guarantees that a point satisfying the strong Wolfe conditions will always be found. It was also proven that the quantum cost functional can not be made convex through regularization on the control terms via a parity argument, thereby justifying the need for linesearches to globalize Newton's method.

The optimal control framework was applied to the problem of inducing state–to–state transitions in open quantum systems and higher dimensional problems. In the case of the open system, perfectly matched layers were introduced to simulate loss to the environment and inequality state constraints were imposed to restrict the probability of particle loss. A semi–smooth Newton method was derived based on the state constraints. An optimal control for the excitation of a particle in a two–dimensional quantum dot from the ground state was computed for both scalar– and vector–valued control fields.

Spectral discretizations of the TDSE in both space and time were proposed on account of the highly oscillatory behavior of the wavefunction in time and the extreme smoothness of the optimal control. Preconditioning strategies were given for fast solution of the state equation with Krylov methods.

It was demonstrated that the standard final–time cost is actually equivalent to a whole family of time–distributed costs. While these two formulations are identical in principle, time–distributed costs may have interesting implications for the numerical solution of optimality equations as it introduces new degrees of freedom into the problem.

Finally directions of future work for further reducing the computational cost of solving quantum optimal control problems through the use of block Krylov methods and changes of dependent variable were proposed. Extension of the optimal control framework to multiple particle systems and spin systems was proposed.

Appendices

Appendix A

An equivalent time-distributed cost

Optimal control of quantum dynamics using the method of Lagrange multipliers has been the subject of increasing interest over the last twenty years, beginning with the landmark paper of Peirce, Dahleh, and Rabitz[32]. In their paper, the authors formulate an cost functional based on the discrepancy between the quantum mechanical wavefunction ψ onto a target state at a final time T. The form of the cost originally followed the approach of optimal control of the heat equation in that the absolute difference of the state variable and target at the final time was penalized.

$$J(\psi, u) = \frac{1}{2}\int_{\Omega} \|\psi(x,T) - \psi^f(x)|^2 d\Omega + \frac{\gamma}{2}\|u\|^2 \tag{A.1}$$

where Ω is the spatial domain and $\psi^f : \Omega \to \mathbb{C}$ is some target state. This is a computationally nice cost functional, however, it does exhibit the physically undesirable feature of phase dependence. That is to say, assuming the normalization $\|\psi(\cdot,t)\|_\Omega = 1$ for all time $t \in [0,T]$ and $\|\psi^f\|_\Omega = 1$, the cost functional can take any value between 0 and 1 due to only a shift in the absolute phase of ψ, which is not a physically observable quantity.

Appendix A. An equivalent time-distributed cost

An alternate cost functional was proposed [82] which makes use of a projection operator. In quantum mechanics all observable quantities have an associated operator. The probability of finding a particle whose dynamics is represented by ψ in a target state φ is given by the magnitude squared of the projection onto the target. Let the projection operator $\mathcal{P}$ be defined as

$$\mathcal{P}\psi(x,t) = \psi^f(x) \int_\Omega \bar{\psi}^f(x)\psi(x,t)d\Omega \tag{A.2}$$

where $\bar{\varphi}$ denotes the complex conjugate of φ. The cost functional which uses this projector is

$$J(\psi,u) = \frac{1}{2}(1 - \|\mathcal{P}\psi(\cdot,T)\|^2) + \frac{\gamma}{2}\|u\|^2 \tag{A.3}$$

For the remainder of this work, we refer to this as the standard cost functional owing to its ubiquity in the literature.

The cost functional as written in the preceding section and in the existing literature is a function of the quantum wave function and the control function. Since the wave function is complex-valued and the cost is real, J can not be an holomorphic function of ψ and indeed depends on its complex conjugate $\bar{\psi}$ as well. As such the cost in not differentiable in the usual sense and there are two basic approaches to taking variations. One option is write a real-variable formulation where the cost is differentiated with respect to real and imaginary parts of the the wave function separately[84]. The alternate approach employs the Wirtinger calculus[74], which allows one to construct linear operators which extract the real or imaginary parts of complex quantities or perform complex conjugation. This idea was first used by Brandwood[72] to define a complex gradient of a cost and similarly the Hessian of an unconstrained problem was introduced subsequently by van den Bos[73]. More recently, a detailed exposition of the Wirtinger calculus was written by [78]. The present work extends the Wirtinger calculus formulation to the constrained optimization problem of quantum optimal control. Additional discussion of the Wirtinger

calculus can be found in appendix D.

The key idea of the method is that by converting a final time cost to an equivalent time-distributed cost. We begin with the standard cost functional

$$J(\psi, \bar{\psi}, u) = 1 - (\bar{\psi}, \mathcal{P}\psi)_T + \frac{\gamma}{2} \int_0^T u^2 dt \tag{A.4}$$

Proposition

There exists a linear operator $\mathcal{A} : Q \to Q$, such that the cost functional of (A.4) may be equivalently written as

$$J(\psi, \bar{\psi}, u) = \int_0^T \frac{\gamma}{2} u^2 + (\bar{\psi}, \mathcal{A}\psi) dt \tag{A.5}$$

Proof. Suppose that instead of $\mathcal{P}$ projecting a solution onto a time-independent final target state $\hat{\psi}(x)$, that we were to choose a space-time trajectory $\varphi(x,t)$ which has the properties that $\varphi(x,0) = \psi^0(x)$ and $\varphi(x,T) = \psi^f(x)$. For convenience, assume that $\varphi : Q \to \mathbb{R}$, although the approach could be generalized to complex-valued trajectories. Let the projection onto this trajectory be defined as

$$\mathcal{P}_\varphi \psi(x,t) = (\varphi, \psi)\varphi(x,t) \tag{A.6}$$

In this case, we have that $(\bar{\psi}, \mathcal{P}_\varphi \psi)_0 = 1$ and $(\bar{\psi}, \mathcal{P}_\varphi \psi)_T = (\bar{\psi}, \mathcal{P}\psi)_T$. By the Fundamental Theorem of Calculus, we have that

$$(\bar{\psi}, \mathcal{P}_\varphi \psi)_0 - (\bar{\psi}, \mathcal{P}_\varphi \psi)_T = -\int_0^T \frac{d}{dt}(\bar{\psi}, \mathcal{P}_\varphi \psi) dt \tag{A.7}$$

Appendix A. An equivalent time-distributed cost

The Ehrenfest theorem relates the time derivative of the expectation of an operator to its commutation relation with the Hamiltonian.

$$\frac{d}{dt}(\bar{\psi}, \mathcal{P}_\varphi \psi) = i(\bar{\psi}, [\mathcal{H}, \mathcal{P}_\varphi]\psi) + (\bar{\psi}, \dot{\mathcal{P}}_\varphi \psi) \tag{A.8}$$

Where the notation means

$$[\mathcal{H}, \mathcal{P}_\varphi]\psi = \mathcal{H}\mathcal{P}_\varphi \psi - \mathcal{P}_\varphi \mathcal{H}\psi, \quad \dot{\mathcal{P}}_\varphi \psi = (\dot{\varphi}, \psi)\varphi(x,t) + (\varphi, \psi)\dot{\varphi}(x,t) \tag{A.9}$$

Therefore, the operator may be formally defined as

$$\mathcal{A} = i[\mathcal{P}_\varphi, \mathcal{H}] - \dot{\mathcal{P}}_\varphi \tag{A.10}$$

For purposes of deriving optimality conditions, we also need the adjoint of this operator. It is easy to see that the adjoint is $\mathcal{A}^* = i[\mathcal{H}, \mathcal{P}_\varphi] - \dot{\mathcal{P}}_\varphi$. □

Proposition

The L^1-norm of the control establishes an upper bound of the projection of the solution onto a target state. Considering a time-dependent Hamiltonian of the form $\mathcal{H} = \mathcal{H}_0 + u(t)v(x)$, with an initial eigenstate $\psi_0(x)$ The probability of finding the particle in the target eigenstate $\varphi(x)$ at the final time is bounded by the estimate

$$(\bar{\psi}, \mathcal{P}\psi)_T \leq 2\|u\|_1 |v|_\infty \tag{A.11}$$

Proof. Let the target state φ be and eigenfunction of $\mathcal{H}_0$ with eigenvalue λ. The probability of finding the particle in state φ at a time T is

$$(\bar{\psi}, \mathcal{P}\psi)_T = (\bar{\psi}, \mathcal{P}\psi)_0 + \int_0^T \frac{d}{dt}(\bar{\psi}, \mathcal{P}\psi)dt \tag{A.12}$$

The term $(\bar{\psi}, \mathcal{P}\psi)_0$ is zero because $\psi(x,0) = \psi_0(x)$ which is orthogonal to φ by virtue of the fact that $\mathcal{H}_0 = \mathcal{H}_0^*$. The Ehrenfest theorem states that

$$\frac{d}{dt}(\bar{\psi}, \mathcal{P}\psi) = i(\bar{\psi}, [\mathcal{H}, \mathcal{P}]\psi) + (\bar{\psi}, \dot{\mathcal{P}}\psi) \tag{A.13}$$

In this case $(\bar{\psi}, \dot{\mathcal{P}}\psi) = 0$ because $\varphi(x)$ is time-independent. Expanding the remaining term gives

$$i(\bar{\psi}, [\mathcal{H}, \mathcal{P}]\psi) = i(\bar{\psi}, (\lambda + uv)\varphi)(\varphi, \psi) - i(\psi, (\lambda + uv)\varphi)(\varphi, \bar{\psi}) \tag{A.14}$$

Note that this can be expressed as $2\Im[(\psi, (\lambda + uv)\varphi)(\varphi, \bar{\psi})]$.

$$\frac{d}{dt}(\bar{\psi}, \mathcal{P}\psi) = 2\Im[\lambda(\psi, \varphi)(\varphi, \bar{\psi})] + 2u(t)\Im[(\psi, v\varphi)(\varphi, \bar{\psi})] \tag{A.15}$$

The term $(\psi, \varphi)(\varphi, \bar{\psi}) = |(\psi, \varphi)|$ is purely real, so this vanishes leaving

$$\frac{d}{dt}(\bar{\psi}, \mathcal{P}\psi) = 2u(t)\Im[(\psi, v\varphi)(\varphi, \bar{\psi})] \tag{A.16}$$

Taking absolute values

$$\left|\frac{d}{dt}(\bar{\psi}, \mathcal{P}\psi)\right| \leq 2|u(t)| \cdot |(\psi, v\varphi)(\varphi, \bar{\psi})| \leq 2|u(t)| \cdot |(\psi, v\varphi)| \leq 2|u(t)| \cdot |v|_\infty \tag{A.17}$$

Finally

$$(\bar{\psi}, \mathcal{P}\psi)_T = \left|(\bar{\psi}, \mathcal{P}\psi)_T\right| \leq 2\int_0^T |u(t)| \cdot |v|_\infty dt = 2\|u\|_1 |v|_\infty \tag{A.18}$$

□

An L^2 control regularization is added.

$$J(\psi, \bar{\psi}, u) = \int_0^T \frac{\gamma}{2}u^2 + (\bar{\psi}, \mathcal{A}\psi)dt \tag{A.19}$$

Appendix B

Hessian blocks for time-distributed cost

In this appendix, we give the blocks of the KKT Hessian in the weak form which arise from taking second variations.

$$\langle \delta\bar{\psi}^1, L_{\psi\psi}\delta\psi^2\rangle = -\langle \delta\bar{\psi}^1, \mathcal{A}\delta\psi^2\rangle \tag{B.1}$$

$$\langle \delta\bar{\psi}^1, L_{\psi u}\delta u^2\rangle = -\langle \delta\bar{\psi}^1, (\mathcal{A}_u\psi + i\mathcal{H}_u\bar{p})\delta u^2\rangle \tag{B.2}$$

$$\langle \delta\bar{\psi}^1, L_{\psi\bar{p}}\delta\bar{p}^2\rangle = -\langle \delta\bar{\psi}^1, (\partial_t + i\mathcal{H})\delta\bar{p}^2\rangle \tag{B.3}$$

$$\langle \delta u^1, L_{\psi u}\delta\psi^2\rangle = \int_0^T \delta u^1[i(p, \mathcal{H}_u\delta\psi) - (\bar{\psi}, \mathcal{A}_u\delta\psi)]dt \tag{B.4}$$

$$\langle \delta u^1, L_{uu}\delta u^2\rangle = \int_0^T \delta u^1[\gamma\delta u^2 - (\bar{\psi}, \mathcal{A}^\dagger_{uu}\psi) + i(p, \mathcal{H}_{uu}\psi) - i(\bar{p}, \mathcal{H}_{uu}\bar{\psi})]dt \tag{B.5}$$

$$\langle \delta u^1, L_{up}\delta p^2\rangle = i\int_0^T (\delta p, \mathcal{H}_u\psi)dt \tag{B.6}$$

$$\langle \delta p^1, L_{\bar{p}\psi}\delta\psi^2\rangle = \langle \delta p^1, (\partial_t + i\mathcal{H})\delta\psi^2\rangle \tag{B.7}$$

$$\langle \delta p^1, L_{\bar{p}u} \delta u^2 \rangle = i \langle \delta p^1, \mathcal{H}_u \psi \delta u^2 \rangle \tag{B.8}$$

All other blocks of the KKT Hessian are either complex conjugates of given blocks or are identically zero.

Appendix C

DG time discretization

A nodal discontinuous Galerkin scheme[80] is used for the time discretization. On each time element, the solution is expanded in the Lagrange polynomials based on the Legendre-Gauss nodes. These points are chosen an they diagonalize the temporal mass matrix and give optimal order of integration.

The method is described here using only an ordinary differential equation with variable to illustrate the concept, but generalizes to the system of ODEs produced by discretizing the Schrödinger equation in space.

$$\dot{y}(t) + a(t)y = f(t), \quad y(0) = y_0, \quad t \in [0, 1] \tag{C.1}$$

We choose the Lagrange interpolating polynomials $\ell_1(t), ..., \ell_n(t)$ which are based on the Legendre-Gauss nodes as test and trial functions. The approximate solution to the IVP expanded in this basis.

$$\tilde{y}(t) = \sum_{k=1}^{n} \hat{y}_k \ell_k(t) \tag{C.2}$$

Substituting the expansion into the IVP gives

$$\sum_{k=1}^{n} \hat{y}_k [\dot{\ell}_k(t) + a(t)\ell_k(t)] = f(t) \tag{C.3}$$

where the $\hat{y}_k$ are the unknown coefficients that we need to compute. Now we multiply the equation by a test function $\ell_j(t)$ and integrate by parts

$$\sum_{k=1}^{n} \hat{y}_k[-(\dot{\ell}_j, \ell_k) + (\ell_j, a\ell_k) + \ell_j(1)\ell_k(1) - \ell_j(0)\ell_k(0)] = (\ell_j, f) \tag{C.4}$$

Now we want to enforce the initial condition. The requirement that $y(0) = y_0$ can be weakly enforced by requiring that $y(0)\ell_j(0) = y_0\ell_j(0)$ for all j.

$$y(0)\ell_j(0) = \sum_{k=1}^{n} \hat{y}_k \ell_j(0)\ell_k(0) \tag{C.5}$$

This term appears within the expansion above so it may be taken to the right hand side

$$\left(\sum_{k=1}^{n} \hat{y}_k[-(\dot{\ell}_j, \ell_k) + (\ell_j, a\ell_k) + \phi_k(1)\phi_j(1)]\right) = (\ell_j, f) + y_0\ell_j(0) \tag{C.6}$$

Let $K \in \mathbb{R}^{n\times n}$ be the called the stiffness matrix with elements $K_{jk} = -(\dot{\ell}_j, \ell_k)$, $S \in \mathbb{R}^{n\times n}$ is the matrix containing the surface terms from the right boundary with elements $S_{jk} = \ell_j(1)\ell_k(1)$, and $A \in \mathbb{R}^{n\times n}$ containing the variable coefficient projected on to the basis functions $A_{jk} = (\ell_j, a\ell_k)$. Let $\hat{f} \in \mathbb{R}^n$ with elements $\hat{f}_k = (\phi_k, f)$ and $\hat{g} \in \mathbb{R}^n$ be a vector for enforcing the initial condition with elements $\hat{g}_j = y_0\ell_j(0)$. The Galerkin Method can now be written as a linear system

$$(K + S + A)\hat{y} = \hat{f} + \hat{g} \tag{C.7}$$

which we can solve for the vector of unknown coefficients $a \in \mathbb{R}^n$.

This approach can then be used to construct a time-stepping method when the time interval is subdivided and the solution on a given time interval is evaluated at the final time and used to as initial data for the solution in the next time interval. This is a discontinuous Galerkin method as the basis functions are not themselves globally time continuous, but rather the surface terms are matched between elements to weakly impose continuity of the solution.

Space-time discretization

The structure of the solution operator for the dipole driven-well, $\partial_t - i\partial_x^2 + iu(t)x$ is such that the numerical approximation is easily written in terms of a sum of tensor products. On the kth time interval, the solution to the Schrödinger equation, or the forced Schrödinger-like equation satisfies the system

$$[M_x \otimes (K_t + S) + iK_x \otimes M_t + iX \otimes U_k]\hat{y}_k = \hat{f}_k + \hat{g}_k \tag{C.8}$$

Where M_x, K_x are the mass and stiffness matrices for the spatial discretization, X is the projection of the position operator x onto the spatial basis. Standard hp-nodal Lagrange polynomial basis functions based on the Legendre-Gauss-Lobatto nodes are used for the spatial discretization. M_t, K_t are the mass and stiffness matrices for temporal discretization, S is the surface operator, and U_k is the control function in the kth interval projected onto the Lagrange polynomials. The forcing and initial conditions are incorporated into $\hat{f}_k$ and $\hat{g}_k$ as described above, but there is a different initial condition for each mode of the spatial expansion.

Appendix D

Complex representation

In the preceding work, it was observed that in quantum optimal control problems, one aims to minimize a real valued cost functional which in some way depends on the quantum mechanical wavefunction, which is a complex quantity. Since the cost must be real, it means that $J(\psi, u)$ must not only be a function of ψ, but also of its complex conjugate $\bar{\psi}$. This means that J can not be an analytic function of ψ and indeed some care is needed in taking variations. The approach taken above was to circumvent this difficulty by using the real matrix representation of complex numbers. As alluded to earlier, there exists an alternate approach of dealing with non-analytic functions and their derivatives; this is the Wirtinger calculus [74].

The idea of the Wirtinger calculus is quite simple. Suppose we have a real-valued scalar function of of many complex variables $f(\mathbf{z})$ where

$$\mathbf{z} = \begin{pmatrix} z_1 & z_2 & \cdots & z_n \end{pmatrix}$$

The fact that $f \in \mathbb{R}$ tells us that f must also depend on $\bar{\mathbf{z}}$, so really the function is $f(\mathbf{z}, \bar{\mathbf{z}})$. Assuming f to be smooth in $\mathbf{z}$ and $\bar{\mathbf{z}}$, it will have a Taylor series and the series must also be real-valued. When f is differentiated with respect to $\mathbf{z}$, the $\bar{\mathbf{z}}$ is treated as constant and vice versa. Additionally, if f is real, it holds that $f_{\bar{\mathbf{z}}} = \bar{f}_{\mathbf{z}}$. The

main difference of the Wirtinger calculus is that the full KKT-Hessian will complex Hermitian instead of real symmetric, although since the control is real-valued, the reduced Hessian will be real symmetric. Taking first variations gives us the term

$$\begin{pmatrix} \delta\mathbf{z}^1, \delta\bar{\mathbf{z}}^1 \end{pmatrix} \begin{pmatrix} f_{\mathbf{z}} \\ f_{\bar{\mathbf{z}}} \end{pmatrix} \tag{D.1}$$

To take second variations we proceed as before but first take the complex conjugate of the term in D.1.

$$\begin{pmatrix} \delta\bar{\mathbf{z}}^1, \delta\mathbf{z}^1 \end{pmatrix} \begin{pmatrix} f_{\mathbf{zz}} & f_{\mathbf{z}\bar{\mathbf{z}}} \\ f_{\bar{\mathbf{z}}\mathbf{z}} & f_{\bar{\mathbf{z}}\bar{\mathbf{z}}} \end{pmatrix} \begin{pmatrix} \delta\mathbf{z}^2 \\ \delta\bar{\mathbf{z}}^2 \end{pmatrix}, \quad f_{\mathbf{zz}} \equiv \nabla_{\mathbf{z}}(\nabla_{\mathbf{z}} f)^* \tag{D.2}$$

The Hessian matrix in D.2 is Hermitian. When we formulate the cost functional for a quantum control problem, we use this approach. Note that the inner products used are taken to be the *real* inner products and conjugation is performed explicitly. This is in contrast to the standard complex inner products of mathematical physics. The primary motivation for using the real inner product is that we do not need to concern ourselves with where in the expression the wavefunction appears to determine if it should be treated as a constant or a variable when taking variations.

References

[1] R.A. Adams, *Sobolev Spaces*, Academic Press, New York-London, 1975.

[2] H. W. Alt, *Lineare Funktionalanalysis. Eine anwendungsorientierte Einführung*, Springer-Verlag, Berlin, 1992.

[3] P.W. Atkins and R.S. Friedman, *Molecular Quantum Mechanics*, Oxford University Press.

[4] R. Becker and B. Vexler, *Optimal control of the convection-diffusion equation using stabilized finite element methods*, Numerische Mathematik,**106** (2007), pp. 349–367.

[5] C.H. Bennett, E. Bernstein, G. Brassard, and U. Vazirani, *Strengths and weakness of quantum computating*, SIAM J. Computing, **26** (1997), pp. 1510–1523.

[6] A. Borzì and U. Hohennester, *Multigrid optimization schemes for solving Bose-Einstein condensate control problems*, SIAM J. Scientific Computing, **30** (2008), pp. 441–462.

[7] A. Borzì, J. Salomon, and S. Volkwein, *Formulation and numerical solution of finite-level quantum optimal control problems*, J. Comput. Appl. Math., **216** (2008), pp. 170–197.

[8] A. Borzì, G. Stadler, and U. Hohenester, *Optimal quantum control in nanostructures: Theory and application to a generic three-level system*, Phys. Rev. A **66**, (2002) 053811.

[9] U. Boscain, G. Charlot, J.-P. Gauthier, S. Guerin, H.-R. Jauslin, *Optimal control in laser-induced population transfer for two- and three-level quantum systems*, Journal of Mathematical Physics,**43** (2002), pp. 2107–2132.

[10] J. Bourgain, *Global Solutions of Nonlinear Schrödinger Equations*, American Mathematical Society Colloquium Publications,**46**. American Mathematical Society, Providence, RI (1999).

[11] P.W. Brumer and M. Shapiro, *Principles of the Quantum Control of Molecular Processes*, Wiley-VCH, Berlin, 2003.

[12] J. Burkardt, M. Gunzburger, and J. Peterson, *Insensitive functionals, inconsistent gradients, spurious minima, and regularized functionals in flow optimization problems*, Int. J. Comput. Fluid Dyn.,**16** (2002), pp. 171-185.

[13] A.G. Butkovskiy and Yu.I. Samoilenko, *Control of quantum-mechanical processes and systems*, Kluwer, 1990.

[14] A.Z. Capri, *Nonrelativistic Quantum Mechanics*, World Scientific Publishing Co. Inc., River Edge, NJ, 2002.

[15] R. Dautray, J.-P. Lions, *Mathematical Analysis and Numerical Methods for Science and Technology. Volume 5: Evolution Problems*, Springer-Verlag, Berlin, 1992.

[16] P. Ditz and A. Borzi, *A cascadic monotonic time-discretized algorithm for finite-level quantum control computation*, Computer Physics Communications, **178** (2008), 393-399.

[17] L.C. Evans, *Partial Differential Equations*, Graduate Studies in Mathematics, vol.**19**, American Mathematical Society, Providence, Rhode Island, 2002.

[18] D. Gaveaux, *Semiconductor lasers: Quantum wells meet nanowires*, Vol. 2, Nature, October 2008.

[19] P. Harrison, *Quantum Wells, Wires and Dots: Theoretical and Computational Physics of Semiconductor Nanostructures*, Wiley, 2005.

[20] M. Hochbruck and C. Lubich, *On Magnus integrators for time-dependent Schrödinger equations*, SIAM J. Numer. Anal.,**41** (2003), pp. 945-963.

[21] A. Iserles, H.Z. Munthe-Kaas, S. Nørsett, and A. Zanna, *Lie-group methods*, Acta Numerica, Cambridge Univ. Press, **9** (2000), pp. 215-365.

[22] R. Kosloff, S.A. Rice, P. Gaspard, S. Tersigni, and D. Tannor, *Wavepacket Dancing: Achieving Chemical Selectivity by Shaping Light Pulses*, Chem. Phys., **139** (1989), pp. 201–220.

[23] J.L. Lions, *Optimal Control of Systems Governed by Partial Differential Equations*, Springer, Berlin, 1971.

[24] D.G. Luenberger, *Optimization by Vector Space Methods*, John Wiley & Sons, Inc.,New York, 1969.

[25] Y. Maday, J. Salomon and G. Turinici, *Monotonic time-discretized schemes in quantum control*, Num. Math., **103** (2006), pp. 323–338.

[26] Y. Maday, J. Salomon, and G. Turinici, *Parareal in time control for quantum systems*, SIAM J. Num. Anal., **45** (2007), pp. 2468-2482.

[27] Y. Maday and G. Turinici, *New formulations of monotonically convergent quantum control algorithms*, J. Chem. Phys., **118** (2003), pp. 8191–8196.

[28] H. Maurer and J. Zowe, *First and second order necessary and sufficient optimality conditions for infinite-dimensional programming problems*, Mathematical Programming, **16** (1979), pp. 98-110.

[29] J. Nocedal and S.J. Wright, *Numerical optimization, Springer Series in Operations Research and Financial Engineering*, Springer, New York, second ed., 2006.

[30] T. Numai, *Fundamentals of Semiconductor Lasers*, Springer-Verlag, New York, 2004

[31] C.C. Paige and M.A. Saunders, *Solution of sparse indefinite systems of linear equations*, SIAM J. Numer. Anal., **12** (1975), pp. 617-629.

[32] A.P. Peirce, M.A. Dahleh, and H. Rabitz, *Optimal control of quantum-mechanical systems: existence, numerical approximation, and applications*, Physical Review A, **37** (1988), pp. 4950-4964.

[33] H. Rabitz, M. Hsieh, and C. Rosenthal, *Quantum optimally controlled transition landscapes*, Science, **303** (2004), p. 998.

[34] H. Rabitz, G. Turinici, and E. Brown, *Control of Molecular Motion: Concepts, Procedures, and Future Prospects*, Ch. 14 in Handbook of Numerical Analysis, Volume X, P. Ciarlet and J. Lions, Eds., Elsevier, Amsterdam, 2003.

[35] M. Reed and B. Simon, *Methods of Modern Mathematical Physics. Volume 1: Functional Analysis*, Academic Press, Inc., Boston, 1980.

[36] B.J. Sussman, D. Townsend, M.Y. Ivanov, and A. Stolow, *Dynamic Stark control of photochemical processes*, Science, **13** (2006) , pp. 278 - 281.

[37] R. Temam, *Infinite-Dimensional Systems in Mechanics and Physics*, Springer-Verlag, New York, 1988.

[38] V. Thomée, *Galerkin Finite Element Methods for Parabolic Problems*, Springer-Verlag, Berlin, 2006.

[39] A. van den Bos, *Complex Gradient and Hessian*, IEEE Proc.-Vis. Image Signal Processing, **141** (6) (1994), pp. 380-82.

[40] G. von Winckel and A. Borzì, Computational techniques for a quantum control problem with H^1-cost, Inverse Problems, **24** (2008), 034007.

[41] K. Yajima, *Existence of Solutions for Schrödinger Evolution Equations*, Communications in Mathematical Physics, **110** (1987), pp. 415-26.

[42] Bandrauk, A. D. and Légaré, F. and Yu, H. T., *QLaser control of molecular states—nonperturbative examples*, Quantum control: mathematical and numerical challenges, CRM proceedings & lecture notes series, Vol. **33**, pp. 41–47, American Mathematical Society, 2004.

[43] W. Bao and Q. Du, *Computing the ground state solution of Bose–Einstein condensates by a normalized gradient flow*, SIAM J. Sci. Comput., **25** (2004), pp. 1674–1697.

[44] W. Bao, D. Jaksch, and P.A. Markowich, *Numerical solution of the Gross-Pitaevskii Equation for Bose–Einstein condensation*, J. Comput. Phys., **187** (2003), pp. 318–342.

[45] W. Bao, S. Jin, and P.A. Markowich, *On time-splitting spectral approximation for the Schrödinger equation in the semiclassical regime*, J. Comput. Phys., **175** (2002), pp. 487–524.

[46] A. Borzì, G. Stadler, and U. Hohenester, *Optimal quantum control in nanostructures: Theory and application to a generic three-level system*, Phys. Rev. A **66**, (2002) 053811.

[47] J. Burkardt, M. Gunzburger, and J. Peterson, *Insensitive functionals, inconsistent gradients, spurious minima, and regularized functionals in flow optimization problems*, Inter. J. Comput. Fluid Dyn., **16** (2002), pp. 171–185.

[48] F. Dalfovo, G. Stefano, L.P. Pitaevskii, S. Stringari, *Theory of Bose–Einstein condensation in trapped gases*, Rev. Mod. Phys., **71** (1999), pp. 463–512.

[49] R. Folman, P. Krüger, D. Cassettari, B. Hessmo, T. Maier, and J. Schmiedmayer, *Controlling Cold Atoms using Nanofabricated Surfaces: Atom Chips*, Phys. Rev. Lett., **84** (2000), 4749.

[50] R. Folman, P. Krüger, D. Cassettari, J. Schmiedmayer, J. Denschlag, and C. Henkel, *Microscopic atom optics: from wires to an atom chip*, Adv. in Atom. Mol. and Opt. Phys., **48** (2002), 263.

[51] J. Fortagh and C. Zimmermann, *Magnetic microtraps for ultracold atoms*, Reviews of Modern Physics, **79** (2007), pp. 235–289.

[52] J.C. Gilbert and J. Nocedal, *Global convergence properties of conjugate gradient methods for optimization*, SIAM J. Opt. **2** (1992), pp. 21–42.

[53] W.W. Hager and H. Zhang, *A New Conjugate Gradient Method with Guaranteed Descent and an Efficient linesearch*, SIAM Journal on Optimization, **16** (2005), pp. 170–192.

[54] W. Hänsel, J. Reichel, P. Hommelhoff, and T.W. Hänsch, *Trapped-atom interferometer in a magnetic microtrap*, Phys. Rev. A, **64** (2001), 063607.

[55] W. Hänsel, P. Hommelhoff, T.W. Hänsch, and J. Reichel, Nature, **413** (2001), pp. 498–501.

[56] M. Heinkenschloss and L.N. Vicente, *An interface between optimization and application for the numerical solution of optimal control problems*, ACM Transactions on Mathematical Software, **25** (1999), pp. 157–190.

[57] U. Hohenester, *Optical properties of semiconductor nanostructures: Decoherence versus quantum control*, to appear in M. Rieth and W. Schommers, (Eds.), *Handbook of Theoretical and Computational Nanotechnology* (American Scientific Publishers, 2005); cond-mat/0406346.

[58] U. Hohenester, P.-K. Rekdal, A. Borzì, J. Schmiedmayer, *Optimal quantum control of Bose Einstein condensates in magnetic microtraps*, Phys. Rev. A, **75** (2007), 023602.

[59] P. Holmes, J.L. Lumley, and G. Berkooz, *Turbulence, Coherent Structures, Dynamical Systems and Symmetry*, Cambridge Monographs on Mechanics, CUP, Cambridge, 1996.

[60] I. Lesanovsky, T. Schumm, S. Hofferberth, L.M. Andersson, P. Krüger, and J. Schmiedmayer, *Adiabatic radio-frequency potentials for the coherent manipulation of matter waves*, Phys. Rev. A, **73** (2006), 033619.

[61] A. Sacchetti, *Nonlinear time-dependent one-dimensional Schrodinger equation with double-well potential*, SIAM J. Math. Anal., **35** (2004), pp. 1160–1176.

[62] V. Schulz, Optimization Methods, SPPOPT spring school. RICAM Linz, March 2007.

[63] D.F. Shanno, *Conjugate gradient methods with inexact searches*, Math. Oper. Res. **3** (1978), pp. 244–256.

[64] T. Schumm and S. Hofferberth, L.M. Andersson, S. Wildermuth, S. Groth, I. Bar–Joseph, J. Schmiedmayer, and P. Krüger, *Matter–wave interferometry in a double well on an atom chip*, Nature Phys., **1** (2005), pp. 57–62.

[65] A. Tarantola, *Inverse Problem Theory and Methods for Model Parameter Estimation*, SIAM, Philidelphia, 2005.

[66] S.H. Tersigni, P. Gaspard, and S.A. Rice, *On using shaped light pulses to control the selectivity of product formation in a chemical reaction: An application to a multiple level system*, J. Chem. Phys., **93** (1990), pp. 1670-1680.

[67] Pechen, A., Prokhorenko, D., Wu, R., and Rabitz, H., *Control landscapes for two-level open quantum systems*, J. Phys. A: Math. Theor. **41** (2008) 045205 (18pp)

[68] Roloff, R., Wenin, M., and Pötz, W., *Optimal Control for Open Quantum Systems: Qubits and Quantum Gates*, J. Computational and Theoretical Nanoscience, Vol. **6**, No. 8. (2 Oct 2009), pp. 1837-1863.

[69] Simon, B. *The definition of molecular resonance curves through complex exterior scaling*, Phys. Lett., **71A** (1979), pp. 211–214.

[70] Levy, M.F. *Perfectly matched layer truncation for parabolic equation models*, Proc. Roy. Soc. London A, **457** (2001) pp. 2609–2624.

[71] Jiang, S., Greengard, L. *Fast evaluation of nonreflecting boundary conditions for the Schrödinger equation in one dimension*, Comput. Math. Appl., **47** (2004) pp. 955–966.

[72] Brandwood, D. H., *A Complex Gradient Operator and its Application in Adaptive Array Theory*, IEE Proc H **130** (1983) pp. 11–16.

[73] van den Bos, A., *Complex Gradient and Hessian*, IEE Proc-Vis. Image Signal Processing, **141** (1994) pp. 380–82

[74] Wirtinger, W., *Zur Formalen Theorie der Funktionen von mehr Complexen Veränderlichen*, Math. Ann., **97** (1927), pp. 357–75

[75] Kreutz-Delgado, K., *The Complex Gradient Operator and the CR Calculus*, June 2009, http://arxiv.org/abs/0906.4835v1

[76] Lefebvre, K. R., Anwar, A. F. M., *Electron escape time from single quantum wells*, IEEE J. Quantum Electronics, **33** (2), pp. 187–191. (1997)

[77] Barrett, R., M. Berry, T. F. Chan, et al., *Templates for the Solution of Linear Systems: Building Blocks for Iterative Methods* , SIAM, Philadelphia, (1994)

[78] K. Kreutz-Delgado, *The Complex Gradient Operator and the CR Calculus*, June 2009, http://arxiv.org/abs/0906.4835v1

[79] J. Shen, *Efficient spectral-galerkin method I. Direct solvers of second- and fourth-order equations using Legendre Polynomials*, SIAM J. Sci. Comp. **15**, (1994), pp. 1489–1505

[80] J.S. Hesthaven and T. Warburton, *Nodal Discontinuous Galerkin Methods: Algorithms, Analysis, and Applications*, volume 54 of Text in Applied Mathematics. Springer Verlag, New York, 2008.

[81] G. Friesecke and M. Koppen, *On the Ehrenfest theorem of quantum mechanics*, J. Math. Phys. **50**, (2009), 082102

[82] D. Tannor, V. Kazakov, and V. Orlov, *Control of photochemical branching: Novel procedures for finding optimal pulses and global upper bounds*, Time-dependent Quantum Molecular Dynamics, J. Broeckhove and L. Lathouwers eds., Plenum Press, New York (1992)

[83] I. Degani, A. Zanna, L. Sælen, and R. Nepstad, *Quantum control with piecewise constant control functions*, SIAM J. Sci. Comput, **31** (2009), pp. 3566–3594

[84] G. von Winckel, A. Borzì, and S. Volkwein, *A globalized Newton method for the accurate solution of a dipole quantum control problem*, SIAM J. Sci. Comp. **31**, (2009), pp. 4176–4203 .

[85] D. Meidner and B. Vexler, *A Priori Error Estimates for Space-Time Finite Element Discretization of Parabolic Optimal Control Problems Part I: Problems Without Control Constraints*, SIAM J. Control Optim. **47**, (2008), pp. 1150–1177.

[86] D. Meidner and B. Vexler, *A Priori Error Estimates for Space-Time Finite Element Discretization of Parabolic Optimal Control Problems Part II: Problems With Control Constraints*, SIAM J. Control Optim. **47**, (2008), pp. 1301–1329.

[87] G. von Winckel and A. Borzì, *QUCON: A fast Krylov-Newton code for dipole quantum control problems*, Comp. Phys. Comm., **181**, (2009), pp. 2158–2163.

[88] E.A. Coutsias, T. Hagstrom, J.S. Hesthaven and D. Torres, *Integration preconditioners for differential operators in spectral tau-methods*. In: A.V. Ilin and L.R. Scott, Editors, Proceedings of the Third International Conference on Spectral and High Order Methods, Houston J. Mathematics, University of Houston, Houston, TX (1996), pp. 21–38.

[89] B. Fornberg, *A Practical Guide to Pseudospectral Methods*, Cambridge Monographs on Applied and Computational Mathematics, Cambridge University Press, 1998.

[90] J.S. Hesthaven, *Integration Preconditioning of Pseudospectral Operators. I. Basic Linear Operators*, SIAM J. Numer. Anal. **35**, (1998), pp. 1571–1593

[91] A.C. Doherty and K. Jacobs, *Feedback Control of Quantum Systems Using Continuous State Estimation*, Phys. Rev. A. **60** (4): 2700.

[92] J. Shen and L.L. Wang, *Legendre and Chebyshev dual–Petrov–Galerkin methods for Hyperbolic equations*, Comput. Methods Appl. Mech. Engrg, **196** (2007), pp. 3785–3797

[93] A.H. Baker, J.M. Dennis, and E.R. Jessup, *An efficient Block Variant of GMRES*, SIAM J. Sci. Comput. **27**, 5 (2006), 1608–1626.

[94] V. Simonici and E. Gallopoulos, *A hybrid block GMRES method for nonsymmetric systems with multiple right–hand sides*, J. Comp. Appl. Math., **66** (1996), pp. 457–469.

[95] M.M. Wagner, P.M. Pinsky, A.A. Oberai, and M. Malhotra, *A Kyrlov subspace projection method for simultaneous solution of Helmholtz problems at multiple frequencies*, Comput. Methods Appl. Mech. Engrg, **192** (2003), pp. 4609–4640

[96] S.D. Garvey, F.T. Tisseur, M.I. Friswell, J.E.T. Penny, and U. Prells, *Simultaneous tridiagonalization of two symmetric matrices*, Int. J. Numer. Meth. Engng, **57** (2003), pp. 1643–1660.